University of
HUDDERSFIELD
Inspiring global professionals

Probing the localisation and function of a novel kinetoplast-associated protein in evolutionarily divergent protists

By
Cameron Jack Stockwell BSc (Hons), AMRSB
The Department of Biological and Geographical Sciences

Supervisors:
Dr Jane Harmer and Prof. Michael Ginger

Thesis submitted to the
University of Huddersfield
In partial fulfilment of the requirements for the degree of Masters of Sciences by Research

Statement of Copyright

In our age, there is no such thing as 'keeping out of politics'. All issues are political issues, and politics itself is a mass of lies, evasions, folly, hatred and schizophrenia

- - George Orwell

Politics and the English Language, 1946

Acknowledgments

To my family and my friends, thank you for reminding me what a work life balance is. I fear sometimes I forget what a break is.

To Kurtis, thank you for your love, patience, understanding and kindness throughout my Bachelor's and Master's Degree. Your support reminds me to keep moving forward daily.

I love you endlessly.

William Turner, and Morgan O'Neill thank you for the litres of coffee. Olivia Fisher, and Abi Broxham, thank you for the unsolicited use of your reagents, glassware and patience.

Thank you to Activia Training and The University of Huddersfield for their generosity in contributing towards the costs associated with this work as well as the financial support from family.

I would like to thank Dr Jane Harmer for her unwavering support, kindness and mentorship over the past two years throughout my dissertation and masters. Thanks to Prof. Michael Ginger for the guidance, support and advice offered.

Many Thanks To:

Asma Belbelazi

Kim Yeardley

Kayleigh Hopkins

Rebecca Reid

And

The Technical Team and Administrative Staff

Abstract

In evolutionary terms, the origin of the kinetoplast remains ambiguous. However, interestingly some components of the TAC are found in the genome of the free-living *Bodo Saltans*. This includes the protein designated *Tb*9260, which is important in kinetoplast organisation during cell division a fragment of the *Bodo saltans Tb*9260 orthologue, named Trett, will be expressed as recombinant protein in *E.coli* in order to raise a *Bs*Trett antibody. This will be utilised for the *in vivo* targeting by confocal and super-resolution microscopy of *Bs*Trett within *Bodo saltans* in order to ascertain its localisation. Additionally, *Bodo saltans* TAC65, TAC60, TAC40 and Trett orthologues will be cloned into a pNUS-GFPcH expression vector and transfected into *Crithidia fasciculata*. The localisations of these orthologous proteins are shown here with some surprising phenotypes. In addition, a cross species bioinformatic analysis of the *Bodo saltans* transcriptome against peptide sequences of putative proteins identified within the *Tb*MitoCarta will aim to identify possible conserved orthologues and future protein targets. *Bodo saltans* is a divergent free-living ancestor of the parasitic trypanosomatids, including species of trypanosomes and *Leishmania*. Similarities between the Kinetoplastids have demonstrated the importance of understanding the evolutionary process which has led to parasitism and the question of whether it evolved from, or separately, to its free-living ancestor remains unanswered. Here I show the localisations of the aforementioned proteins and their similarities between the free-living and parasitic organisms.

Table of Contents

List of Tables

Tables of Figures

Table of Abbreviations

BLAST	Basic Local Alignment Search Tool
Bs	*Bodo saltans*
Cf	*Crithidia fasciculata*
CSB	Conserved Sequence Blocks
DAPI	4',6-diamidino-2-phenylindole
DIC	Diffuse Interference Contrast
DM	Differentiated Membranes
EtOH	Ethanol
EZF	Exclusion Zone Filaments
GFP	Green Fluorescent Protein
HRP	Horse Radish Peroxidase
IF	Immunofluorescence
kDNA	Kinetoplast DNA
LB	Lysogeny Broth
NaOAc	Sodium Acetate
OM	Outer Membrane
PBS	Phosphate Buffered Saline
PDVF	Polyvinylidine fluoride
TAC	Tripartite Attachment Complex
Tb	*Trypanosoma brucei*
TBCC	Tubulin Binding Co-factor C
TCA	Tricarboxylic Acid Cycle
TRITC	Tetramethyrhodamine-5-isothiocyanate
ULF	Unilateral Filaments
UMSBP	Universal Minicircle Sequence Binding Protein
VDAC	Voltage Gated Anion Channel

1.0 Introduction

1.1 The Tripartite Attachment Complex

Approximately 2.3 billion years ago the great oxidation event introduced free oxygen into our oceans allowing evolution of a α-proteobacterium capable of oxidative phosphorylation and its introduction into early archaeon (Käser *et al.*, 2017; Santos, Makiuchi and Nozaki, 2018). The origins of mitochondria have been traced via fossil remains identifying the moment this evolutionary important, oxidative phosphorylation permitting organelle, arose (Dacks *et al.*, 2016; Schneider and Ochsenreiter, 2018). Unlike their mammalian counterparts, Kinetoplastid organisms possess a singular large mitochondrion which is distributed through the full length of the cell (Figure 1) and features a mitochondrial genomic cassette known as kinetoplast DNA (kDNA) (Fidalgo and Gille, 2011). The segregation of kDNA has been extensively studied revealing the networks and linkage complex required to allow cell division. The Tripartite Attachment Complex (TAC) of *T. brucei* was first described in 2003 by Ogbadoyi *et al.*,and secures the kinetoplast to the basal body of the cell to ensure faithful replication and division of the kDNA throughout the cell cycle and cytokinesis. The TAC is comprised of distinct subdomains with each being morphologically unique (Figure 2). The three subdomains of the *Trypansoma brucei* Tripartite Attachment Complex were designated: (i) the Exclusion Zone Filaments (EZF), (ii) the Unilateral Filaments (ULF), and (iii) the Differentiated Mitochondrial Membranes (DM) (Ogbadoyi, Robinson and Gull, 2003; Schneider and Ochsenreiter, 2018). The EZF are 5-10 nm wide electron dense filaments spanning the cytoplasm, thereby creating a ribosome free zone; the EZF extends from the basal body to the mitochondrial outer membrane of the cell. The EZF connect to the DM which lack cristae and appear resistant to detergent (Ogbadoyi, Robinson and Gull, 2003). Extending from the DMs to the kDNA disc; the ULFs, a tightly packed filamentous mass, are observed and, comprised of a kDNA-proximal domain and a domain close to the inner-DM. *T. brucei* is often used for kinetoplast studies as *T. brucei* has been extensively studied and is its importance within human disease and the effects of the African economy.

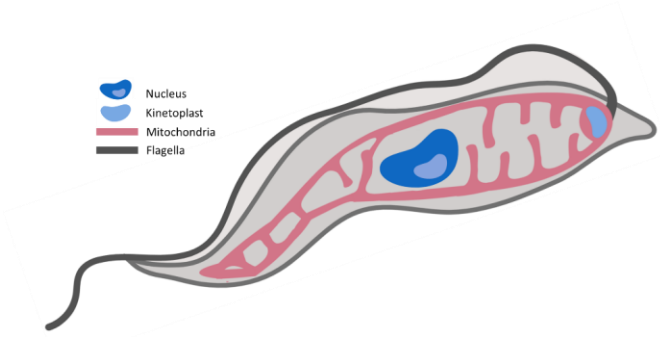

Figure 1: Cartoon of *Trypanosoma brucei*: The large elongate mitochondrion, kinetoplast and nucleus are depicted. The kinetoplast sits within the mitochondrial matrix space and is secured via the Tripartite Attachment Complex (TAC) to the basal body and flagellum.

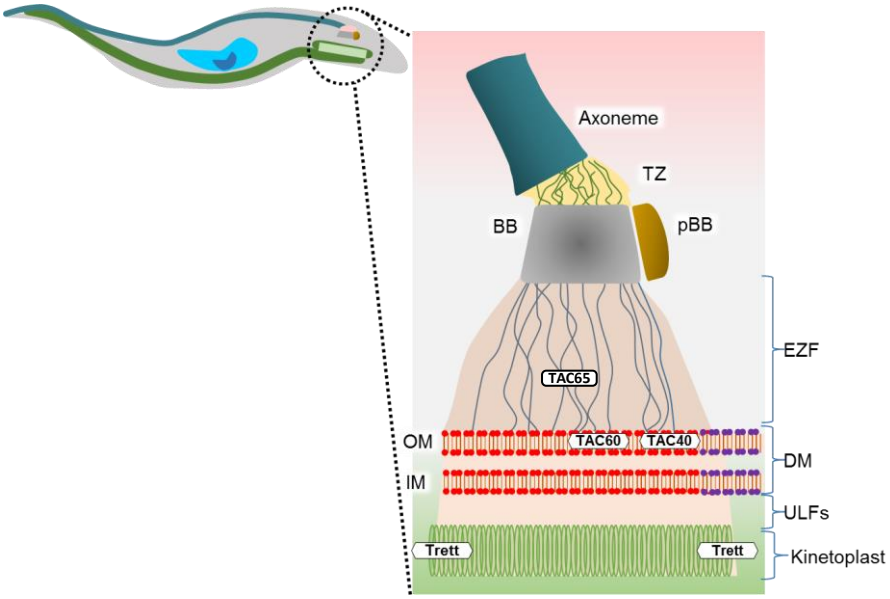

Figure 2: Schematic of the Tripartite Attachment Complex: Localisations of proteins studied within this thesis are labelled, loci are specific to studies within *T. brucei*. TAC40 and TAC60 have been shown to localise to the differentiated membranes. TAC65 is specific to the Exclusion Zone Filaments and previous unpublished work by our lab shows localisation of Trett (*Tb*927.3.2630::YFP) to the kinetoplast antipodal sites.

Commented [CS(1]: Not changes to site as the literature commonly uses the plural e.g Lukes et al 2003

1.2 Proteins Involved Tripartite Attachment Complex Assembly

Misreplication of the kDNA disc is often a sign of a defective TAC. Several proteins have been shown to associate, via localisation studies, with the TAC and proteomic ablation often results in several abnormal phenotypical changes, such as enlarged kinetoplasts, diskinetoplasty or cell cycle interruption (Table 1). The localisation within the TAC of each of these proteins is depicted within Figure 3.

RNA-interference of conserved Tubulin Binding Co-factor C (TBCC) domain-containing protein 1 (*Tb*TBCCD1) within *T. brucei* results in incommensurate division of the kinetoplast and disorganisation of the bi-lobe and problematic cell division (Andre *et al.*, 2013). *Tb*TBCCD1 localises at the anterior cell body and the basal body bi-lobe, while canonical TBCCD1 is an EZF protein that is also responsible for cytoskeletal filament formation (Andre *et al.*, 2013; Schneider and Ochsenreiter, 2018).

BBA4 is representative of a basal body probe within the cytoskeleton of *T. brucei*. Antigen immunofluorescence (IF) of the protein shows it decorates the pro-basal and basal body very early within TAC biogenesis (Woods *et al.*, 1989), being the first proximal basal body component to be assembled into the new TAC at the start of each cell cycle (Woods *et al.*, 1989; Hoffmann *et al.*, 2018). BBA4 expression has previously been shown to be dependent on another protein, p197 for its expression. A study utilising RNAi targeting p197 in *T. brucei*, showed complete loss of BBA4, however no phenotypical changes are observed overall (Hoffmann *et al.*, 2018). p197 localises between the kDNA disc and the basal body. RNAi of p197 produced no effect on basal body structure. However, kDNA becomes missegregated and TAC associated proteins mislocalised (Hoffmann *et al.*, 2018; Schneider and Ochsenreiter, 2018). Mab22 recognises basal body structures and is strongly present within the Exclusion Zone Filaments throughout the cell cycle (Bonhivers *et al.*, 2008). Similar to BBA4, Mab22 also detects an unknown antigen and localisation is p197 dependant (Woods *et al.*, 1989; Bonhivers *et al.*, 2008; Hoffmann *et al.*, 2018; Schneider and Ochsenreiter, 2018). Unlike other EZF protein, TAC65 forms part of a protein complex with peripheral archaic translocase of the outer membrane 36 (pATOM36) that is crucial for normal TAC functionality. Ablation of TAC65 was shown to affect overall health of *T. brucei* cell lines. Also, 4′,6-diamidino-2-phenylindole (DAPI) stained cells showed enlarged kinetoplasts or diskinetoplasty (Käser *et al.*, 2016). TAC65 is also known to associate with the differentiated membrane protein, pATOM36. Because of its cellular function, *Bs*TAC65 is a candidate protein for localisation within this thesis.

pATOM36 is an outer membrane (OM) protein which localises exclusively to the differentiated membranes of the TAC and throughout the OM demonstrating its dual functionality as an ATOM protein biogenesis factor and in kDNA inheritance (Käser *et al.*, 2016, 2017; Schneider and Ochsenreiter, 2018). RNAi knock-down of pATOM36 is seen to primarily cause disruption to OM

proteins; ATOM sub-unit proteins (ATOM-14,-46 and POMP6) which form a protein import complex in the OM were seen to be most affected by pATOM36 ablation (Käser *et al.*, 2016). Furthermore, overall kDNA quantity present in cells was rapidly depleted and cells which had kDNA remaining showed enlarged kinetoplasts (Käser *et al.*, 2016).

TAC40, TAC42 and TAC60, form a complex, alongside pATOM36 (Käser *et al.*, 2017; Schneider and Ochsenreiter, 2018). TAC40, a 40kDa, β-barrel protein is integral for TAC-kDNA linkage and inheritance of a single mitochondrial genome (Felix Schnarwiler *et al.*, 2014). TAC40 belongs to the Voltage Dependent Anion Channel (VDAC) family of proteins and RNAi knock-down revealed kDNA mis-segregation and cell cycle arrest. TAC60, like TAC40 localises to the mitochondrial OM and RNAi knock-down of TAC60 resulted in TAC40 loss and vice versa (Käser *et al.*, 2016; Hoffmann *et al.*, 2018). TAC42, like TAC60, co-fractionates with ATOM40 and localises between the kDNA and basal body. TAC42 lacks transmembrane domains and depends on Sam50 signalling for localisation (Käser *et al.*, 2017). Alternatively edited protein 1 (AEP-1) is another crucial mitochondrial protein that localises at the DM. Further investigations in the DM subdomain of the TAC in *Trypanosoma brucei* found that alternative splicing of mRNA *cox3* transcript results in a 4 transmembrane domain protein which localises between the basal body and kDNA – AEP-1 (Ochsenreiter *et al.*, 2008; Käser *et al.*, 2017; Schneider and Ochsenreiter, 2018). Mitochondrial targeting of the soluble domain of AEP-1 (also observed to bind with kDNA) shows growth arrest and an increase in diskinetoplastic (kinetoplast lacking) and dikinetoplastic cells (Schneider and Ochsenreiter, 2018). In summary; the DM subdomain of the TAC requires further investigation, both in terms of localising proteins inhabiting the TAC, but also to gain further insights into their canonical functions.

TAC102 is a non kDNA interacting, structurally basic protein that associates with both isolated flagella (Hoffmann *et al.*, 2018; Schneider and Ochsenreiter, 2018) and, more specifically, with the unilateral filaments (Trikin *et al.*, 2016). RNAi ablation of the protein results in disproportionate kDNA segregation where upon cell division, one daughter cell acquires an enlarged kinetoplast, and the other complete kDNA loss. TAC102 is utilised for kDNA segregation and not replication, as RNAi showed no apparent effect on organelle morphology, replication or cell organogenesis (Trikin *et al.*, 2016). One of the first characterised TAC components was p166, a 166 kDa acidic protein which localises to the ULFs, between the mitochondrial inner membrane (DM) and the kDNA (Trikin *et al.*, 2016; Hoffmann *et al.*, 2018). p166 possesses a transmembrane region that may be required for its functionality. Like TAC102, p166 is stably associated with the TAC in isolated flagella, and upon RNAi knock-down exhibits a similar phenotype of apparent inhibition of kDNA segregation (Zhao *et al.*, 2008) in an exponential number of cells exhibiting an enlarged kinetoplast or no kinetoplast at all. However, basal body duplication and replication remained unaffected. Another ULF inhabiting protein is α-KDE2 - the E2 subunit of α-ketoglutarate dehydrogenase – with experiments showing it localises to the antipodal

sites of the kDNA disc and also throughout the mitochondria due to its secondary function in the tricarboxylic acid cycle (TCA - Sykes & Hajduk, 2013). In *Saccharomyces cerevisiae* α-KDE2 associates with mtDNA nucleoids and in *T.brucei* was shown to maintain antipodal distribution throughout the cell cycle (Sykes and Hajduk, 2013). Ablation of the protein in bloodstream form *T. brucei* revealed a similar phenotype to AEP-1 ablation, thereby suggesting that as well being involved in the TCA cycle, α-KDE2 is also involved in kDNA segregation.

Protein	Gene ID	Localisation	Features	pI/ mW	Orthologs
TbTBCCD1	Tb927.11.2440	EZF	Tubulin binding co-factor C D1, maintains bi-lobe structure	8.23/ 59 kDa	BS, CF, LM, TC
BBA4	-	EZF	Can be utilised as a pro-basal body probe	N/A	-
p197	Tb927.10.15750	EZF	Ablation causes kDNA missegregation	7.48/ 197 kDa	BS, CF, LM, TC
Mab22	-	EZF	Detects an unknown antigen	N/A	-
TAC65	Tb927.5.830	EZF	Forms a complex pATOM36	10.09/ 65 kDa	BS,CF, LM, TC
pATOM36	Tb927.7.5700	DM	Transiently localises to DM and has dual functionality	10.66/ 35 kDa	BS, CF, LM, TC
TAC40	Tb927.4.1610	DM	VDAC protein like and forms supercomplex with TAC42 and TAC60	7.1/ 40 kDa	BS, CF, LM, TC
TAC42	Tb927.7.3060	DM	Forms complex with TAC40 and TAC60	6.61/ 42 kDa	BS, CF, LM, TC
TAC60	Tb927.7.1400	DM	Forms a complex with TAC42 and TAC40	4.95/ 60 kDa	BS, CF, LM, TC
p166	Tb927.11.3290	DM	Stably associates with isolated flagellar	5.13/ 166 kDa	BS, CF, LM, TC
AEP-1	-	ULF	Ablation causes growth arrest	N/A	-
TAC102	Tb927.7.2390	ULF	Non kDNA interacting	9.42/ 102 kDa	CF, LM, TC
a-KDE2	Tb927.11.11680	ULF	Secondary function in TCA cycle.	8.27/ 41 kDa	BS, CF, LM, TC
TbTrett	*Tb*927.3.2630	Kinetoplast	Antipodal site localisation	7.95/ 85 kDa	BS, CF, LM, TC

Table 1: Major components of the Tripartite Attachment Complex: Sub domains are abbreviated (Exclusion Zone Filaments: EZF, Differentiated membranes: DM and unilateral filaments: ULF) Species: BS, *Bodo saltans*; CF, *Crithidia fasciculata ;* LM, *Leishmania major*; TC, *Trypanosoma*

cruzi. pI/mW: isoelectric point and molecular weight in kDa. Adapted from Schneider and Ochsenreiter, 2018.

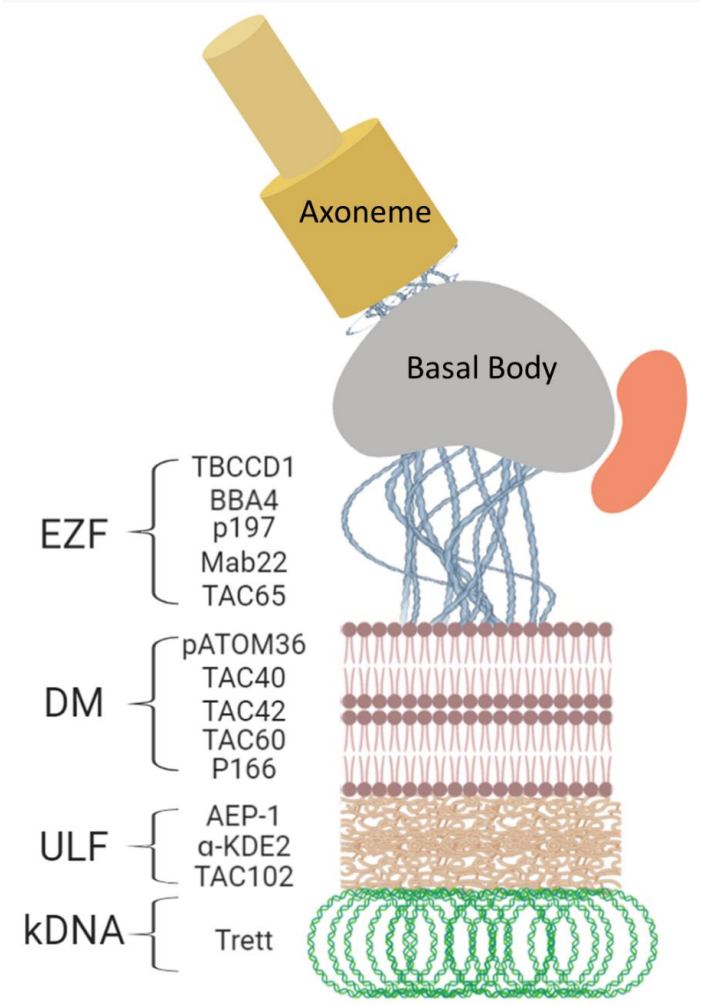

Figure 3: Drawing of Tripartite Attachment Complex: Each known protein localisation is listed. The Exclusion Zone Filaments secure the basal body to the mitochondrial membrane, and the unilateral filaments secure the kinetoplast DNA to the mitochondrion, and in turn the basal body to the cell. Trett is an unpublished protein uniquely described in this thesis.

1.3 Overview of the Kinetoplast

Eukaryotic DNA is packed within a nucleosome comprised of histones and DNA whereas prokaryotes, on the other hand, utilise histone-like proteins (known as bacterial DNA binding proteins) such as H-NS, HU and IHF which bind to DNA without sequence specificity (de Souza *et al.*, 2017; Kamashev *et al.*, 2017). The endosymbiotic origins of the mitochondria have resulted in massive mitochondrial genome loss. DNA condensing by HMG-like and histone H1-like proteins compact mtDNA within trypanosomatids to form the tight kinetoplast structure. This is substantially different from that of eukaryotic chromatin and bacterial nucleoids (Kamashev *et al.*, 2017). Here, mitochondrial DNA is seen to be highly condensed forming a kDNA network at the base of the mitochondria. This characteristic and unique mitochondrial DNA packing has led to much interest about the mechanisms that form this kinetoplast disc. Alanine and lysine rich proteins called Kinetoplast Associated Proteins (KAPs), similar to H1-like proteins found within bacteria, carry out the mtDNA packing with KAP2, KAP3 and KAP4 genes encoding p16, p17 and p18 proteins respectiviely that have been shown to localise throughout the kDNA network (Xu *et al.*, 1996). Despite KAPs appearing to have moonlighting capabilities within the cell, canonical KAPs ensure proper mtDNA packing and segregation, with ablation of *Cf*KAP1, *Tc*KAP4 and *Tc*KAP6 all resulting in kinetoplast disruption and disorganisation (Kamashev *et al.*, 2017). Interestingly knock-outs of KAP3 within *Trypanosoma cruzi* (shown to localise to the kinetoflagellar zone throughout the cell cycle) showed no overall morphological change to the cell or the kinetoplast, possibly resulting from compensation from other kinetoplast-associated proteins (Souza *et al.*, 2010).

The most studied kDNA network is that of *Crithidia fasciculata.* It contains five thousand 0.5 to 10 kb DNA rings, known as minicircles, and approximately twenty-five, 20 to 40 kb rings known as maxicircles (Lukeš *et al.*, 2002). The kDNA network presents itself as a dense structure, organised like medieval chain maille through catenations of circular DNA (Lukeš *et al.*, 2002; Schneider and Ochsenreiter, 2018) (Figure 4). Minicircles are catenated to 3 neighbours with larger maxicircles threaded within the kDNA matrix scaffold. In *Trypanosoma equiperdum*, maxicircles are concatenated within the network and form distinct rosette shaped aggregates (Shapiro, 1993). Maxicircles encode classical mitochondrial gene products such as rRNAs and electron transport chain complexes; for example in *Trypanosoma brucei* two mtrRNAs and ~18 oxidative phosphorylation subunit proteins are encoded (Shapiro, 1993; Schneider and Ochsenreiter, 2018). The kinetoplast structure is as diverse as the organisms it inhabits. Because of this, several distinct kinetoplast structures have been observed: Pan-kDNA, Mega-kDNA, Poly-kDNA, Pro-kDNA, and the classical kDNA network.

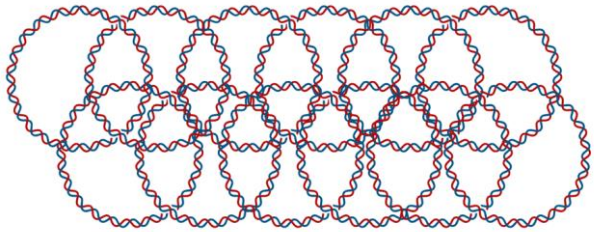

Figure 4 kDNA Catenation: kDNA packing within the kinetoplast network forms distinct aggregates. Mini and maxicircles are intertwined forming a chain maille complex. Each DNA mini and maxicircle are linked to one and other by close covalent bonds.

1.3.1 Pan-kDNA

Kinetoplast DNA harvested from *Cryptobia helicis*, a parasite of fish (also often referred to as *Trypanoplasma sp.*), presents itself as monomeric supercoiled minicircles (Lukeš *et al.*, 1998) with some concatenated oligomers and dimers present. The kDNA is spread throughout the elongated *C. helicis* mitochondria with no distinct loci but typical minicircle motifs (such as the Universal Minicircle Sequence-binding protein – UMSBP) were found. *C. helicis* minicircles also present a bent DNA helix, indicative of poly-A stretches (~10 bp tracts) within the minicirles – this topology is observed within many kinetoplast structures (Lukeš *et al.*, 1998, 2002; Harteis and Schneider, 2014). The bending of the DNA helix may facilitate many roles including kDNA packing within the mitochondria and allow for recognition by DNA-binding proteins (Hajduk, Siqueira and Vickerman, 1986; Lukeš *et al.*, 2002; Harteis and Schneider, 2014). Pan-kDNA has also been postulated in *Bodo caudatus* and *Cryptobia branchialis* (Hajduk, Siqueira and Vickerman, 1986; Lukeš *et al.*, 2002).

1.3.2 Mega-kDNA

Trypanoplasma borreli is an early branching parasite of fish, and an example of a mega-kDNA containing organism (Jackson *et al.*, 2016). Presenting tandemly linked minicircle-like sequences, mega-kDNA is characterised by uniformly spread large circular molecules within the mitochondria. Each of these approximately 200 kb molecules also feature UMS-like sequences and display a lack of minicircles (Lukeš *et al.*, 2002). Unlike Pan-kDNA, mega-kDNA does not exhibit a bent helix.

1.3.3 Poly-kDNA

Distinct from its mega-kDNA counterpart, poly-kDNA is present as scattered condensed foci within the mitochondrial lumen (Lukeš *et al.*, 2002). Like its predecessors, no classical kDNA network is found but covalently closed, relaxed minicircles are (1.2 to 2.0 kb; species dependant). Dimers have been

found within *Cruzella marina* (an intestinal parasite of the Ascidian sea squirts), but information on minicircle dimers is lacking for other parasitic, and free living organisms, as is sequence composition. Maxicircles were found to be present within the kinetoplastid, *Dimastilgella trypaniformis*, but conformation of these maxicircles is unknown (Marande, Lukes and Burger, 2005).

1.3.4 Pro-kDNA

Most pro-kDNA structures have been divulged from electron microscopy of thin layers of organisms such as the heterotrophic microflagellates *Bodo designis*, *Procryptobia sorokina*, *Rhynchomonas nastuta and Bodo saltans*. Bundle-like kDNA organisations resembling a kDNA disc was found at the basal body of the flagellum, thereby providing insights into the evolution of the kDNA network. Pro-kDNA comprises few small-catenations of minicircles (~1.4 kb) which are closed covalently and are relaxed (Blom *et al.*, 1998). DAPI staining of the *B. saltans* kDNA revealed a distinct globular mass of kDNA which was more prominent than the nucleus. *In situ* hybridisation of the bundle by Gažiová & Lukeš, 2003 revealed the pro-kDNA disc is located within the mitochondria anterior at the base of the flagellum. Minicircles were found to contain two gRNAs, DNA bending (similar to that of pan-DNA minicircles) and a highly conserved UMS sequence (~350 bp in length). The mtDNA of *B. saltans* showed more similarity to *Trypanosomes* than its predecessors. Editing of *cox2* and MURFR2 RNAs is found in the same location as on trypanosomatids with slightly different editing. Pro-kDNA Minicircles and Maxicircles form dimer and trimers, which ultimately give rise to the kDNA network seen across all trypanosomes, but the order of genes, editing patterns and size differ. (Blom *et al.*, 1998, 2000; Lukeš *et al.*, 2002; Gažiová and Lukeš, 2003). Pro-kDNA of these heterotrophic microflagellates is strikingly similar to kDNA networks found within the trypanosomes; perhaps unsurprising due to the evolutionary placement of *Bodo saltans.*

1.4 Mini and Maxicircles

Maxicircles comprise the minority of kDNA within the kinetoplast network. Maxicircle sizes usually range from 20 to 40 kb, dependent upon species, and encode mitochondrial gene products (e.g. *cox2*). Two major regions form the maxicircle; the first encodes classical mitochondrial genes observed within a variety of eukaryotes with the second being a divergent, variable and non-coding region. The majority of the maxicircle encoded genes are cryptogenic, where multiple uridine moieties have to be inserted or deleted to allow functional mRNA transcripts (Wong *et al.*, 2015; Käser *et al.*, 2017). Botero et al., (2018), summarised the coding region as containing two rRNA genes (12S and 9S rRNA) and 14 protein coding genes (ND -1, -2, -3, -4, and -5, RSP12, COI and COII). A further four genes of unknown function and several guide RNAs (gRNAs) were also described..

The largest portion of the kDNA network is comprised of minicircles. Minicircles within the network are present as thousands of copies, each of varying length and sequence. In *T. brucei*, minicircles encode the majority of gRNAs (Aphasizhev and Aphasizheva, 2014) and tend to encode highly conserved sequences blocks (CSBs). These CSBs vary in length from 8 to 12 bp and have been extensively studied. For example, CSB-3 (UMSBP), present in all kinetoplastids, is involved in kDNA replication and segregation (Lukeš *et al.*, 2002; Aphasizhev and Aphasizheva, 2014; Botero *et al.*, 2018) and RNAi ablation demonstrated the overall importance of the UMSBP for survival. Ablation of *Tb*UMSBP resulted in inhibited minicircle segregation, interrupted minicircle replication initiation and blocked nuclear division. Further studies demonstrated UMSBP deletion could result in apoptosis and unregulated parasitic virulence within mice (Milman *et al.*, 2007; Botero *et al.*, 2018).

1.5 Kinetoplast DNA Replication

Mini- and Maxicircles are interlocked and secured via the Tripartite Attachment Complex (TAC) which connects the kinetoplast to the basal body of the flagellum and replicates 5' to 3' (Ogbadoyi, Robinson and Gull, 2003; Povelones, 2014). Four distinct stages occur during kDNA replication. First, replication begins at the start nuclear S phase. Second, Ligase κα, Polymerase β-PAK and primase locate to the inner kDNA disc. Topoisomerase II (TopoII), Polymerase β, Ligase κβ and Structure Specific Endonuclease 1 (SSE1) localise to the antipodal sites (Figure 5) and Polymerase 1C, Polymerase 1B and UMSBP locate to the kinetoflagellar zone (Liu *et al.*, 2005; Liu and Englund, 2007). These enzymes surround the kDNA creating a replicative complex. Third, covalently closed Minicircles are released from the kDNA network by Topo II and locate to the unilateral filaments of the TAC; maxicircles remain attached to the kDNA network throughout replication. Here minicircles replicate as theta structures via primase, UMSBP and DNA pol 1B and 1C catalysation. UMSBP initiates replication by binding to the replication origin, and primase synthesises a RNA primer for *de novo* DNA synthesis (Abeliovich, Tzfati and Shlomai, 1993; Liu *et al.*, 2005; Povelones, 2014; Käser *et al.*, 2017). Fourth, SSE1 facilitates primer removal (Liu, Motyka and Englund, 2005); gap filling between Okazaki fragments is completed by DNA pol β before nick sealing by DNA ligase κβ (Robinson and Gull, 1994; Liu *et al.*, 2005; Povelones, 2014). The minicircles are then translocated to the antipodal sites via an unknown mechanism and reattached to the kinetoplast periphery by Topo II (Guilbride and Englund, 1998). In *T. brucei* this produces a Cassinian oval (a dumbbell shape), as kinetoplast replication progresses creating a central concentration of maxicircles between the sister kinetoplasts.

The mechanism of kinetoplast division is strikingly different between *Trypanosoma brucei* and *Crithidia fasciculata* with *T. brucei* possessing a much more inhomogeneous population of minicircles in comparison to other Trypanosomatids. *Crithidia* possesses a larger kDNA network requiring complete rotation of the kinetoplast during division. Networks within *Leishmania donovani* and *Trypanosoma cruzi* present torus morphology when partially replicated (Robinson and Gull, 1994; Liu *et al.*, 2005). Within the more recently evolved Trypanosomatids (*L. tarentole*, *C. fasciculata* and *T. cruzi*), minicircles are distributed uniformly throughout the kinetoplast poles. Rotation of the kinetoplast between the antipodal sites then gives rise to a ring instead of the dumbbell topology observed within *T. brucei* (Liu *et al.*, 2005).

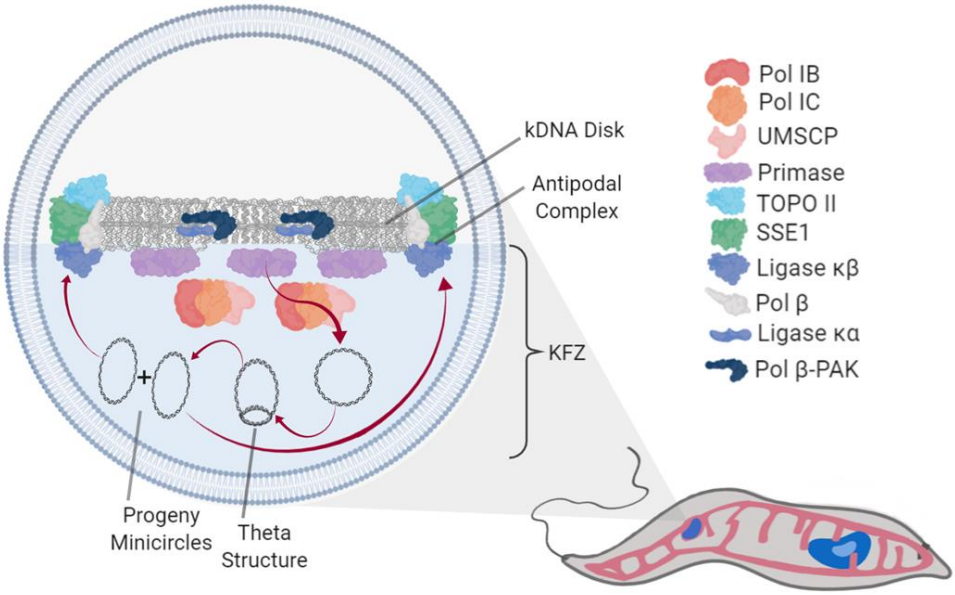

Figure 5 Replication Mechanism of kDNA in *C. fasciculata* : Replication of the mini and maxicircle cassette, the kDNA, is a complex process in which the kinetoplast rotates between the antipodal sites (such as in *C. fasciculata*) or forms a dumbbell shape from release of minicircles and reattachment when replicated at the kinetoplast periphery. The above process is seen across the trypanosomatids.

1.6 History and Phylogeny of *Bodo saltans*

The kinetoplastae Bodonid, *Bodo saltans* is a heterotrophic free-living organism that inhabits a diverse range of aquatic environments and feeds primarily on bacteria via phagocytosis. Bacterial macromolecules are degraded within a phagolysomal system prior to metabolic absorption (Jackson, Quail and Berriman, 2008; Opperdoes *et al.*, 2016). The Bodonids possess classical kinetoplastid morphology, featuring flagella protruding from a flagellar pocket, a glycosome (a dedicated pocket which confines glycolytic activity) and a Pro-kDNA disc at the flagellar base (Blom *et al.*, 1998; Opperdoes *et al.*, 2016) (Figure 6A). Unlike the parasitic Trypanosomatids, *Bodo saltans*, features two flagella, with the nucleus closely positioned to the flagellar pocket. *Leishmania sp, Trypanosoma sp* and *Crithidia sp.* often present nuclei more distal to the flagellar pocket and the kinetoplast, compared to the *Bodonids* (Figures 6B-C). The draft *B. saltans* genome is 39.8 Mbp and covers ~18,943 proteins, substantially larger than that observed with the heteroxenous and dixenous kinetoplastid parasites (Zhou *et al.*, 2010; Jackson *et al.*, 2016). The sub-Saharan trypanosome *Trypanosoma brucei* and obligatory intracellular protozoan *Leishmania*, have many parasitic adaptations within their genetic repertoire, yet the evolutionary pathway leading to parasitism is yet to be fully resolved. Perhaps explaining their curtailed genome size, moonlighting capabilities present in conserved ancient proteins have been shown to aid pathogenicity and the proliferation of the obligatory parasites (Ginger, 2014). Free living *B. saltans* is one of the closest known evolutionary partners of the parasitic trypanosomatids, giving it suitable candidacy to address evolutionary development of pathology and the kinetoplast evolution pathway (Jackson, Quail and Berriman, 2008).

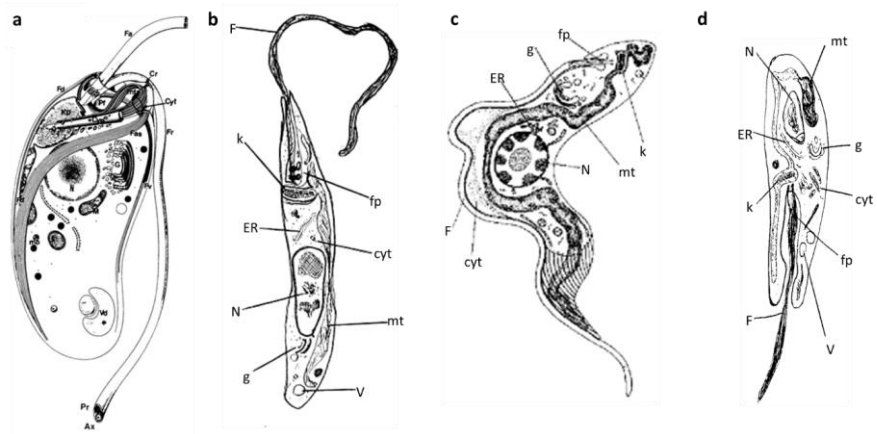

Figure 6 Drawings of Parasitic and Free Living Kinetoplastids: Zoological drawings of the morphology of *Bodo sp.* (A), *Leishmania donovani* promastigote (B), *Trypanosoma brucei* blood stream slender (C) and *Crithidia fasciculata* (D). Cyt: cytosol ER: endoplasmic reticulum, fp: flagellar pocket, F: flagellum, g: golgi apparatus, mt: mitochondria, N: nucleus, V: vesicle. *Bodo* saltans is the free living ancestor of the Trypanosomatids but possesses many of the classical features, including

flagellum and a pro-kinetoplast. Image a: taken from Brugerolle, G., Lom, J., Nohỳnkovà, E., & Joyon, 1979; Image c: taken from Gould, 2009 with author permissions.

1.7 Evolutionary Relations of the Kinetoplastids

Kinetoplastida (Eukaryota, Excavata and Euglonozoa) belong to one of the more well studied groups of eukaryotes due to their medical, agricultural and veterinary significance (Simpson, Lukes and Roger, 2002; Harmer *et al.*, 2018). The ancestral beginnings of the parasitic trypanosomatids are now widely accepted to have arisen from the morphologically diverse and free-living Euglenids (Cavalier-Smith *et al.*, 2014). Previous thought placed the basal branch of the clade with the *Trypanosoma* genus indicating ancestral trypanosomatids arose within vertebrates. However, fossil evidence of an amber-encapsulated tumescent sand fly places the divergence of the parasitized Kinetoplastids at ~150 million years ago (Poinar, 2011) which would place the emergence of dixenous species in the late Cretaceous period (145 million to 66 million years ago), approximately 85 million years ago and in line with the divergence of mammalian orders, thereby challenging the previous placement of the trypanosomatids within vertebrata (Lukeš *et al.*, 2014).

The dixenous Trypanosomatids occupy a minority niche and are responsible for devastating human and animal malady. Diseases include; Human African Trypanosomiasis (Sleeping Sickness) – caused by *Trypanosoma brucei*, Chagas disease – attributed to *Trypanosoma cruzi*, and Leishmaniasis, of which twenty species of *Leishmania* are responsible (Kaufer *et al.*, 2017). The origins of the dixenous progeny have been widely investigated and; concluded that *Leishmania* and *Phytomonus* originated in parasitical insect vectors (Lukeš *et al.*, 2014; Kaufer *et al.*, 2017). Recent classification and phylogenetic studies employed 18S rDNA trees and placed *Diplonema* and Kinetoplastae groups together as a single subphylum (termed Glycomonada due to their shared glycosomes). Within Kinetoplastae, HSP90 trees and 192-gene trees placed *Bodo* as a sister group to the trypanosomatids (Flegontov *et al.*, 2013; Maslov *et al.*, 2013; Lukeš *et al.*, 2014; Cavalier-Smith, 2016; Kaufer *et al.*, 2017) and a maximum-likelihood phylogeny (using the the SSU rRNA gene) resolved the Bodonids to be earliest branching clade in Kinetoplastae (Flegontov *et al.*, 2013). Within the Kinetoplastida group, Trypanosomatids are higher branching than Bodonids and separate into twelve major clades (Figure 7a). Further molecular evidence strongly supports the origins of the obligatory parasitic trypanosomatids to be from the *Bodonidae* clade organism *Bodo saltans* (Maslov *et al.*, 2013; Kaufer *et al.*, 2017). These major clades represent several subfamilies: *Leishmania*, the endosymbiont bearing clade which include *Stringomonas* and *Angomonas* and *Phytomonas* (Maslov *et al.*, 2013; Cavalier-Smith, 2016; Harmer *et al.*, 2018). Additionally concatenated protein alignments from 18 species of the Kinetoplastea further identified *Bodo saltans* as the free-living common ancestor of the trypanosomatids (Cavalier-Smith *et al.*, 2014; Opperdoes *et al.*, 2016). *Paratrypanosoma confusum* was then designated the earliest branching parasitic trypanosomatid

prior to *Trypanosoma sp., Phytomonas sp., Leptomonas sp., Endotrypanum* and finally *Leishmania sp* (Figure 7b).

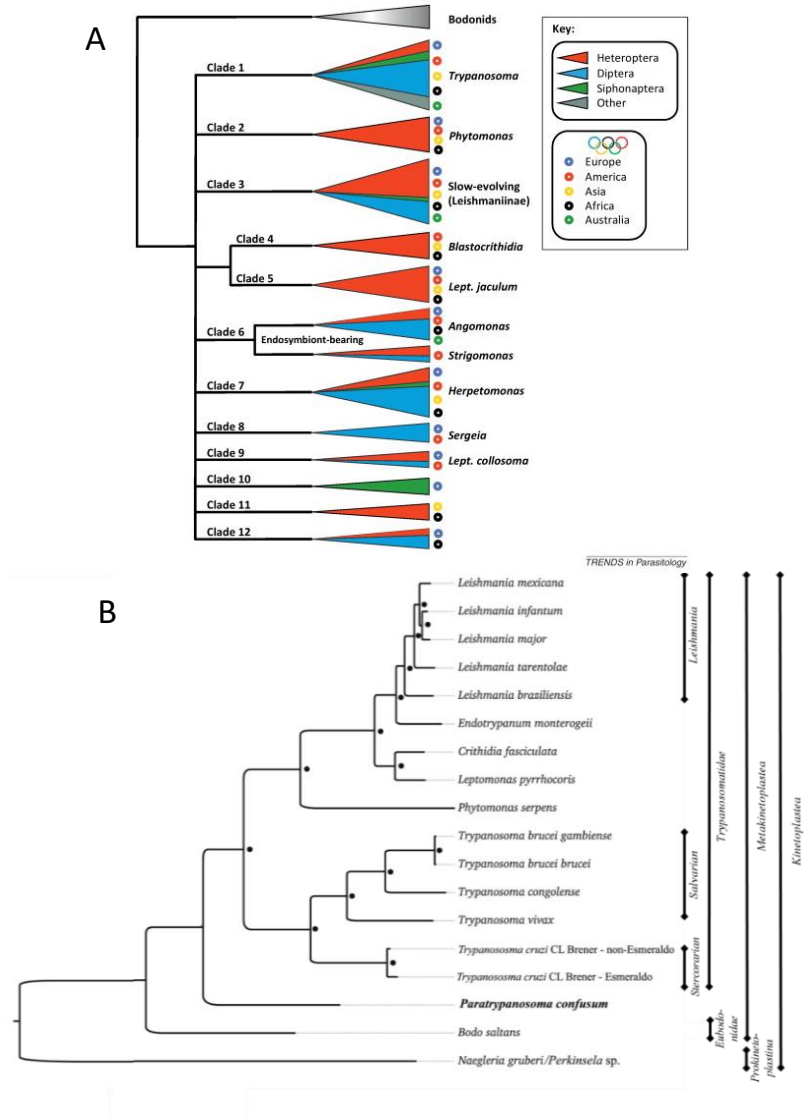

Figure 7 A Major Clades of Trypanosomatidae: Major clades of Trypanosomatidae. Geographical distributions identified (Taken from Maslov *et al.*, 2013). The Trypanosomatids emerges as a sister group *Bodo saltans* whereas *Leishmania* and *Phytomonas* emerge as amongst monoxenous groups. **Figure 7 B Phylogenetic Tree of Kinetoplastids:** Maximum-Likelihood Phylogenetic tree of 18 Kinetoplastids from Flegontov *et al., 2013.* Based on protein concatenation and adapted to show Kinetoplastea taxonomy.

1.8 Comparative Lifecycles of the Parasitic Trypanosomes

The close evolutionary relationships between the Kinetoplastea class have prompted the study of their digenetic and monogenetic lifecycles which are crucial for their pathogenicity and survival. The lifecycles of human infective *Leishmania* and *Trypanosoma* are remarkably similar and comprise of three basic stages; mammalian infection via feeding, multiplication *in vivo* and re-uptake via the vector. *Leishmania* infections present two common forms, cutaneous leishmaniasis and visceral leishmaniasis which can be caused by more than 20 *Leishmania* species (Borghi *et al.*, 2017). Within phlebotomine sand flies, *Leishmania* first present promastigote morphology (Sunter and Gull, 2017), with differentiation within the sand fly midgut forming procyclic promastigotes from amastigotes . Second, procyclic promastigotes become nectomonad promastigotes attaching themselves to the midgut microvilli prior to differentiation to leptomonad promastigotes within the thoracic midgut (Figure 8a). It is here where intraconversion into metacyclic infective promastigotes occurs within the salivary glands before transmission into the mammalian host through the sand fly proboscis (Borghi *et al.*, 2017; Sunter and Gull, 2017). Following a blood meal, sand flies deposit the parasites into the bite wound. During the establishment of a *Leishmania* infection, the mammalian hosts' phagocytes uptake the deposited parasites following an immune response and high motility of *Leishmania* means that the phagocytic uptake of the parasite could occur far from the original bite site (Séguin and Descoteaux, 2016; Sunter and Gull, 2017).

Inside the macrophage, differentiation from promastigote to amastigote occurs after 24 to 48 hours post infection. The overall cascade triggering metamorphosis from promastigote to amastigote are yet to be fully understood but acidation of the peroxisomal vacuole and temperature changes are thought to play a major role (Séguin and Descoteaux, 2016). Flagella restructuring facilitates a reduction in cellular volume, thereby enabling parasite survival within the phagocytic peroxisome, but this is at cost of reduced cellular division from metabolic downregulation (Séguin and Descoteaux, 2016; Sunter and Gull, 2017). Slow multiplication of amastigotes could also prevent overwhelming the hosts immune system, allowing better disease transmission throughout the host organism before reuptake by the sand fly (Borghi *et al.*, 2017).

The genus *Trypanosoma*, the causative agents of Chagas disease and Human African Trypanosomiasis, represents one of the better studied lifecycles within the trypanosomes (Figure 8B). *T. brucei* has four major developmental stages within its lifecycle; epimastigotes, procyclic forms, bloodstream slender trypomastigotes and blood stream stumpy metacyclic trypomastigotes (Rodrigues, Godinho and de Souza, 2014). Both *Trypanosoma brucei rhodesiense* and *Trypanosoma brucei gambiense* are transmitted into the vector hosts via the bite of the *Glossina* spp. Tsetse fly. Upon feeding, the parasites enter the midgut and differentiate into procyclic cells which multiply via binary fission before

continuing into the proventricles (Silvester, McWilliam and Matthews, 2017). Within the salivary gland, procyclic epimastigotes continue to divide until they transform into non-proliferative short metacyclic cells. This development takes approximately 20 – 30 days within the Tsetse fly (Fenn and Matthews, 2007). During a blood meal, short stumpy metacyclic trypomastigotes are injected into a mammalian host coupled with the transformation into blood stream slender trypomastigotes. The blood-stream slender cells continue to proliferate and divide via binary fission (Figure 3b), increasing overall parasitaemia (Fenn and Matthews, 2007; Rodrigues, Godinho and de Souza, 2014; Silvester, McWilliam and Matthews, 2017). At maximum parasitaemia, stumpy induction factor promotes cell cycle arrest to form stumpy cells. Indeed, the change from bloodstream slender to stumpy form has intermediates, but are yet to be fully described (Fenn and Matthews, 2007).

The protist genus *Crithidia*, are flagellate parasites which only infect and inhabit insects. *Crithidia* represents a monogenetic lifecycle, unlike *T. brucei*, and *Leishmania sp* (Figure 7A-C), and are responsible for pollinator decline (though much of this is due to human impact on the global climate (Alcolea *et al.*, 2014)). *Crithidia bombi*, and *C. fasciculata* represent the better studied of the genus (Koch and Schmid-Hempel, 2011) with *Bombus terrestris* (the common bumble bee) and *Cuclicidae* (nectar consuming mosquitoes) the most famed insect hosts of the genus (Koch and Schmid-Hempel, 2011). The lifestyle is more closely related to *Leishmania*, comprising immotile amastigotes which attach to the gut epithelium, differentiating into motile choanomastigotes (Alcolea *et al.*, 2014; Borghi *et al.*, 2017) (Figure 7C). Once differentiated they parasitise the gut and are excreted within the hosts faeces as amastigotes, contaminating freshwater or flowers when the host takes a meal. Transmission in aquatic environments by faecal matter or dead insects leads to infection of larval and pupil instars which are then transmitted into adult insects post metamorphosis (Alcolea *et al.*, 2014). The overall biochemistry of the life cycle, and the processes involved are relatively understudied and therefore little information is currently available on difference of lifecycles within the *Crithidia* genus.

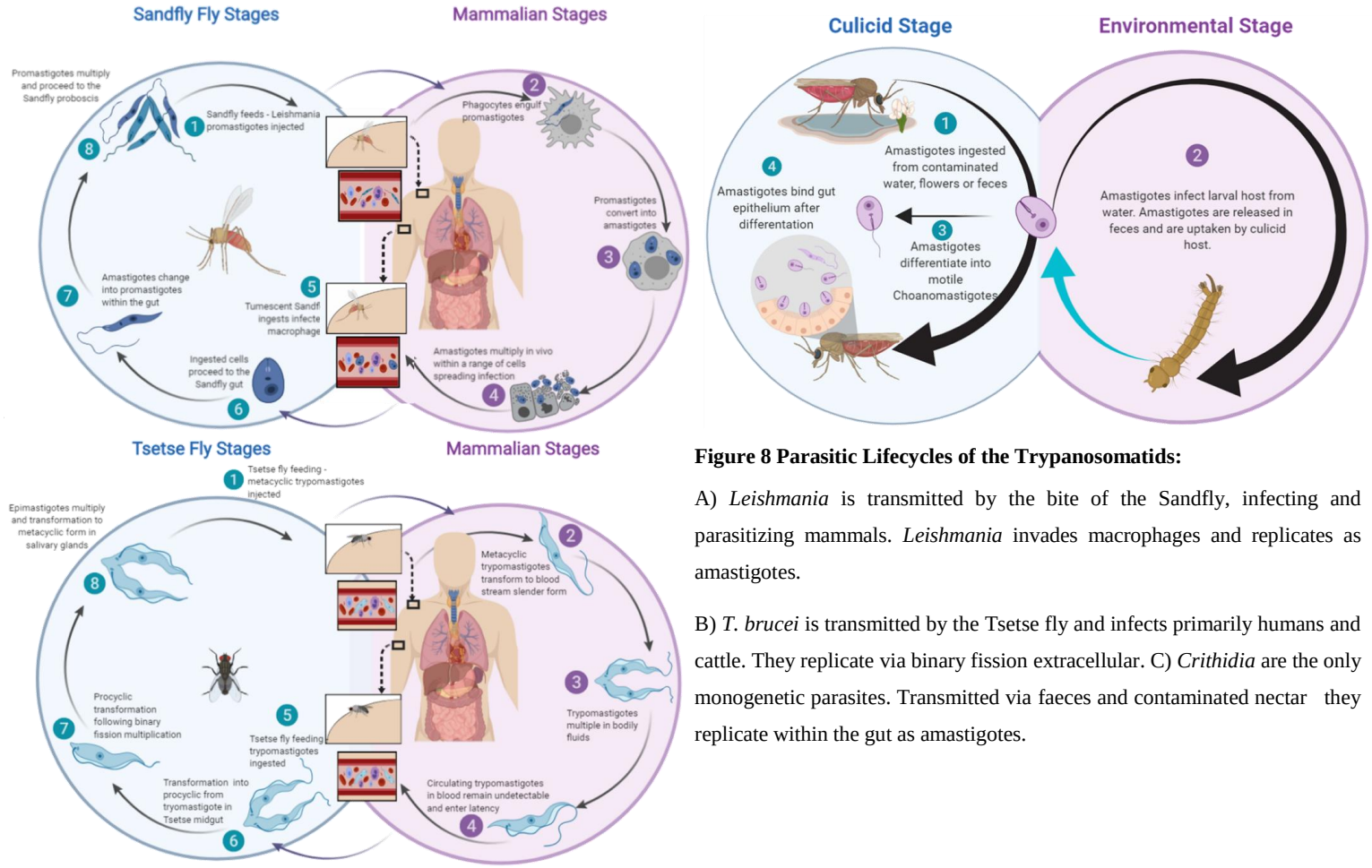

Figure 8 Parasitic Lifecycles of the Trypanosomatids:

A) *Leishmania* is transmitted by the bite of the Sandfly, infecting and parasitizing mammals. *Leishmania* invades macrophages and replicates as amastigotes.

B) *T. brucei* is transmitted by the Tsetse fly and infects primarily humans and cattle. They replicate via binary fission extracellular. C) *Crithidia* are the only monogenetic parasites. Transmitted via faeces and contaminated nectar they replicate within the gut as amastigotes.

1.9 Aims and Objectives

In evolutionary terms, the origin of the kinetoplast remains ambiguous. However, interestingly some components of the TAC are found in the genome of the free-living *Bodo Saltans*. This includes the protein designated *Tb*9260, which previous work by this group has shown to localise to the antipodal sites, important in kinetoplast organisation during cell division of the kinetoplast in *T. brucei*. A fragment of the *Bodo saltans Tb*9260 orthologue, named Trett, will be expressed as recombinant protein in *E.coli* and purified via Ni-NTA in order to raise a *Bs*Trett antibody. Once purified the antibody will utilised for the *in vivo* targeting by confocal and super-resolution microscopy of *Bs*Trett within *Bodo saltans* in order to to ascertain its localisation. Additionally, the localisation of *Bodo saltans* TAC65, TAC60, TAC40 and Trett orthologues will be cloned into a pNUS-GFPcH (inclusive of a GFP protein) vector and transfected into *Crithidia fasciculata*. Ascertaining the localisations of these proteins could potentially give us an insight into their functionally, both through their localisation *per se* but also through any adverse phenotypic effects evident from their expression. In addition, a cross species bioinformatic analysis of the *Bodo saltans* transcriptome against peptide sequences of putative proteins identified within the *Tb*MitoCarta (Zhang *et al.*, 2010) will aim to identify possible conserved orthologues and future protein targets. *Bodo saltans* is a divergent free-living ancestor of the parasitic trypanosomatids, including species of trypanosomes and *Leishmania*. Similarities between the lifecycles of *Leishmania* sp. and *T. brucei* sp. have demonstrated the importance of understanding the evolutionary process which has led to parasitism and the question of whether it evolved from, or separately from its free-living ancestor remains unanswered.

2.0 Materials and Methods

2.1 General laboratory equipment and reagents

2.1.1 Microscopes

Zeiss Stemi 305 Compact Greenough Stereo Microscope

Zeiss Axio Inverted Wide Field Microscope

Zeiss LSM 880 with Airyscan Confocal laser scanning microscope.

Nikon Diaphot 300 Inverted Phase Contrast Microscope

2.1.2 Growth Medias

Media Type	Component	Amount	Notes
Lysogeny Broth (LB)[a]	Tryptone	10 g	Deionised water is used to bring total volume to 1L. pH to 7.0 with NaOH and autoclave. Relevant antibiotic can be added at 55°C[b]
	NaCl	10 g	
	Yeast Extract	5 g	
Warren's Media	Brain Heart Infusion	9.25 g	For hemin; 600 mg hemin in 250 mL ddH_2O with 0.5 M NaOH. Filter sterilise media when made and seal in laminar flow hood.
	Hemin	0.75 mL	

[a] 20g of agar can be added to 1 L LB prior to autoclaving for production of growth plates
[b] This is to prevent degradation of the antibiotic, working concentrations of antibiotics are below

Table 2 Growth Media Utilised for Microbial Work: Growth media for microbiological work with *E. coli and C. fasciculata.* LB and Warren media were sterilised via autoclave or 20 nm filter respectively.

2.1.3 Transfection Buffers

Cytomix is utilised for the transfection of protist cell cultures.

Media Type	**Component**	**Concentration**	**Amount**
Cytomix Transfection	KCl	120 mM	2.2 g
Buffer 250 mL[3]	HEPES pH7.6	25 mM	1.48 g
	K_2HPO_4/KH_2PO_4 pH7.6[1]	10 mM	25 mL
	$MgCl_2.6H_2O$	5 mM	254.1 mg
	EGTA pH7.6	2 mM	380.3 mg
	$CaCl_2$	150 µM	4.1 mg
	Glucose	0.5% (w/v)	1.25 g
	BSA	100 µg/ mL	25 mg
	Hypoxanthine[2]	1 mM	2.5 mL

[1]Of a 10X K_2HPO_4/KH_2PO_4 pH7.6 stock (8.66 mL, 1M, K_2HPO_4; 1.34 mL, 1 M, KH_2PO_4 in 90 mL water (store at room temperature)
[2]Of a 100X Hypoxanthine solution: 0.6 NaOH, 100 mL H_2O, 1.36g Hypoxanthine. Store at -20°C
[3]Filter sterilised the Cytomix when raised to 250 mL and replace cap in laminar flow hood.

Table 3 Cytomix Transfection Buffer Components: Transfection buffers for *Crithidia,* a Biorad pre-programme (1700 V, 2 seconds electroporation) for transfections of *E. coli* was utilised throughout this work.

2.1.4 Antibodies

Antibody	Host	Immunogen	Concentration	Clonality
6X-His Tag	Mouse	6X His synthetic peptide	1 mg/ mL	Monoclonal
Anti-Mouse HRP conjugate	Rabbit	Mouse IgG light chains	1 mg/ mL	Polyclonal
Anti-c-Myc	Mouse	C-terminus synthetic myc tag	0.5 mg/ mL	Monoclonal
Anti-Mouse IgG Secondary, TRITC	Goat	Mouse γ IgG heavy and light chains	2 mg/ mL	Polyclonal
Anti-Tubulin [YL1/2]	Rat	Full length native tubulin	100 µg/ mL	Monoclonal
Anti-Rat IgG Secondary, TRITC	Goat	Rat γ IgG heavy and light chains	2 mg/ mL	Polyclonal
Anti-*Bs*Trett	Rabbit	*Bodo saltans* Trett C-terminus	N/A	Polyclonal
Anti-Rabbit IgG Secondary, Rhodamine	Goat	Rabbit IgG heavy and light chains	2 mg/ mL	Polyclonal

Table 4 Anti-bodies Used Within This Work: Dilutions of each will be described throughout.

2.2 Microbiology

2.2.1 Bacterial Strains

Bacterial strains utilised in this work are tabulated below:

***Escherichia coli* Strains used in this work**		
Strain	**Strain Genotype**	**Source**
XL1 Blue	*recA1 endA1 gyrA96 thi-1 hsdR17 supE44 relA1 lac [F´ proAB lacIq ZΔM15 Tn10 (Tetr)]*	Agilent Technologies, Inc
BL21 (DE3)	B F– *dcm ompT hsdS(rB – mB –) gal λ(DE3) [pLysS Camr]*	Agilent Technologies, Inc

Table 5 Bacterial Strains Used and Respective Genotype: Cloning was carried out within XL1 blue strains, recombinant protein expressions were carried out within BL21 (DE3) cells.

2.2.2 Plasmids use in this study

Plasmid	Antibiotic Selection	Phenotype	Source
pGEM®-T easy	100.00 µg/ mL ampicillin	amp^R	Promega UK
pET-28a (+)	50.00 µg/ mL kanamycin	kan^R	Novagen
pNUS-GFPcH with modified myc tag	100.00 µg/ mL ampicillin and 10.00 µg/ mL	amp^R hph^R	(Tetaud *et al.*, 2002)

Table 6 Antibiotic Working Concentrations By Plasmid: Plasmids for cloning, recombinant protein expression and for protein expression within *C. fasciculata*. pNUS-GFPcH encodes intergenic regions specific for *C. fasciculata* and was used for fluorescent studies

Features of plasmids used in this study

Plasmid Type	Use of Vector	Features	Promoter	Plasmid Map
pGEM®-T easy	Rapid ligation, PCR cloning	Contains a 3' terminal thymidine at both ends	T7	N/A
pET-28a (+)	Expression vector	Bacterial expression vector featuring a T7 *lac* promoter, a C- and N-term His_6 tag encoding	T7	Sup 5
pNUS-GFPcH	Expression vector	*Crithidia* expression modified to include a C- and N-term myc tag and a GFP tag.		Sup 4

Table 7 Plasmids Utilised for Cloning and Protein Expression: Plasmids for cloning, recombinant protein expression and for protein expression within *C. fasciculata*. pNUS-GFPcH encodes intergenic regions specific for *C. fasciculata* and was used for fluorescent studies. pGEM®-T easy was used for cloning of inserts and pET-28a (+) for recombinant protein expression. Maps are in section 8.0.

2.2.3 Kinetoplastid Strains

Kinetoplastid strains used within this work

Organism	Media	Source
Bodo saltans	8 mL Chalkley's media supplemented with 40 µL *Mesorhizobium sp.* and 2 mL original culture	Lancaster University
Crithidia fasciculata	Warren's media supplemented with hemin.	(Galvez Rojas *et al.*, 2008)

Table 8 Kinetoplastids Used and Their Growth Media: *Crithidia fasciculata* cultures were utilised for localisation studies post transfection with a GFP::myc encoding plasmid (pNUS-GFPcH).

Mesorhizobium sp. was streaked onto a LB plate and grown at 25°C for 48 hours. A colony was picked and grown in 10 mL LB with vigorous shaking at 25°C and 40 µL utilised to feed *B. saltans* culture in 10 mL Chalkley's solution. *C. fasciculata* cultures were maintained at a cell density of $5x10^6$ cells/ mL^{-1} in aseptic Warren's media at 26°C. Healthy log phase cultures were used for making whole cell mounts for imaging, and whole cell equivalents for SDS-PAGE analysis.

2.2.4 Antibiotics

Ampicillin is a broad spectrum antibiotic derived from penicillin. Ampicillin was made up to a 100 µg/ mL for high copy plasmids, or 50.00 µg/ mL for low copy number plasmids. Kanamycin A is an aminoglycoside which irreversibly inhibits 30S-subunit proteins of 16S rRNA. The working concentration used in this project was 50.00 µg/ mL. Hygromycin B is an aminoglycoside antibiotic from *Streptomyces hygroscopicus* which is used with both eukaryotic and prokaryotic cells by targeting translocation of the 70S ribosomal subunit resulting in mRNA misreading (Ro, Scheffter and Patterson, 1997), the working concentration was 100 µg/ mL for *C. fasciculata*.

2.3 Cross Species Bioinformatic Analysis of *Tb*MitoCarta

Putative and hypothetical proteins from the *Trypanosoma brucei* mitochondria compiled within the *Tb*MitoCarta were accessed via the acquisition numbers through www.tritryp.org. tBLASTn of these sequences against the *Bodo saltans* transcriptome were conducted and results filtered to E-04. *B. saltans* orthologues of *T. brucei* were then confirmed via reciprocal Basic Local Alignment Search Tool (BLAST). Additionally, BLASTp (www.tritryp.org) and tBLASTn (www.ncbi.nlm.nih.gov/) analysis of the *T.b.brucei* (TREU927 strain) acquisitions were performed against *Crithidia fasciculata*, *Trypanoplasma borreli*, *Perkinsela sp.*, *Leishmania major friedlin* and *Trypanosoma brucei. T. brucei brucei* was utilised to confirm the quality of sequence, *L.m.friedlin* was utilised as it represents the highest quality sequence and the other organisms were present to gain insight into the conservation of the proteins analysed.

Following analysis by BLAST, *B. saltans* orthologues were analysed for any domains, repeats, motif or protein feature via Interpro analysis to gain insight into possible features of the protein orthologues. Results were filtered by reciprocal BLASTp E-values to gain insight into orthology or homology for the acquisitions. Orthologues were defined as ≤E-11, homologous as ≥E-10 to ≤E-4 or poor at ≥E-4.

2.4 Recombinant DNA Methodologies

2.4.1 Preparation of plasmid DNA

All recombinant plasmids were prepared from transformant *E. coli* grown overnight at 37ºC with 180 rpm shaking in 3 mL LB supplemented with 100. 00 µg/ mL ampicillin. Plasmid DNA was extracted using the GeneJET Plasmid Miniprep kit (ThermoFischer, U.K) following the manufacturer's protocols.

2.4.2 Primer Sequences

Primer	Fragment	Sequence
BsForward	N-terminal	5′-AAT GGA TCC ATG AAT CGC TCA CGC GCT CTG C -3′
BsReverse	N-terminal	5′-AAT CTC GAG CTC TGT GCG ACA ACG GCT CAC -3′
BsForward1	Middle	5′-AAT GGA TCC ATG GTG GAT CTC ATC CGA TTG CAG-3′
BsReverse 1	Middle	5′-AAT CTC GAG GTG GAC GAG CGG GAG AAA CGT TGG-3′
BsForward 2	C-terminal	5′-AAT GGA TCC CTG GTC TTA AAG GTC CTT GAG-3′
BsReverse 2	C-terminal	5′-AAT CTC GAG GTT TCG GGG AGG TGG TGT CTC-3′
NdeI Forward	Full Length	5′-AAT CAT ATG ATG AAT CGC TCA CGC GCT CTG C -3′
KnpI Reverse	Full Length	5′-AAT GGT ACC CTC TGT GCG ACA ACG GCT CAC -3′

Table 9 Primer Sequences for Trett Amplification: All primers encoded site specific mutations for restriction endonuclease sites for downstream cloning and protein expression work.

2.4.3 Polymerase Chain Reaction

PCR allows for the amplification of DNA from a genomic template. Synthetic pre-designed oligonucleotides (primers) bind to a complementary nucleotides flanking the gene of interest on denatured DNA. DNA polymerase synthesises the region between these primers during an extension phase. This reaction repeats to generate a full double strand gene compliment. PCR was utilised within this set of work to amplify the BS69260 gene from *Bodo saltans* gDNA. BS69260 will be referred to as Trett throughout this work in honour of A.Trett who previously worked on the gene.

PCRs were optimised through the addition of a primer annealing step (*T*m*)* which was adjusted dependant on the gene fragment amplified. Addition of 0.2 µL of $MgCl_2$ can be used increase the amount of PCR by increasing Taq polymerase efficiency, however, this comes at the loss of polymerase specificity. PCR was used within this study for amplification of the *Bs*Trett gene fragments. The reaction mixture is tabulated below.

Components	Volume (µL)
Nuclease Free Water	11.2
5x HF Phusion® Buffer[a]	4.0
10 mMol dNTPs	0.4
FOR 10µMol primer	1.0
Rev 10µMol Primer	1.0
gDNA Template	2.0
Phusion® HF DNA Polymerase[b]	0.2
$MgCl_2$ 50 mM	0.2

[a]Phusion Buffer contains 1.5 mM $MgCl_2$ in the final reaction.
[b]Phusion polymerase storage buffer contains 20 mM Tris-HCl (pH 7.4 at 25ºC), 0.1 mM EDTA, 1 mM DTT, 100 mM KCl, 200 µg/ mL BSA in 50% glycerol.

Table 10 Standard PCR Reagents and Volumes: Individual PCR reactions were optimised throughout this work. Details are specified where necessary.

The primer annealing *T*m was set to 50ºC and adjusted to 48ºC for greater amplification. The PCR protocol is tabulated below:

Step	Temperature (ºC)	Time (Seconds)
Initial Denaturation	95	180
Denaturation	95	30
Primer Annealing	50	30
Extension (20x Cycles)	72	180
Final Extension	72	300
Hold	8	-

Table 11 PCR Conditions and Run Times: Polymerase chain reaction temperatures and run time per cycle. Annealing temperatures were adjusted for each fragment of *Bs*Trett being targeted

Following the PCRs a GeneJet PCR purification kit (ThermoFisher, U.K) was utilised and DNA eluted to 20 µL following the manufacturer's instructions. Phusion® high fidelity DNA polymerase generates blunt ended products. For cloning a TA overhang was generated using *Taq* DNA polymerase, a 1:1 DNA to Dream*Taq* Green PCR master mix was used. Samples were incubated at 78ºC for 30 minutes in a thermocycler and then cleaned as before. All DNA samples were stored at -20ºC.

2.4.4 Ligation of pGEM®-T Easy with insert DNA

Plasmid vector/insert ligations were conducted as tabulated below. All ligations were left on the bench overnight.

Components	Volume (µL)
Cleaned PCR Product	3
pGEM®-T easy (50ng/ µL)	1
2X Rapid Ligation Buffer[a]	5
T4 DNA Ligase	1

[a]Rapid ligation buffer and T4 DNA Ligase contain: 60 mM Tris-HCl (pH 7.8), 20 mM $MgCl_2$, 20 mM DTT, 2 mM ATP, 10% polyethelene glycol (ACS Grade)

Table 12 Volumes of Ligation Components: Ligations were incubated at 20°C for 6 h prior to bacterial transformations

2.4.5 Restriction Endonuclease Digestions

DNA for expression vectors were prepared through double digestion of pGEM®-T easy vectors and excision of insert DNA from agarose following the GeneJet PCR purification kit (ThermoFisher, U.K) protocol. pET-28a (+) was prepared through restriction endonuclease digestion (buffers and enzymes supplied by New England Biolabs™). All double digestions were incubated at 37ºC overnight. Components and conditions are below.

Components*	Volume (µL)	Incubation Time	Analysis
DNA [a]	2 OR 20	Overnight in a 37ºC incubator	0.7% Agarose TAE horizontal gel electrophoresis
10x NEB 3.1 buffer [b]	1 OR 3		
BamHI restriction endonuclease [c]	0.5 OR 2		
XhoI restriction endonuclease [c]	0.5 OR 2		
Nuclease Free Water	6 OR 3		

[a] DNA stored in 10 mM Tris-HCl, pH 8.5, from GeneJet Kits
[b] NEB 3.1 buffer components: 100 mM NaCl, 50 mM Tris-HCl, 10 mM $MgCl_2$, 100 µg/ mL BSA pH 7.9 at 25ºC
[c] Restriction endonuclease storage buffer: 10 mM Tris-HCl, 1 mM DTT, 50 mM KCl, 0.1 mM EDTA, 200 µg/ mL BSA, 50% glycerol, pH 7.4 at 25ºC
*For use in a pNUS expression vector restriction *knpI* and *ndeI* were used in the same quantities with NEB2.1 buffer.

Table 13 Restriction Endonuclease Digestion Reagents: Restriction endonuclease digestion components and enzymes were adjusted dependant on the plasmid being used. Digestions for bacteriological work utilised *BamHI and XhoI* restriction endonuclease, whereas digestions for *C. fasciculata* DNA utilised *knpI* and *ndeI*

2.4.6 Horizontal Agarose Gel Electrophoresis

Agarose gel electrophoresis was used to analyse, separate and purify DNA fragments. 0.7% agarose TAE gels supplemented with SYBR™ Safe DNA Gel Stain were used to visualise DNA fragments under ultra-violet light. 1 kb DNA ladder (NEB, UK) was used to determine fragment size. DNA was extracted from agarose using a GeneJet PCR purification kit (ThermoFisher, UK) with adaptations made for agarose following the manufacturer's protocol.

2.4.7 Quantification of DNA

DNA quantity was determined using a NanoDrop™ 2000c Spectrophotometer (ThermoFischer, UK). 1 µL of elution buffer was used as a blank and nucleic acid concentration was determined using in house software provided with the equipment. 1 µL of recombinant DNA was utilised for DNA quantification.

2.4.8 Ligation of pET-28a (+) and pNUS-GFPcH

Following exhaustive unsuccessful PCR amplification attempts, synthetic constructs *Bs*Trett C-terminal fragment (*Bs*Trett$^{\Delta 1324\text{-}2092}$) and full length were synthesised. DNA was excised from the backbone and quantified via nanodrop prior to ligation into pNUS-GFPcH and pET-28a vectors; insertion of inserts was confirmed via sanger sequencing. Components are listed below:

Components	Volume (µL)
DNA insert	Determined by nanodrop
pNUS-GFPcH(50 ng/ µL)	Determined by nanodrop
10 X T4 DNA Ligase Buffer[a]	1
T4 DNA Ligase	1
ddH_2O	Made up to 10 µL

[a]T4 DNA ligase buffer and T4 DNA Ligase contain: 60 mM Tris-HCl (pH 7.8), 20 mM $MgCl_2$, 20 mM DTT, 2 mM ATP, 10% polyethelene glycol (ACS Grade)

Table 14 Ligation Components for Protein Expression: Ligations were incubated at 20℃ for 6 h prior to bacterial transformations

2.5 Recombinant Protein Expression

2.5.1 Transformation of Bacteria with DNA

Transformations into *Escherichia coli* were utilised for plasmid cloning and protein expression. Cell lines used are tabulated above. All transformations were carried out over ice to prevent damage to cells. Cell lines were stored at -80℃. Growth media was purchased from Fischer Bioreagents™ and autoclaved to sterilise.

XL1-Blue and BL21 (DE3) competent cells were purchased from Aligent. Competent cells (30 µL) were defrosted on ice. 3 µL of recombinant DNA was introduced and incubated on ice for 30 minutes. Cells were heat shocked at 42℃ for 45 seconds and transferred onto ice. For plasmids encoding kanamycin resistance, 900 µL LB was added, and cells incubated at 37℃ with 180 rpm shaking for one hour. Cells were centrifuged (6,000 rpm, 2 minutes) and 900 µL supernatant removed, cells were resuspended in the remaining media. Cells were spread onto LB-plate supplemented with the appropriate antibiotic and grown overnight at 37℃.

2.5.2 Small Scale Protein Expression

Cells expressing pET-28a (+) vector phenotype were picked and grown in 3 mL LB supplemented with kanamycin and grown overnight at 37℃ with 180 rpm shaking. 100 µL overnight culture was used to inoculate 3 mL LB media with antibiotic. Protein expression was induced with 1 mM Isopropyl β-D-1-thiogalactopyranoside (IPTG; ThermoFisher™, UK.) Cultivation continued for 4 hours post induction at 37℃ with 180 rpm shaking.

2.5.3 SDS-PAGE Analysis

A 10% SDS-PAGE Tris/Bis gel was made by combining the below reagents. The resolving gel was prepared and set prior stacking gel addition. 100 µL 1X SDS loading buffer (500 µL 1X PBS, 100 µL DTT, 400 µL 2X SDS Loading buffer [100 mM Tris-HCl, 0.2% Bromophenol blue, 20% glycerol]) was added to each pelleted overnight sample (6,000 rpm, 2 mins). Samples were boiled for 5 minutes, 8 µL was loaded onto the gel – 8 µL of 10-250 kDa PageRuler™ Prestained Protein Ladder (Bio-Rad, UK) was used. The gel was run at 200 V for 45 minutes and stained with InstantBlue™ Ultrafast Protein Stain (SigmaAldrich/Merck, UK).

	10 mL Resolving Gel	
Component	**mL**	**µL**
H2O	4.0	4000
30% Acrylamide	3.3	3300
1.5 M Tris (pH8.8)	2.5	2500
10% SDS	0.1	100
10% APS	0.004	4
TEMED		
	4 mL Stacking Gel	
Component	**mL**	**µL**
H2O	2.1	2100
30% Acrylamide	0.5	500
1.5M Tris (pH6.8)	0.33	330
10% SDS	0.03	30
10% APS	0.003	3
TEMED		

Table 15 Components for SDS-PAGE Gels: SDS-PAGE analysis was used for protein production analysis and purification of recombinant protein via NiNTA. Gels were stained with InstantBlue™ Ultrafast Protein Stain or Coomasie Brilliant Blue protein dye.

2.5.4 Western Blot

After SDS-PAGE protein samples were transferred by electropheric transfer (Towbin, Staehelin and Gordon, 1979) on ice. PVDF membrane was cut and rehydrated for 10 seconds in 100% methanol and followed by a 10 second wash in ultrapure water. Membrane, chromatography paper and foam pads were equilibrated in transfer buffer (25 mM Tris, 192 mM Glycine, 20% methanol (v/v) and 0.18% SDS) before electrophoretic transfer (100V, 60 mins). Following transfer, the membrane was blocked in blocking buffer [5% (w/v) non-fat dry milk (Marvel, Premier Foods, Thame, UK) 0.05% (v/v) Tween 20 in PBS] for one hour on an orbital shaker. The membrane was then incubated with a primary anti His IgG in blocking buffer for 1 hour followed for two subsequent 10-minute washes in PBS-Tween 20 (0.05% v/v). After the final wash the membrane was incubated in a secondary anti mouse IgG with a horseradish peroxidase conjugate. The membrane was washed twice in PBS-Tween 20 followed by incubation with 1 mL HRP substrate peroxide solution (Millipore, USA) for five minutes prior to X-ray film exposure and development.

2.5.5 Large Scale Protein Induction and NiNTA Purification

pET-28a(+)-*Bs*Trett BL21(DE3) transformant cells from a glycerol stock were streaked onto a LB-kanamycin plate and incubated (30°C, overnight). A colony was picked and grown in 50 mL LB-kanamycin overnight. 2% (v/v) culture was used to inoculate 1200 mL LB. Culture was grown with vigorous shaking until OD_{600} reached 0.5-0.6. Prior to induction 1 mL T=0 sample was taken. Protein

induction initialised by addition of 1.2 mL 1mM IPTG and grown for 5 hours at 37°C with shaking. Culture was harvested via centrifugation (8,000*g*, 4°C) for 30 minutes. Supernatants were discarded and pellets resuspended in 20 mL insoluble lysis buffer (6 M Guanidine, 20 mM Tris-HCl (pH 8.0), 500 mM 0.02% Triton-X, 20 mM Imidazole, 10% Glycerol) and incubated for 30 minutes. After resuspension, 200 µL phenylmethylsulfonyl fluoride (PMSF) was added and cells lysed by application of a Sonics, Vibra-cell TM VCX130 Ultrasonic Liquid Processor (5 seconds active, 10 seconds cooling, 10 minutes total). Lysates were centrifuged (35,000 rpm, 1 h, 4°C). Supernatants were retained for purification.

500 µL Amintra NiNTA His· Affinity Agarose (Expedeon, UK) suspension was placed onto glass wool compacted in a syringe. The resin was settled through gravity and equilibrated with 2.5 mL insoluble lysis buffer and incubated on an end-over-end shaker for 30 minutes and supernatants removed. 20 mL lysate was added and the tube and incubated (16 h, 4°C, 15 rpm). Flow through was collected. The column was washed with 5 mL wash buffer (20 mM Tris-HCl (pH 8.0), 300 mM NaCl, 0.02% Triton-X, 20 mM Imidazole, 10% Glycerol). This was repeated three times ensuring each elution was collected. 0.5 mL elution buffer (20 mM Tris-HCl (pH 8.0), 300 mM NaCl, 0.02% Triton-X, 500 mM Imidazole, 10% Glycerol) was added and the column incubated on a shaking end-over-end table for 15 minutes. This was repeated five times. Fractions were analysed using 10% SDS-PAGE.

2.5.6 Purification of *Bs*Trett Antibodies

Following purchase of *Bs*Trett Rabbit anti-sera, 200 mL of LB supplemented with kanamycin was inoculated with 5 mL *Bs*Trett$^{\Delta 1324\text{-}2092}$ *E.coli* culture and protein production induced with 1mM IPTG. After 3 hours of growth post induction the protein was purified following methods described in section 2.5.5 and 6 mL of protein eluted. A column was prepared with 2 mL AminoLink® Plus Coupling Resin (Thermo Scientific, UK) was placed onto glass wool compressed in a 20 mL syringe and drained. The column was then washed with 5 mL coupling buffer (in 100 mL 2.941 g of 0.1 M $Na_3C_6H_5O_7$ and 105.99 g 0.05 M Na_2CO_3 (pH 7.2)). The column was sealed and primed with 6 mL *Bs*Trett$^{\Delta 1324\text{-}2092}$ protein diluted in 6 mL coupling buffer and incubated for 4 h. at RT. The column was cleared and washed with 5 mL coupling buffer. 2 mL coupling buffer was added to the column to resuspend the resin and 40 µL sodium cyanoborohydride (in 1M NaOH; Sigma Aldrich, UK) added and incubated for 4 h. The column was cleared and 4 mL 1 M Tris·Cl (pH 7.4) with 40 µL cyanoborohydride (1 M NaOH) added before a 30 minute incubation. The column was drained and washed in 20 mL 1 M NaCl twice followed by five washes in 1X PBS before resuspension in 4 mL NaN_3 in PBS.

The column was then equilibrated with three 5 mL washes with elution buffer (200 mM glycine, pH 2.3) and neutralised with 200 mL PBS. 8 mL anti-sera supplemented with 800 µL 10X PBS prior to

addition to the column and incubated overnight at 4℃ on a rotorwheel. Elutions were collected and the column washed in 80 mL 1X PBS. 20 mL 500 mM NaCl in 1X PBS was added and eluted before a final wash with 20 mL 1X PBS. The collected anti-sera was then reapplied to the column and incubated overnight at 4℃ on a rotorwheel. The following day the washing procedure was repeated. To elute the purified antibodies, 9 mL 200 mM glycine (pH 2.3) was added to the column and 1 mL fractions collected and 100 µL Tris·Cl (pH 8.8) added.

2.6 Cell Culture and Fluorescence Microscopy

2.6.1 Transfection of *Crithidia fasciculata*

Plasmid DNAs were precipitated (10% v/DNA 3 M NaOAc, 2.5X EtOH v/DNA) and resuspended in 50 µL sterile 10mM Tris-HCl (pH 8.5). Wild type *Crithidia fasciculata* was harvested via centrifugation (18000 rpm, 10 min, 4℃) and resuspended in Cytomix buffer. 25 µL plasmid (75 ng/µL) was utilised for transfecting $3x10^7$ log phase cells per electroporation. BioRad Gene Pulser apparatus was utilised for two, 5 second pulses at 1700 V. Transfected cells were placed on ice for 5 minutes then placed in 10 mL fresh Warren's media for a 4-hour recovery, 26℃. *C. fasciculata* cultures were passed to $5x10^5$ cells/ mL^{-1} and supplemented with hygromycin B (Sigma-Aldrich, UK). Cultures were left to grow to healthy log-phase before subsequent passages.

2.6.2 Fluorescence Microscopy

C. fasciculata cells were centrifuged (8,000 rpm, 3 mins, 4℃) and pellets washed three times with 1X PBS prior to resuspension in 50 µL 1X PBS (Melford, UK). Cells were settled onto Superfrost™ adhesion slides (ThermoFisher, UK) for 30 minutes and fixed directly with 4% paraformaldehyde in PBS. Following a 15 minute incubation, slides were dehydrated in -20℃ methanol. Cells were rehydrated in 1X PBS and dyed with 4',6-diamidino-2-phenylindole (DAPI) mounting medium (VECTASHIELD®, UK). A coverslip was applied and sealed prior to visualisation.

2.6.3 Immunofluorescence Slide Preparation

Whole cell mount slides were prepared as before and then rehydrated for 10 minutes in 1X PBS. Following rehydration, cell mounts were permeabilised with 0.5% Triton X-100 in 1X PBS for five minutes, followed by two, five minute washes in 1X PBS. Fixed cells were then blocked (1% BSA (w/v), 0.05% Tween 20 (v/v), 1X PBS) and incubated in a wet chamber for 1 hour. Primary mouse myc IgG in block solution was added to cells and incubated for 1 hour. Three subsequent washes in PBS-Tween 20 (5 mins each) followed by addition of tetramethylrhodamine-5-isothiocyanate (TRITC)-conjugated anti-mouse IgG in blocking solution and incubation for 1 hour. Prior to mounting with DAPI mounting medium, slides were washed three times in PBS-Tween 20. For basal body localisations,

YL1/2 anti-tubulin rat monoclonal antibodies were utilised as primary and a secondary anti-rat TRITC conjugated IgG following the above protocoll.

2.6.4 Whole Cell Cytoskeletal Mounts

Cytoskeletons were prepared from live cultures settled on poly-L-lysine coated adhesion slides. Soluble cell components were extracted with 1% (v/v) NP-40 in PEME buffer (100 mM PIPES, 1 mM $MgSO_4$, 0.1 mM EDTA, 2 mM, EGTA [pH 6.0]) for 30 to 60 seconds before fixation with 4% PFA for ten minutes, then dehydrated in -20°C methanol (10 mins). Slides were rehydrated in 1X PBS for ten minutes prior to embedding in VECTASHIELD® mounting medium with DAPI prior to visualisation.

2.6.5 Whole Cell Mounts and Fluorescent Micrscopy of *B.saltans*

B. saltans cells were centrifuged (8,000 rpm, 3 mins, 4°C) and pellets washed three times with 1X PBS prior to resuspension in 30 µL 1X PBS (Melford, UK). Cells were settled onto Superfrost™ adhesion slides (ThermoFisher, UK) for 30 minutes and fixed directly with 4% paraformaldehyde in PBS. Following a 30 minute incubation, slides were dehydrated in -20°C methanol overnight. Cells were rehydrated in 1X PBS for 10 minutes and dyed with 4',6-diamidino-2-phenylindole (DAPI) mounting medium (VECTASHIELD®, UK). A coverslip was applied and sealed prior to visualisation.

For Immunofluorescence slides the same protocol as before was followed (2.6.3). Primary anti-Trett antibodies were utilised in a 1:10 dilution as the antibody concentration was not quantified due to time restraints. Following a 1 hour incubation and subsequent washes, a secondary anti-rabbit IgG with a conjugated Rhodamine tag was utilised in a 1:200 dilution and slide incubated for 1 hour. Three, five minute washes in PBS-Tween-20 solution followed before mounting with VECTASHIELD® DAPI mounting media. Negative controls followed the same steps above in absence of primary Trett antibodies and simple incubation in fresh blocking buffer (1% BSA, 1xPBS, 0.05% Tween-20)

2.7 Western Blot Detection from Cell Equivalents

$1x10^7$ *C. fasciculata* cells were harvested from each culture for *Bs*TAC65, 60, 40 and Trett along with Wild type *C. fasciulata* culture as a control. Cultures were centrifuged (8,000 rpm, 3 minutes) and supernatants aspirated and discarded. Cell pellets were resuspended in loading dye (see 2.5.3) and boiled for five minutes before vortexing. After SDS-PAGE and electropheric transfer (see 2.5.3) (Towbin, Staehelin and Gordon, 1979) the PVDF membrane was blocked in blocking buffer [5% (w/v) non-fat dry milk (Marvel, Premier Foods, Thame, UK) 0.05% (v/v) Tween 20 in PBS (Melford, UK) for one hour on an orbital shaker. The membrane was then incubated with a primary anti myc IgG in blocking buffer for 1 hour followed for two subsequent 10 minute washes in PBS-Tween 20 (0.05% v/v). After the final wash the membrane was incubated in a secondary anti mouse IgG with a horseradish peroxidase conjugate. The membrane was washed twice in PBS-Tween 20 followed by incubation with

1 mL HRP substrate peroxide solution (Millipore, USA) for five minutes prior to X-ray film exposure and development.

3.0 Results

3.1 Bioinformatic Analysis of *B. saltans* Orthologues

Following compilation of possible *T. brucei* orthologues from the *Bodo saltans* transcriptome (from Sanger Welcome, UK), 117,328 *B. saltans* acquisitions were produced for 92 *T. brucei* hypothetical/ putative proteins analysed from the *Tb*MitoCarta. Results were then filtered revealing 2,087 candidate acquisitions for analysis covering 97 *T. brucei* predicted proteins. Of these 2,087 acquisitions, 862 were analysed representing either singular results, or the hits with the lowest E-value for *T. brucei* proteins with multiple *Bodo saltans* predicted orthologues. These results were then subject to a second reciprocal BLASTp of the *T. brucei* peptide sequence against *B. saltans, L. major, C. fasciculata, T. borreli* and *Perkinsela sp,* representing evolutionary divergent members of Kinetoplastae.

BLASTp of *T. brucei* sequence against *T. brucei* showed 99.5% of hypothetical proteins analysed returned >E-10, confirming the majority of the *T. brucei* sequences analysed were well annotated. Overall one peptide sequences from *T. brucei* (Tb972.2.2940) produced an empty database. Three sequences produced an E value of <E-4 to >E-10 (Tb09.160.0550, Tb09.160.1280 and Tb09.160.0360), the remaining 858 acquisitions showed complete agreement with the original sequence. For *Leishmania major* Friedlin strain 4.80% of BLASTp analyses resulted in >E-4, 1.75% <E-4 to >E-10 and the majority (99.5%) of results were orthologous to the *T. brucei* 927 hypothetical proteins. Similar results were seen for *C. fasciculata*. 4.64% of results appeared to not be conserved, 2.44% appeared homologous to *T. brucei* and 92.92% peptide sequences were potental orthologous. *B. saltans*, the free living evolutionary ancestor of the Trypanosomatids showed a different story from the trypanosomatids. 19.14% of acquisitions analysed either resulted in an empty database, or had an E-value >E-4, a larger proportion of peptide sequences appeared to be homologous (8.82%) and the remaining 621 are potential *T. brucei* protein orthologues (<E-10).

Trypanoplasma borreli (an endoparasitic haematozoon of fish) which is higher branching than *Perkinsela* within Metakinetoplastea showed less orthology to *T. brucei* peptide sequences than *Bodo saltans.* The majority of tBLASTn analyses resulted in E-values above E-4 (65.5%), 31 peptide sequences appeared homologous to *T. brucei* (3.53%) and last, 30.97% peptide sequences resulted in orthologous values. The prokinetoplastina organism, *Perkinsela sp.* is the lowest branching Kinetoplastea organism analysed within this work. All 862 acquisitions from *B. saltans* analysed resulted in either an empty database or an E-value above E-3. Following determination of homology via BLASTp and tBLASTn, each *Bodo saltans* acquisition obtained originally was analysed using Uniprot and Interpro for domains, repeats, motifs and any other predicted feature. The details of each of these were noted and tabulated to highlight any proteins which are candidates for analysis during future work (Figure 12).

Naturally, *T. brucei* showed the greatest orthology to itself and was utilised to confirm sequence quality. *Leishmania major* Friedlin was utilised as it is the most well annotated strain of the *Leishmania* genus, *Leishmania* had the second highest count of orthologous proteins to *T. brucei* and *C. fasciculata* the third. Moreover, *Bodo saltans* appears to present the fourth highest similarity to the *T. brucei* hypothetical mitochondrial proteins (Figures 9-11).

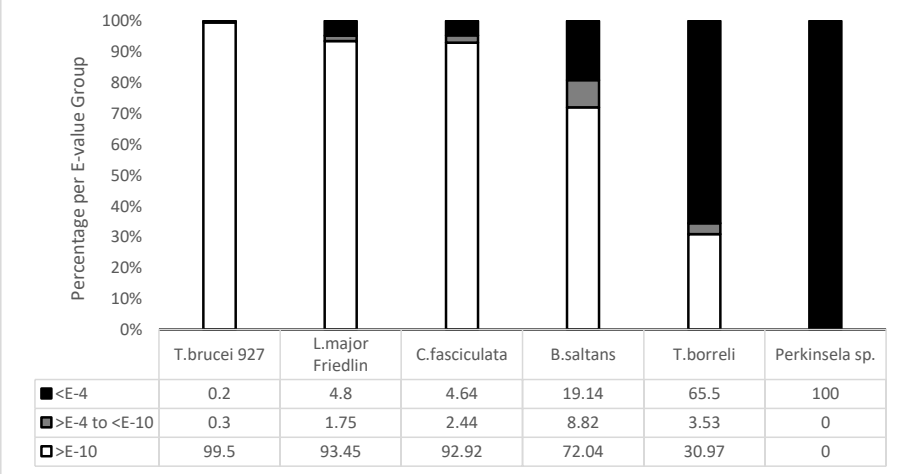

	T.brucei 927	L.major Friedlin	C.fasciculata	B.saltans	T.borreli	Perkinsela sp.
<E-4	0.2	4.8	4.64	19.14	65.5	100
>E-4 to <E-10	0.3	1.75	2.44	8.82	3.53	0
>E-10	99.5	93.45	92.92	72.04	30.97	0

Figure 9 Stacked percentile bar chart of E-value groups within each species: *Perkinsela* presented no E-value >E-4 and presents a 100% stack for <E-4. Greater homology to *T. brucei* is present within higher branching Kinetoplastea organisms. *Leishmania* and *Crithidia* present similar values for proteins analysed. Table shows percentile of each group within each species.

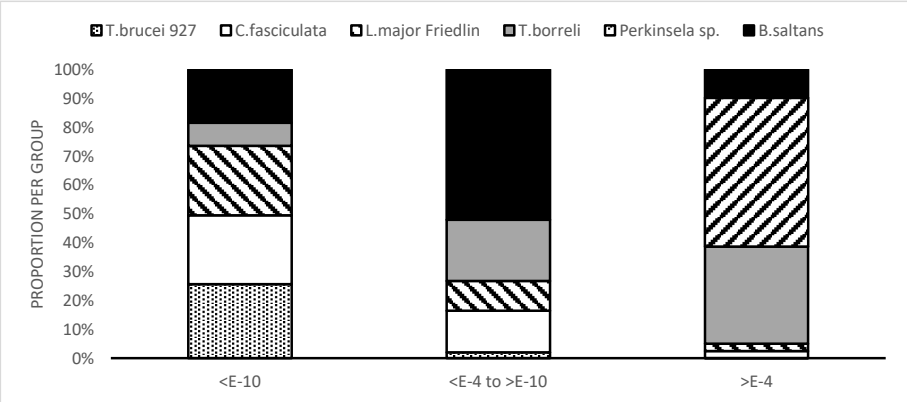

Figure 10 Stacked percentile chart grouped by E-value. *T. brucei* was anchored to itself to confirm sequence quality. *Leishmania* has the greatest orthology to *Tb*Mitocarta hypothetical proteins. *Perkinsela sp.* presented the largest group with no homologous proteins (>E-4), then *Trypanoplasma borreli.*

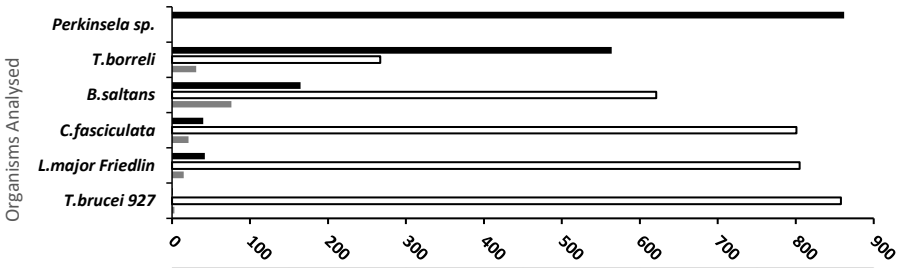

	T.brucei 927	L.major Friedlin	C.fasciculata	B.saltans	T.borreli	Perkinsela sp.
■ <E-4	1	42	40	165	564	862
□ >E-10	858	805	801	621	267	0
■ >E-4 to <E-10	3	15	21	76	31	0

Figure 11 E-values separated by quantity for each organism: *Perkinsela* presented no E-value >E-4. Greater homology to *T. brucei* is present within higher branching Kinetoplastea organisms. *Leishmania* and *Crithidia* present similar values for proteins analysed. Table shows by value the number of proteins within each E-value bracket. 862 *Bodo saltans* acquisitions were analysed overall.

Tb04.24M18.150						BLAST Sequences with Significant Alignment				
***Bs* Acquisition**	**E-value**	**Peptide Length**	**Superfamily**	**Reciprocal BLASTp**	**Notes**	***T.brucei***	***C.fasciculata***	**T.borreli**	**Perkinsela sp.***	***L.major Friedlin***
BS73360	4.45E-49	390	-	8.20E-33	No domains or superfamilies predicted	6.00E-130	2.00E-51	×	×	2.00E-51
Tb09.160.0360						**BLAST Sequences with Significant Alignment**				
***Bs* Acquisition**	**E-value**	**Peptide Length**	**Superfamily**	**Reciprocal BLASTp**	**Notes**	***T.brucei***	***C.fasciculata***	**T.borreli**	**Perkinsela sp.***	***L.major Friedlin***
BS53885	1.25E-10	292	-	1.10E-06	No domains or superfamilies predicted	6.00E-09	×	×	×	×
Tb09.160.0370						**BLAST Sequences with Significant Alignment**				
***Bs* Acquisition**	**E-value**	**Peptide Length**	**Superfamily**	**Reciprocal BLASTp**	**Notes**	***T.brucei***	***C.fasciculata***	**T.borreli**	**Perkinsela sp.***	***L.major Friedlin***
BS53100	5.52E-113	410	Ubiquitin-Like	9.80E-87	350 - 397 Ubiquitin Like superfamily	1.00E-110	2.00E-125	**3.70E-32**	×	2.00E-121
Tb09.160.0470						**BLAST Sequences with Significant Alignment**				
***Bs* Acquisition**	**E-value**	**Peptide Length**	**Superfamily**	**Reciprocal BLASTp**	**Notes**	***T.brucei***	***C.fasciculata***	**T.borreli**	**Perkinsela sp.***	***L.major Friedlin***
BS02295	4.61E-53	830	-	2.30E-41	Intrinsic protein disorder at 40-70 predicted	2.00E-51	4.00E-142	×	×	9.00E-155
Tb09.160.0540						**BLAST Sequences with Significant Alignment**				
***Bs* Acquisition**	**E-value**	**Peptide Length**	**Superfamily**	**Reciprocal BLASTp**	**Notes**	***T.brucei***	***C.fasciculata***	**T.borreli**	**Perkinsela sp.***	***L.major Friedlin***
BS02175	1.53E-14	198	-	2.50E-25	Intrinsic disorder 72-91 and 104-140	4.00E-92	3.00E-40	**2.70E-16**	×	2.00E-37
BS02370	1.50E-14	205	-	1.10E-24	Intrinsic protein disorder at 112-147 predicted	4.00E-92	3.00E-40	**2.70E-16**	×	2.00E-37
Tb09.160.0550						**BLAST Sequences with Significant Alignment**				
***Bs* Acquisition**	**E-value**	**Peptide Length**	**Superfamily**	**Reciprocal BLASTp**	**Notes**	***T.brucei***	***C.fasciculata***	**T.borreli**	**Perkinsela sp.***	***L.major Friedlin***
BS23420	8.70E-11	388	-	8.10E-09	Predicted cytoplasmic domain 1-67 and none cytoplasmic domain 87-388	2.00E-05	2.00E-33	×	×	3.00E-18
Tb09.160.0760						**BLAST Sequences with Significant Alignment**				
***Bs* Acquisition**	**E-value**	**Peptide Length**	**Superfamily**	**Reciprocal BLASTp**	**Notes**	***T.brucei***	***C.fasciculata***	**T.borreli**	**Perkinsela sp.***	***L.major Friedlin***
BS38545	7.77E-154	354	AB_hydrolase_1	1.00E-112	128-337 alpha beta hydrolase fold predicted	1.00E-149	0	×	0.19	0
Tb09.160.0890						**BLAST Sequences with Significant Alignment**				
***Bs* Acquisition**	**E-value**	**Peptide Length**	**Superfamily**	**Reciprocal BLASTp**	**Notes**	***T.brucei***	***C.fasciculata***	**T.borreli**	**Perkinsela sp.***	***L.major Friedlin***
BS08740	3.11E-12	418	SAM-dependent_MTases	1.40E-10	74-225 SAM-dependant_Mtases signature	2.00E-09	2.00E-55	**1.70E-31**	×	2.00E-59
Tb09.160.1020						**BLAST Sequences with Significant Alignment**				
***Bs* Acquisition**	**E-value**	**Peptide Length**	**Superfamily**	**Reciprocal BLASTp**	**Notes**	***T.brucei***	***C.fasciculata***	**T.borreli**	**Perkinsela sp.***	***L.major Friedlin***
BS25455	1.70E-21	676	Ribosomal_L34Ae	3.40E-18	Non-cytoplasmic domain 22-676	8.00E-16	7.00E-85	**1.40E-15**	×	7.00E-82
Tb09.160.1280						**BLAST Sequences with Significant Alignment**				
***Bs* Acquisition**	**E-value**	**Peptide Length**	**Superfamily**	**Reciprocal BLASTp**	**Notes**	***T.brucei***	***C.fasciculata***	**T.borreli**	**Perkinsela sp.***	***L.major Friedlin***
BS65585	0	716	TCAIM	2.50E-118	3-64 domain of unknown function	0	0	**1.20E-156**	×	0
Tb09.160.1760						**BLAST Sequences with Significant Alignment**				
***Bs* Acquisition**	**E-value**	**Peptide Length**	**Superfamily**	**Reciprocal BLASTp**	**Notes**	***T.brucei***	***C.fasciculata***	**T.borreli**	**Perkinsela sp.***	***L.major Friedlin***
BS56150	1.41E-06	310	Ankyrin_rpt-contain_sf	0.0017	Ankyrin_rpt-contain_sf domain fromn 92-282	2.00E-17	7.00E-17	**3.80E-15**	×	1.00E-16

Figure 12 First twelve *Bodo saltans* and their analysis: Significant alignments of representative evolutionary partners are tabulated and potential features of each are listed. The remaining 850 proteins are omitted from this work due to file size and being surplus to requirement.

3.2 Polymerase Chain Reaction

gDNA obtained from *B. saltans* was of sufficient quantity for PCR amplification of *Bs*Trett fragments. PCR was attempted to amplify N-terminal (532 bp), middle (810 bp), C-terminal (848 bp) and the full length (2091 bp) of the *Bs*Trett gene (BS69260). Successful amplification of the middle fragment was observed. $MgCl_2$, concentrations and *T*m were adjusted to amplify the additional fragments (Figure 13). Amplification for the full length of *Bs*Trett appeared successful but fragment length was dramatically shorter than the gene size. Amplification of the full length was thought to be observed when 0.2 µL $MgCl_2$ was added to the PCR mix with *T*m adjusted to 47°C.

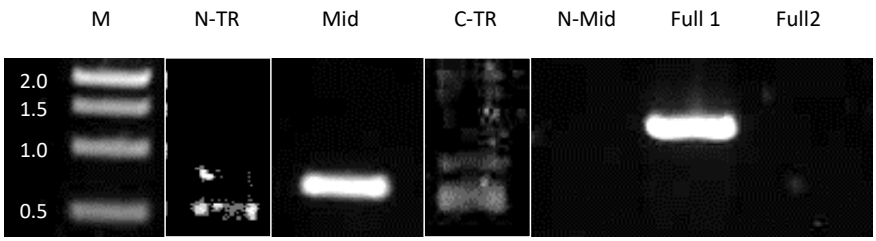

Figure 13 Horizontal gel electrophoresis of PCR amplifications: M: 1kb DNA marker, N-TR: N-terminus of *Bs*Trett, Mid: Middle fragment, C-TR: C-terminus fragment, N-Mid: N terminus and middle fragment, Full 1 : Full length of *Bs*Trett with restriction sites for pET-28a (+) plasmids, Full 2: Full length of *Bs*Trett with restriction sites for pNUS-GFPcH plasmids.

3.3 Recombinant pGEMT-EZ vector production

Recombinant pGEMT-EZ vectors were constructed after TA tailing with Taq polymerase. Double digestion of cloned recombinant vectors revealed successful insertion of the N-terminal and C-terminal fragments into pGEMT-EZ vectors (Figure 14) pGEMT-Nterm and pGEMT-Cterm vectors were sequenced via Sanger sequencing (Source Bioscience, Cambridge).

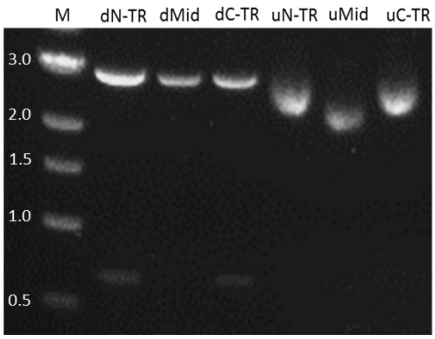

Figure 14 Digestions of recombinant pGEMT-EZ vectors: Labelling follows the same system from Figure 13 where d indicates digestion with restriction endonuclease and u indicates the vector has remained uncut for comparison. Successful insertion for the N-terminal and C-terminal fragment can be seen.

3.4 Bioinformatic Analysis of Sequenced Vectors

M13 reverse primers were utilised for Sanger sequencing. Received sequences are below. EcoR1 sites are in yellow, BamHI green, XhoI pink and *Bs*Trett fragment sequence highlighted in grey.

N-terminal

GGGGNAANNCCGCCNAACGTGGCGAGNAAGGAAGGGAAGAAAGCGAAAGGAGCGGGCGCTAG
GGCGCTGGCAAGTGTAGCGGTCACGNTGCGCGTAACCACCNNCACCCGCCGCGCTTAATGCG
CCGCTACAGGGCGCGTCCATTCGCCATTCAGGCTGCGCAACTGTTGGGAAGGGCGATCGGTG
CGGGCCTCTTCGCTATTACGCCAGCTGGCGAAAGGGGGATGTGCTGCAAGGCGATTAAGTTG
GGTAACGCCAGGGTTTTCCCAGTCACGACGTTGTAAAACGACGGCCAGTGAATTGTAATACG
ACTCACTATAGGGCGAATTGGGCCCGACGTCGCATGCTCCCGGCCGCCATGGCGGCCGCGGG
AATTCGATTAATGGATCCATGGTGGATCTCATCCGATTGCAGACAGGTGGGGAAAGAAACTC
CAAGTTGGCCGCAATGTACTCTGGAAAATTCAAGACGCTCATTTTTTGTTCTTTCTTTCGAC
TCTCTTGGTTTTGGTTTGTTTGTCAATAATCGCTACTCTCTTTCACTGTGTCGCTAGCACAA
CACATCAAAATTCAATGAAGAAGTTACAAAGAGCAGCATTAGGACACACGCGACATGACATA
TGACACAGTAAGATACGTGCGAGTTTTTTGGGAGGACCATCTGTGTGGTCTCCTTCTTGATT
AACCGGTTGAAGTGTTGTTATGATGAATAAATACGGCAGAATACAGGAAGACTTTTTTGTTG
TTCGTTTCTTGTTTGGTGCCTACAGCGTCGGCGGGTCCTCAAACAGCAAATTCGCCGCTCTC
TCAATGCTTCGGTTTGCTAGGAAGAAGGCAGCTGTGCATTGCTCCGTCGTGAAGCCCAAATG
CGTAAGGCCTTCAATCTTTTGCTTGTCATCGTCGGAAATCACCAGCGGAATCGAGCCGCGTT
GGCGTGATGTCGGTACCGTTGTTGCACCTTCGCTGTTGTTCACTTCCGTGTTGGTGTCATTG
TTTGAAGTGGAGATGTTATCATCAGCACCGCCGTCGCTCACGGTACTGCGAAGGCTGTCCAG
GATCTGTGTCGCATTGCGCCCCAACGTTTCTCCCGCTCGTCCACCTCGAGATTAATCACTAG
TGAATTCGCGGCCGCCTGCAGGTCGACCATATGGGAGAGCTCCCAACGCGTTGGATGCATAG
CTTGAGTATTCTATAGNNCANNNNNNNNNNN

C-terminal

ANNNGGCGAGAAAGGAAGGGAAGAAAGCGAAAGGAGCGGGCGCTAGGGCGCTGGCAAGTGTA
GCGGTCACGCTGCGCGTAACCACCACACCCGCCGCGCTTAATGCGCCGCTACAGGGCGCGTC
CATTCGCCATTCAGGCTGCGCAACTGTTGGGAAGGGCGATCGGTGCGGGCCTCTTCGCTATT
ACGCCAGCTGGCGAAAGGGGGATGTGCTGCAAGGCGATTAAGTTGGGTAACGCCAGGGTTTT
CCCAGTCACGACGTTGTAAAACGACGGCCAGTGAATTGTAATACGACTCACTATAGGGCGAA
TTGGGCCCGACGTCGCATGCTCCCGGCCGCCATGGCGGCCGCGGGAATTCGATTAATGGATC
CATGGTGGATCTCATCCGATTGCAGACAGGTGGGGAAAGAAACTCCAAGTTGGCCGCAATGT
ACTCTGGAAAATTCAAGACGCTCATTTTTTGTTCTTTCTTTCGACTCTCTTGGTTTTGGTTT
GTTTGTCAATAATCGCTACTCTCTTTCACTGTGTCGCTAGCACAACACATCAAAATTCAATG
AAGAAGTTACAAAGAGCAGCATTAGGACACACGCGACATGACATATGACACAGTAAGATACG
TGCGAGTTTTTTGGGAGGACCATCTGTGTGGTCTCCTTCTTGATTAACCGGTTGAAGTGTTG
TTATGATGAATAAATACGGCAGAATACAGGAAGACTTTTTTGTTGTTCGTTTCTTGTTTGGT
GCCTACAGCGTCGGCGGGTCCTCAAACAGCAAATTCGCCGCTCTCTCAATGCTTCGGTTTGC
TAGGAAGAAGGCAGCTGTGCATTGCTCCGTCGTGAAGCCCAAATGCGTAAGGCCTTCAATCT
TTTGCTTGTCATCGTCGGAAATCACCAGCGGAATCGAGCCGCGTTGGCGTGATGTCGGTACC
GTTGTTGCACCTTCGCTGTTGTTCACTTCCGTGTTGGTGTCATTGTTTGAAGTGGAGATGTT
ATCATCAGCACCGCCGTCGCTCACGGTACTGCGAAGGCTGTCCAGGATCTGTGTCGCATTGC
GCCCCAACGTTTCTCCCGCTCGTCCACCTCGAGATTAATCACTAGTGAATTCGCGGCCGCCT
GCAGGTCGACCATATGGGAGAGCTCCCAACGCGTTGGATGCATAGCTTGAGTATTCTATAGN
NCNNNNNNNNN

Analysis of the nucleotide sequences showed little alignment to Bs69260 but revealed a 97% sequence homology to Bs14930 (1.3E-67) when investigated via BLASTN (Figure 15A), indicating potential off-target amplification. Clustal omega alignment of Bs14930 and Bs69260 (BsTrett) showed 84.4% agreement to the *Bs*Trett$^{\Delta 1324\text{-}2092}$ region (Figure 15B). Interpro analysis showed detailed signature matches for XPC and UBA domains within Bs14930 and similar domain homology across the Trypanosomatids. Because of this synthetic plasmids of the full length and C-terminal *Bs*Trett (*Bs*Trett$^{\Delta 1324\text{-}2092}$) were purchased (ThermoFischer, UK).

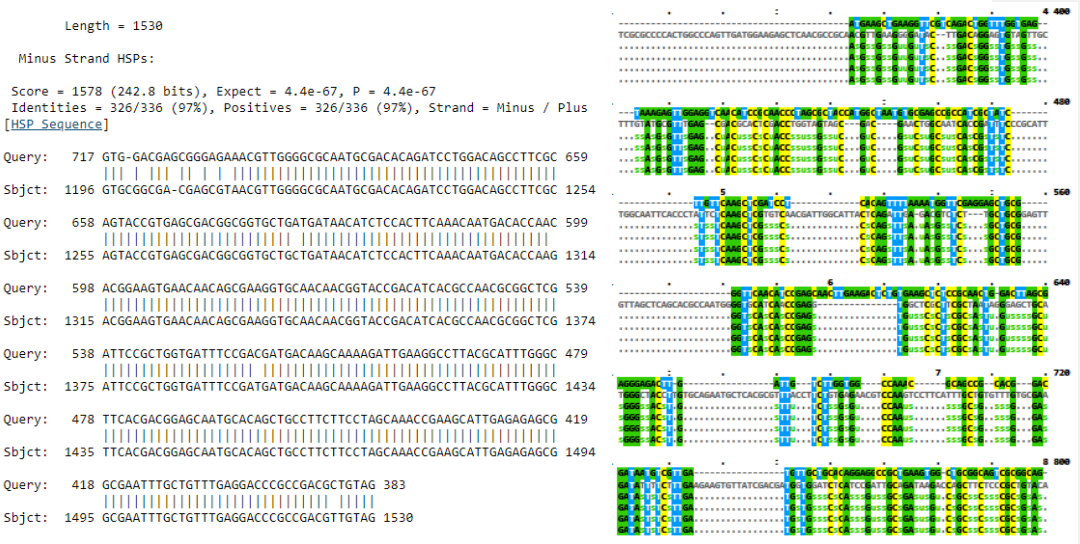

```
       Length = 1530

 Minus Strand HSPs:

 Score = 1578 (242.8 bits), Expect = 4.4e-67, P = 4.4e-67
 Identities = 326/336 (97%), Positives = 326/336 (97%), Strand = Minus / Plus
[HSP Sequence]

Query:   717 GTG-GACGAGCGGGAGAAACGTTGGGGCGCAATGCGACACAGATCCTGGACAGCCTTCGC 659
            ||| | ||| || | | |||||||||||||||||||||||||||||||||||||||||||
Sbjct:  1196 GTGCGGCGA-CGAGCGTAACGTTGGGGCGCAATGCGACACAGATCCTGGACAGCCTTCGC 1254

Query:   658 AGTACCGTGAGCGACGGCGGTGCTGATGATAACATCTCCACTTCAAACAATGACACCAAC 599
            ||||||||||||||||||||||||| ||||||||||||||||||||||||||||||||||
Sbjct:  1255 AGTACCGTGAGCGACGGCGGTGCTGCTGATAACATCTCCACTTCAAACAATGACACCAAG 1314

Query:   598 ACGGAAGTGAACAACAGCGAAGGTGCAACAACGGTACCGACATCACGCCAACGCGGCTCG 539
            ||||||||||||||||||||||||||||||||||||||||||||||||||||||||||||
Sbjct:  1315 ACGGAAGTGAACAACAGCGAAGGTGCAACAACGGTACCGACATCACGCCAACGCGGCTCG 1374

Query:   538 ATTCCGCTGGTGATTTCCGACGATGACAAGCAAAAGATTGAAGGCCTTACGCATTTGGGC 479
            |||||||||||||||||| ||||||||||||||||||||||||||||||||||||||||||
Sbjct:  1375 ATTCCGCTGGTGATTTCCGATGATGACAAGCAAAAGATTGAAGGCCTTACGCATTTGGGC 1434

Query:   478 TTCACGACGGAGCAATGCACAGCTGCCTTCTTCCTAGCAAACCGAAGCATTGAGAGAGCG 419
            ||||||||||||||||||||||||||||||||||||||||||||||||||||||||||||
Sbjct:  1435 TTCACGACGGAGCAATGCACAGCTGCCTTCTTCCTAGCAAACCGAAGCATTGAGAGAGCG 1494

Query:   418 GCGAATTTGCTGTTTGAGGACCCGCCGACGCTGTAG 383
            ||||||||||||||||||||||||||||||| |||||
Sbjct:  1495 GCGAATTTGCTGTTTGAGGACCCGCCGACGTTGTAG 1530
```

Figure 15 A: BLASTN of Sanger sequencing data against Bs14930: 97% sequence homology was seen, indicating off target amplification. **Figure 15 B: Clustal omega alignment of Bs14930 against *Bs*Trett** 84.4% homology was seen between both sequences.

3.5 Recombinant pET-28a (+) and pNUS-GFPcH production

Following cloning of synthetic plasmids, inserts were extracted via digestion with BamHI and XhoI for *Bs*Trett$^{\Delta 1324\text{-}2092}$ fragment extraction and *Nde*I, *Knp*I for the full length fragment extraction from the synthetic backbone. Inserts and digestion sizes were confirmed on 0.8% TAE agarose by gel electrophoresis (Figure 16, 1-6). Digestions showed successful excision of the inserts. Inserts extracted from agarose were then ligated into the appropriate vectors post Nanodrop quantification.

To confirm successful insertion of gene fragments into the vectors a series of restriction endonuclease digestions were conducted. Digestions of each vector showed insertion of the *Bs*Trett gene and each fragment ran at the predicted length (Figure 16, 7-15). To further confirm insertion of the *Bs*Trett$^{\Delta 1324\text{-}2092}$ and full length Trett 100 ng/µL recombinant vector was sequenced.

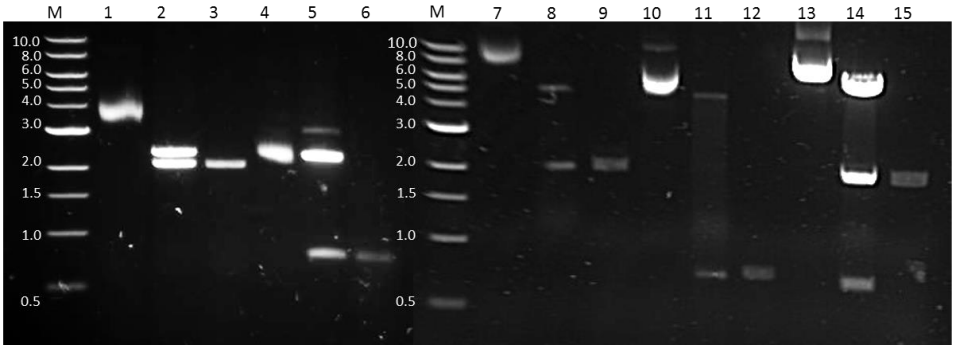

Figure 16 Plasmids and Insert Digestions: M: 1kb DNA ladder, 1: Uncut *Bs*Trett in backbone, 2 *Bam*HI *xho*I *Bs*Trett, 3: Purified insert of *Bs*Trett, 4: Uncut *Bs*Trett$^{\Delta 1324\text{-}2092}$in backbone, 5: *Bam*HI *xho*I, 6: Purified C *Bs*Trett$^{\Delta 1324\text{-}2092}$ insert, 7-9: pET-28a-TrettFull, Digest showing pET-28a and *Bs*Trett insert, 10-12: pET-28a- *Bs*Trett$^{\Delta 1324\text{-}2092}$, Digest showing pET-28a backbone and the *Bs*Trett$^{\Delta 1324\text{-}2092}$, 13-15: *Bs*Trett::GFP::myc, Digest revealing pNUS-GFPcH backbone and *Bs*Trett full length and Insert. 0.8% Agarose, 1kb DNA ladder (NEB,UK)

3.5 Expression of *Bs*Trett and purification via NiNTA

Sodium dodecyl sulphate polyacrylamide gel electrophoresis (SDS-PAGE) and Western Blot analysis revealed successful inductions with 1mM IPTG for *Bs*Trett$^{\Delta 1324\text{-}2092}$ (Figure 17A). Small scale induction revealed a band at ~29 kDa indicating a successful induction. To confirm presence of this a second SDS-PAGE was run and transferred to a PDVF membrane for Western Blot analysis. Targeting of the His tag of *Bs*Trett$^{\Delta 1324\text{-}2092}$ via a mouse anti-His IgG and an anti-mouse HRP conjugated secondary antibody and chemiluminescence visualisation produced bands at ~29 kDa confirming presence of *Bs*Trett$^{\Delta 1324\text{-}2092}$ (Figure 17B). Following the primary western, the same protocol for expression was followed, and cells lysed to confirm the solubility of *Bs*Trett $^{\Delta 1324\text{-}2092}$ via SDS-PAGE and Western Blot analysis. Following PDVF transfer and anti-His targeting as before a corresponding band was revealed within insoluble fractions. Large scale production and purification of the recombinant protein fraction was successful. SDS-PAGE analysis of the solubilised protein purified via Ni-NTA produced bands corresponding to the predicted molecular weight of the *Bs*Trett C-terminus within each elution. Elution 3 was more dilute that other fractions due to the use of a homemade column. *Bs*Trett recombinant protein samples were all of sufficient quantity and purity for rabbit antisera production by Eurogenetec

(Cambridge, UK), this antiserum will be purified for *in vivo* targeting of Trett within *Bodo saltans* via IF imaging.

0

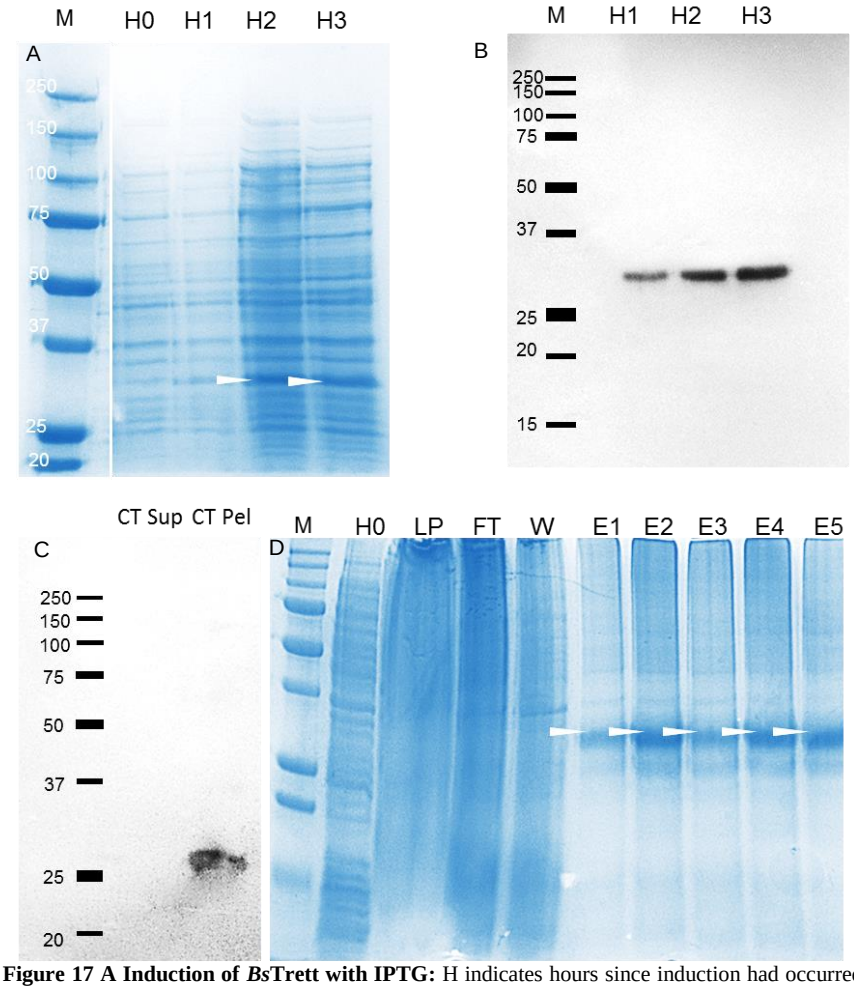

Figure 17 A Induction of *Bs*Trett with IPTG: H indicates hours since induction had occurred. The overall concentration of *Bs*Trett$^{\Delta 1324\text{-}2092}$ increases as time progresses, Full length expression proved unsuccessful. **Figure 17 B Western blot analysis of 17 A**: Anti-His mouse IgG were used. Bands are predominant indicating presence *Bs*Trett$^{\Delta 1324\text{-}2092}$ at 29 kDa**. Figure 17 C Western blot analysis of solubility fractions of *Bs*TrettΔ1324-2092:** Western shows recombinant protein inhabits insoluble fraction. **Figure 17 D NiNTA purification of *Bs*Trett$^{\Delta 1324\text{-}2092}$**: LP: Lysis pellet fraction, FT: Flow through, W: Wash, E1-5: Elutions 1 to 5. Elution 3 appears lighter due to the fraction being slightly

more dilute due to use of a homemade column. Elutions 1 - 5 were run on a 10% SDS-PAGE and the large singular band excised for downstream antibody production.

3.6 *Bs*Trett antibody purification

To produce an anti-*Bs*Trett$^{\Delta 1324\text{-}2092}$ IgG, C-terminal fragments of *Bs*Trett were recombinantly expressed using a pET-28a (+) vector and purified via Ni-NTA. Purified elutions were run on 10% SDS-PAGE, stained with Coomassie-blue before the band at 29 kDa was excised for antibodies to be made. To purify the rabbit anti-sera, an amino-link column was primed with *Bs*Trett following 2.5.5 and the protein left uneluted. Following incubation with anti-sera and washes, rabbit anti- *Bs*Trett$^{\Delta 1324\text{-}2092}$ were eluted and analysed via western blot. Analysis revealed full, heavy chain (HC) and light chain (LC) fragments of the antibody. To confirm *Bs*Trett$^{\Delta 1324\text{-}2092}$ antibodies were functional, recombinant *Bs*Trett$^{\Delta 1324\text{-}2092}$ was run on 10% SDS-PAGE and transferred to a PDVF membrane. A 1:10 dilution of Trett antibody to blocking buffer was utilised as primary with an anti-rabbit HRP conjugate IgG as secondary. Protein samples prior to induction (H0) showed no band at 29 kDa whereas a band was present following 5 hours of induction (H5) confirming overall functionality of the antibody (Figure 18B)

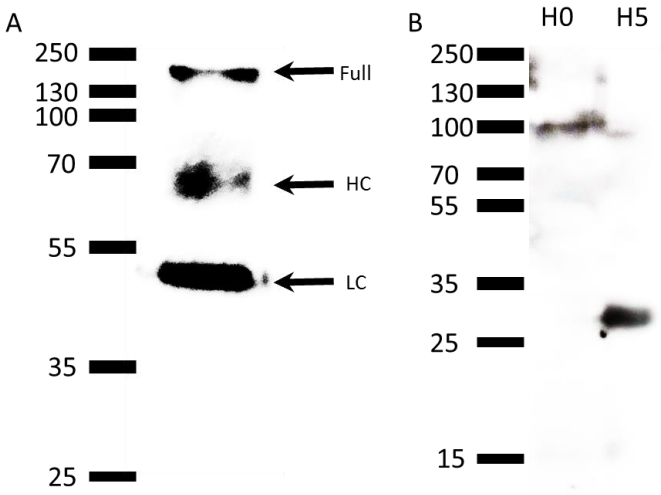

Figure 18 A) Western blot analysis of BsTrett Antibodies: Trett antibodies were transferred onto PDVF membranes following SDS-PAGE. Targeting with anti-rabbit IgG with a HRP conjugate revealed Heavy chains (HC), Light chains (LC) and full length antibodies. **Figure 18 B) Western blot analysis of small scale induction with Trett antibodies:** Following a small scale protein expression, samples were run on SDS-PAGE and analysed by western blot with Trett antibodies as primary. 0 hours from induction (H0) shows not band for Trett (albeit there is possible none specific binding), 5 hours

post induction (H5) shows a clear band at 29 kDa equivalent to Trett C-terminal fragments confirming functionality of the antibodies.

3.6 Production of *Crithidia fasciculata* Cell Lines

3.6.1 Western Blot Analysis of Whole Cell Equivalents

Transfection protocols of *C. fasciculata* were refined and transformants expressing *Bs*Trett::GFP::myc, *Bs*TAC40::GFP::myc, *Bs*TAC60::GFP::myc and *Bs*TAC65::GFP::myc were produced. $2x10^7$ cell equivalents were loaded into each well were run on SDS-PAGE and analysed via Western Blot following transfer onto PDVF membrane (Figure 19). The chimeric myc tags flanking both the N- and C- terminals of GFP (Sup 4) were targeted with anti-myc antibodies. 1:200 mouse anti-myc IgG was utilised with 1:2000 anti-mouse Horseradish peroxidase conjugated IgG and bands visualised through enhanced chemiluminescence (ECL). Wild type controls showed no myc signal, where *Bs*TAC60 and *Bs*TAC40 showed low levels of GFP expression which was reflected in whole cell mount imaging indicating either poor transfection efficiency or proteomic truncation within *C. fasciculata*. Reflecting observations during fluorescence imaging, *Bs*Trett::GFP::myc and *Bs*TAC65::GFP::myc had the greatest level of myc::GFP::myc expression. Western blot analysis of each protein produced a band at ~29 kDa indicative of a cleaved myc::GFP::myc in each chimeric protein. Recently *Lesihmania sp.* inducible CRISPR-Cas9 systems have been developed to produce stably expressive GFP to overcome truncation of the protein by direct insertion of the recombinant gene into *Leishmania* and *Crithidia* this system could have potential use downstream to prevent GFP cleavage (Zhang and Matlashewski, 2015).

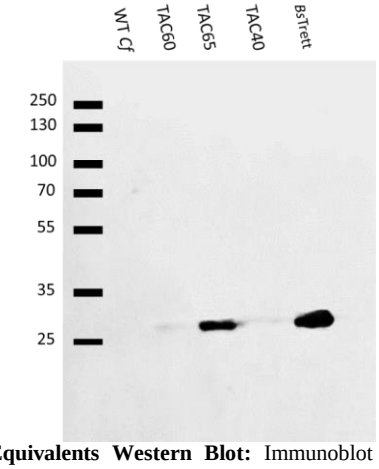

Figure 19 Whole Cell Equivalents Western Blot: Immunoblot of TAC components showed comparable differences of expression levels of each protein. Truncation of the chimeric GFP is apparent given bands produced at ~29 kDa. *Crithidia fasciculata* wild type (WT *Cf*) was indicative of no GFP::myc expression and was utilised as a negative control. TAC60 and TAC40 myc-targeted blots

with HRP-conjugated IgGs indicate poorer levels of expression than other TAC components. PDVF membrane was probes for myc expression within *Bs*Trett, *Bs*TAC65, *Bs*TAC60 and *Bs*TAC40.

3.7 Mitochondrial and Kinetoplast-associated localisations of *Bodo saltans* Trett, TAC40, TAC60 and TAC65

To localise *Bodo saltans* Trett (Bs69260), TAC65, TAC60 and TAC40 we expressed the proteins fused to a chimeric C-terminus green fluorescent protein and a chimeric myc tag (*Bs*Trett::GFP::myc, *Bs*TAC65::GFP::myc and *Bs*TAC60::GFP::myc, *Bs*TAC40::GFP::myc). Using a modified pUC18 plasmid (pNUS-GFPcH) with appropriate intergenic regions specific for *C. fasciculata* trans-splicing and protein expression, recombinant pNUS-GFPcH vectors were introduced to *C. fasciculata* cell lines. Visualisation of *Bs*Trett::GFP::myc, *Bs*TAC65::GFP::myc, *Bs*TAC60::GFP::myc and *Bs*TAC40::GFP::myc throughout the *Crithidia* cell cycle revealed promising insights about the localisation of each protein.

Previous unpublished work by our group localised *Tb*Trett to the antipodal sites of the *T. brucei* kinetoplast. Visualisation of *Bs*Trett::GFP::myc revealed several foci within the cell (Figure 20). First, a diffuse localisation throughout the mitochondrial matrix can be seen. Distinct localisations are observed around the kinetoplast with possible antipodal localisation. Second, nuclear segregation reveals a more localised signal for *Bs*Trett::GFP::myc with foci surrounding the kinetoplast forming a ring complex. This ring complex was observed throughout the majority of cells. Third, dual fluorescence of $2N^{M}2K^{D}$ cells, present standard thread linkage of the dividing kinetoplast over parent and daughter cell with *Bs*Trett localisations proximal to the dividing kinetoplast. *Bs*Trett movements were tracked throughout the cell cycle. Kinetoplast signals appear antipodal throughout nuclear replication

*Bs*TAC65::GFP::myc fluorescence was similar to *Bs*Trett signals for whole cell mounts. Mitochondrial signals surround the kinetoplast laterally and appears to localise strongly to the basal body and flagellar canal of *C. fasciculata* (Figure 21). $1N^{S}1K$ cells showed diffuse localisation of *Bs*TAC65 throughout the mitochondria with puncta again surrounding the kinetoplast. Transfection efficiency of *Bs*TAC65::GFP::myc encoding plasmids was low with the vast majority of expressing cells being 1N1K.

*Bs*TAC60::GFP::myc produced low levels of fluorescence. However, preliminary data presented within this body of work indicates *Bs*TAC60::GFP::myc localises throughout the mitochondrial with affiliation to the kinetoplast (Figure 22). Targeting with myc antibodies shows some co-localisation of the protein to the kinetoplast, but not enough data was available to confirm this with confidence.

Additionally *Bs*TAC65::GFP::myc cells were targeted using a YL1/2 primary antibody which targets tubulin and a secondary TRITC conjugate allowing localisation of the basal body.

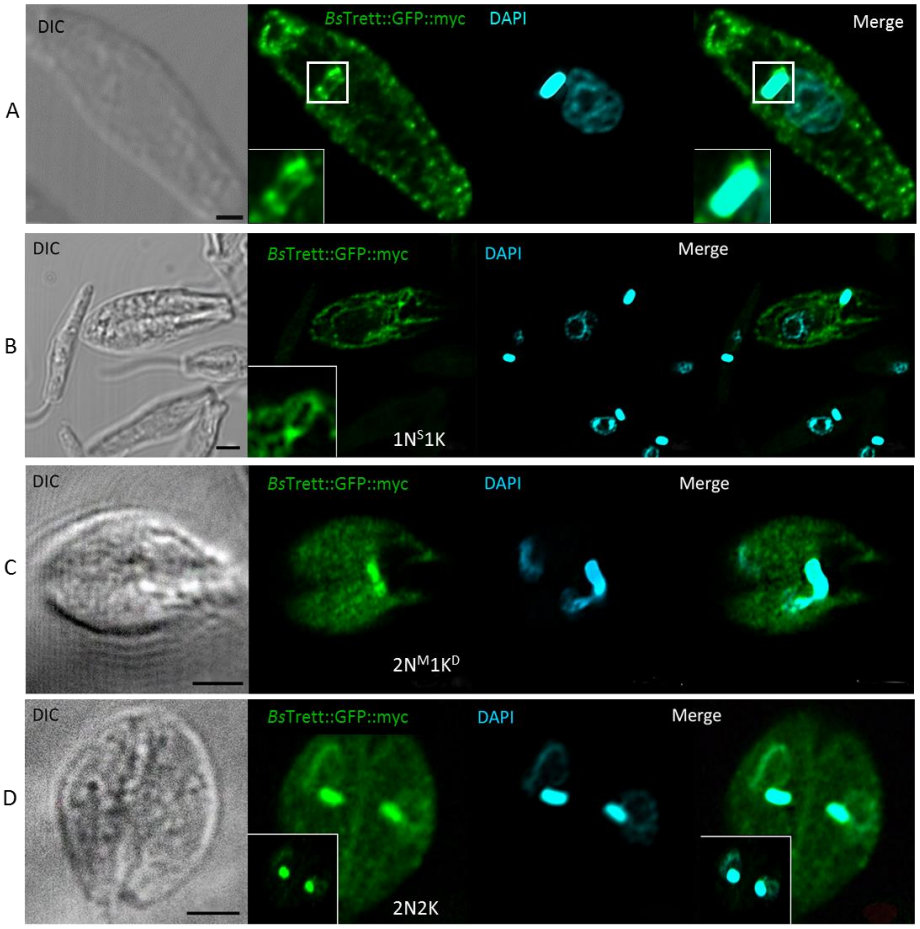

Figure 20 *Bs*Trett Movement Through the Cell Cycle: Nucleus and kinetoplast were stained with DAPI (blue), and *Bs*Trett tagged via a chimeric GFP::myc (green). For each cell the number of nuclei (N) and kinetoplasts (K) are shown. M for nuclear mitosis, S for s-phase and D for kinetoplast division. A: *C. fasciculata* cell in cell cycle arrest. *Bs*Trett localisation around antipodal sites of the kinetoplast can be seen. B: Inset panel shows clear punctate antipodal localisations of *Bs*Trett forming a ring around the kinetoplast. C: *Bs*Trett localisations follow the movement of the kinetoplast (forming a nabelschur – a bridge complex formed by the kinetoplast over replicating cells) across the diving cell. Nuclear

mitosis is also present. D: Cell has entered late stage mitosis with complete segregation of the kinetoplast and of the nucleus. Scale bar 2nm.

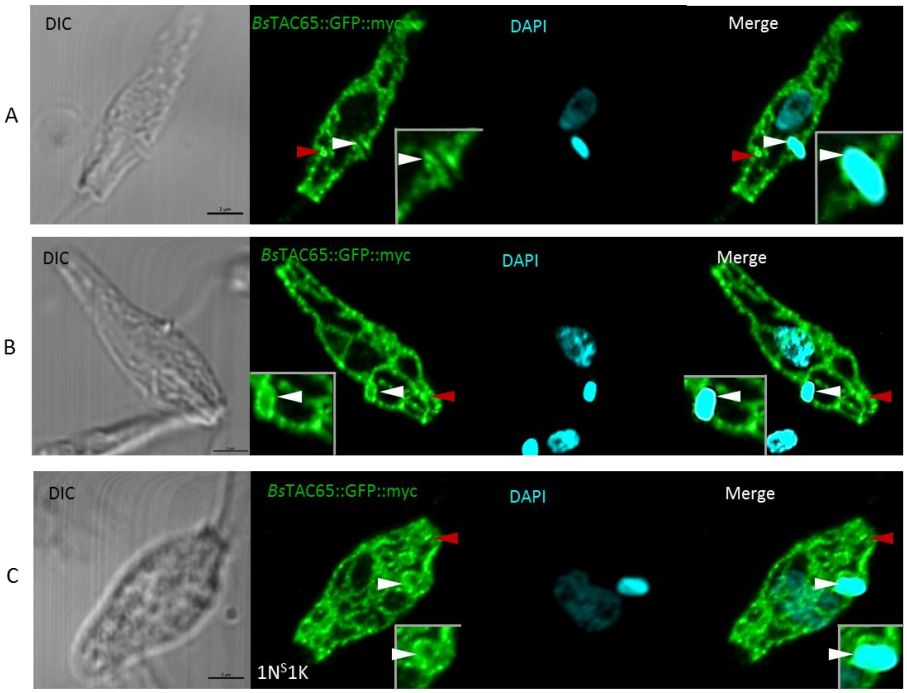

Figure 21 *Bs*TAC65 Movement Through The Cell Cycle: Events during the cell cycle in *C. fasciculata* detected via fluorescence microscopy. Nucleus and kinetoplast DNA was stained with DAPI (blue), and *Bs*TAC65 tagged via a chimeric GFP::myc (green). For each cell the number of nuclei (N) and kinetoplasts (K) are shown, S-phase (S). A: *C. fasciculata* cell in cell cycle arrest. *Bs*TAC65 localisation are lateral the kinetoplast (White arrow – magnified in the inset panel). B: Inset panel shows clear punctate localisations of *Bs*TAC65 forming a ring around the kinetoplast (White arrow). C: *Bs*TAC65 localisations are diffuse during S-phase. White arrows: Lateral localisations to kinetoplast. Red arrows: Possible basal body localisations. Scale bar 2nm.

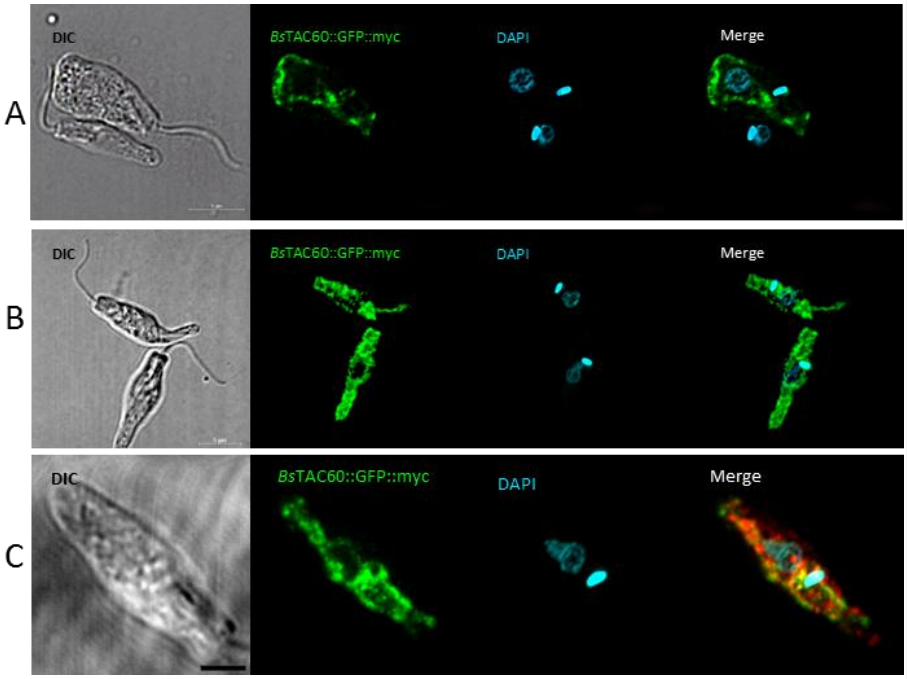

Figure 22 *Bs*TAC60 Fluorescence in *C. fasciculata*: GFP signals of *Bs*TAC60 showed dispersed puncta throughout the cell mitochondrion with the majority being at the mitochondrial periphery. Some kinetoplast loci are visible however this represented the minority of the fluorescent population. TAC60 is known to co-localise with TAC40 within *T. brucei.* Scale bar: 2 µm.

3.8 Immunofluorescence

3.8.1 Wild Type Controls Show No fluorescence

To ensure no background signal or auto fluorescence were giving rise to fluorescent signals, positive and negative immunofluorescence (IF) controls were prepared. IF slides lacking a primary myc antibody and utilising a primary myc antibody were produced. Slides were imaged and processed using identical parameters for the laser and post image processing. GFP signals were not apparent with no background or bleed through signal present. DAPI signals were bright and identical to the signals seen in transfected cell lines. The positive and negative controls produced no signal in both. Negative controls indicate that no auto fluorescence is occurring from the TRITC conjugate, but also indicate proper washing of slides as no residual signal can be seen from the controls. Images were taken of *C. fasciculata* throughout the cell cycle with no indication of auto fluoresce from wild type cells. Interestingly, *C. fasciculata* cells undergoing cell death appeared to produce bright green signals, possible due loss of phenolic compounds from exosomes and vacuoles following membrane degradation. However, this has only previously been observed within plant tissue and further study is required to properly deduce the cause of these properties (Koga *et al.*, 1988; Talamond, Verdeil and Conéjéro, 2015).

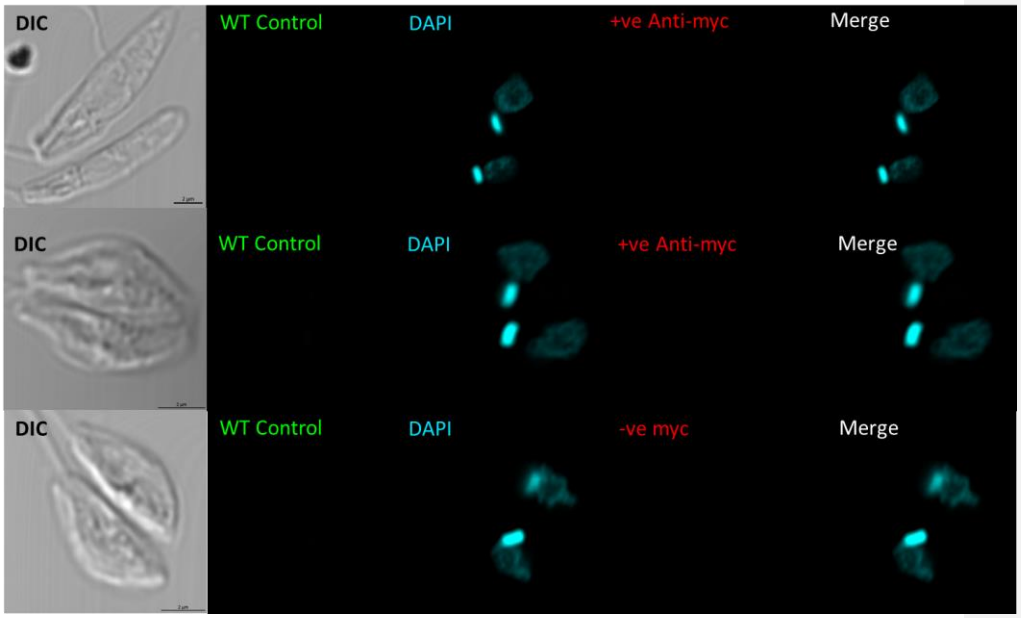

Figure 23 Wild Type Controls: Super resolution confocal microscopy of wild type immunofluorescence controls. Positive controls were treated with a 1 hour incubation myc primary antibody (1:50), negative controls lacked primary antibody. All controls utilised 1:200 secondary antibody. All controls showed no background or auto fluorescence. Scale bar 2 µm.

3.8.2 *Bs*Trett::GFP::myc Associates To the Kinetoplast and Tripartite Attachment Complex

Previously, fluorescence of *Bs*Trett revealed potential kinetoplast localisations. Myc antibodies were utilised to further target the myc tag of the GFP chimera, co-localisations around the kinetoplast and cell posterior were present within expressing cells. However, low level expression of *Bs*Trett::GFP::myc were also detected by the antibody giving diffuse signal within a majority of cells. Whole cell mounts of *C. fasciculata* cells expressing the *Bodo saltans* Trett orthologue were blocked and targeted with mouse anti-myc IgGs and proteomic movement through the cell cycle were captured through confocal microscopy. Airyscan, super-resolution images further confirmed that Trett remains distributed both throughout the mitochondria but also primarily at the kinetoplast. IF produced confirmatory data of the localisation at the kinetoplast (Figure 24; inset panels). S phase cells ($1N^{S}1K$) show foci primarily at the kinetoplast with diffuse mitochondrial localisations elsewhere, myc signals were again concentrated at the kinetoplast. Nuclear mitosis and kinetoplastic division ($2N^{M}1K^{D}$) mounts show typical nabelschnur complexes during division. Interestingly, mitochondrial signal appears recovered and dispersed throughout the mitochondrion. Myc antibodies confirmed presence of *Bs*Trett::GFP::myc with focus again being kinetoplastic. Finally, upon cytokinesis 2N2K cells show a dense concentration of both Trett and myc at the kinetoplast and nucleus.

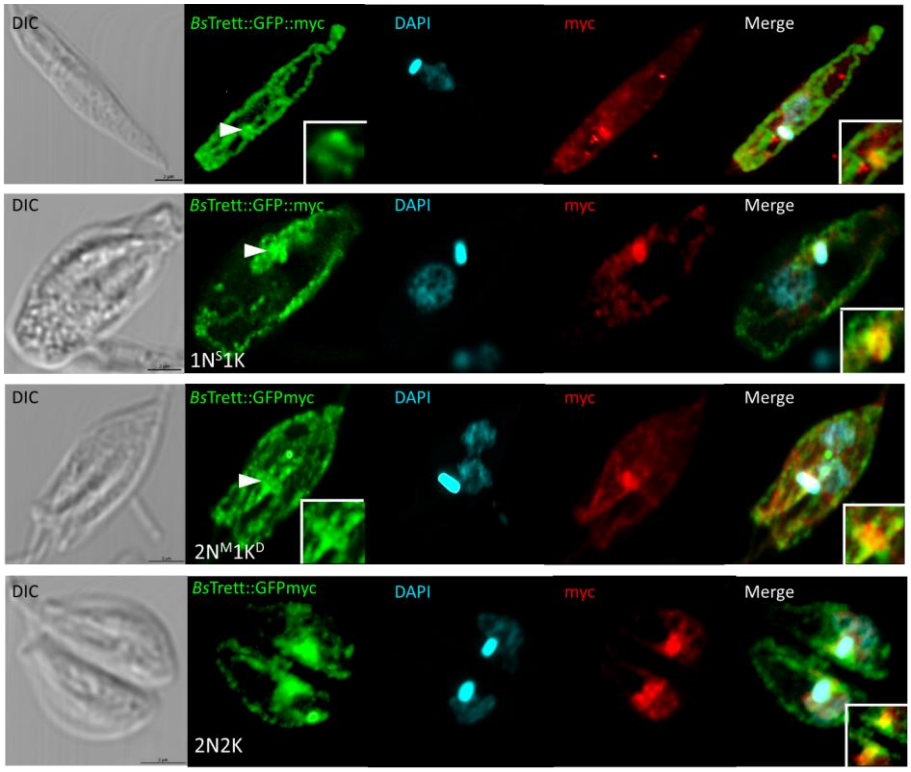

Figure 24 Myc Antibody Targeting of *Bs*Trett in *C. fasciculata*: Myc antibody immunofluorescence of *Bs*Trett::GFP::myc throughout the cell cycle. All inset panels are 2µm across. *Bs*Trett remains distributed throughout the mitochondrion during kinetoplast division and G0 cells. Insets show confirmation of myc GFP colocalisation.

3.8.3 *Bs*TAC65::GFP::myc Localises to the Flagellar Pocket and Basal Body

Following imaging of *Bs*TAC65::GFP::myc fluorescence, targeting of full-length native tubulin with rat YL1/2 IgG was conducted. YL1/2 targets tyrosinated α-tubulin (Andre *et al.*, 2013), which comprises the flagellar pocket, and the basal body allowing more precise localisation of TAC65 within the cell; previous literature describes *Cf*TAC65 as a basal body and kinetoplast associating protein. TRITC conjugated fluorescence of YL1/2 shows the flagellar pocket and the basal body clearly when cells are permeabilised with 0.1% Triton X-100 prior to blocking. A bright puncta at the posterior cell end can be seen indicative of the basal body and some cells exhibited striations indicative of the flagellar pocket. Previously, *Bs*TAC65::GFP::myc signals showed bright puncta at the anterior cell end and along the cell periphery. Dual fluorescence with YL1/2 was utilised to give better insights into these localisations. The flagellar pocket of the cell was revealed with TAC65 signals dual localising down

the full length of the pocket. Additionally, the typical lateral kinetoplast puncta can be seen flanking the kinetoplast top and bottom as-well-as the cell basal body (Figure 25).

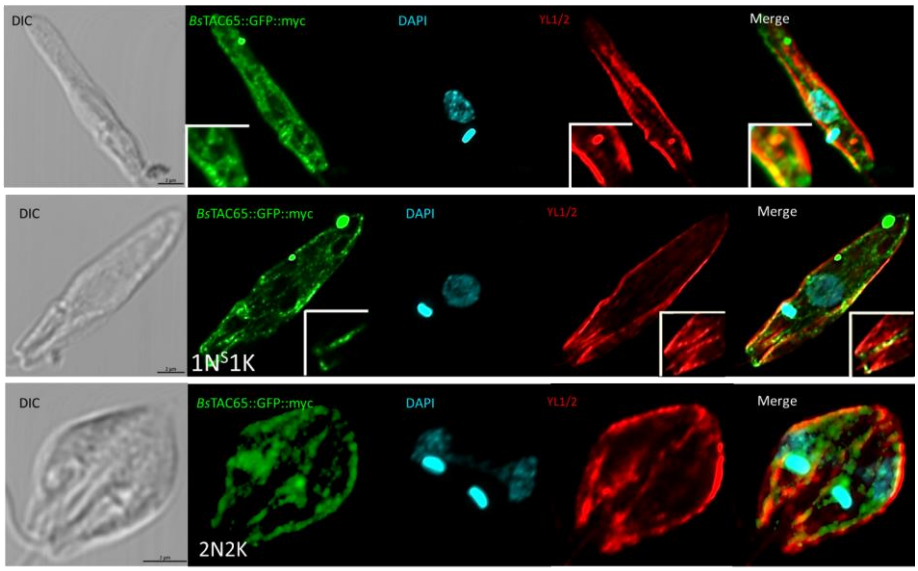

Figure 25 YL1/2 Targeting and *Bs*TAC65 Movement: Top panel – i) *Bs*TAC65::GFP::myc localises close to the flagellar pocket and elongates down the lateral structure. ii) Vibrant puncta are seen at the cell anterior and around the mitochondrial periphery. iii) Fluorescence labelling of tubulin with YL 1/2 confirmed co-localisation to the cell posterior, basal body and distal to the kinetoplast. Bottom panel: Inset YL 1/2 panel identifies the basal body clearly with colocalisation of *Bs*TAC65 to this loci. As before TAC65 appears to focus primarily to the cell posterior but again vibrant puncta are seen at the cell anterior end. Scale bar 2µm.

3.8.4 *Bs*TAC65::GFP::myc Remains at the Kinetoplast throughout the Cell Cycle

Unlike the other TAC associating proteins within this study, the mitochondrial signal of *Bs*TAC65 remains distributed throughout the mitochondrion of the cell and flanks the kinetoplast throughout the cell cycle. 1N1K cells present a signal surrounding the kinetoplast with concentrated signals at the cell anterior (similar to *Bs*Trett). Upon the start of S phase the signal becomes greatly concentrated at the TAC, towards to the cell posterior, before the production of a signal around the nabelschnur complex and bright puncta at the anterior. These dense, signals are present during cytokinesis and flank both *de novo* kinetoplasts (Figure 21). Anti-myc TRITC conjugated antibodies were used to target the chimeric myc tag, yellow puncta around the kinetoplast and the base of the cell are seen within G0 and S phase cells. Additionally, myc antibodies also confirmed some presence of the signal during cell division,

however low levels of myc expression was also detected by the antibodies, as shown by the diffuse signals present within the cell mounts.

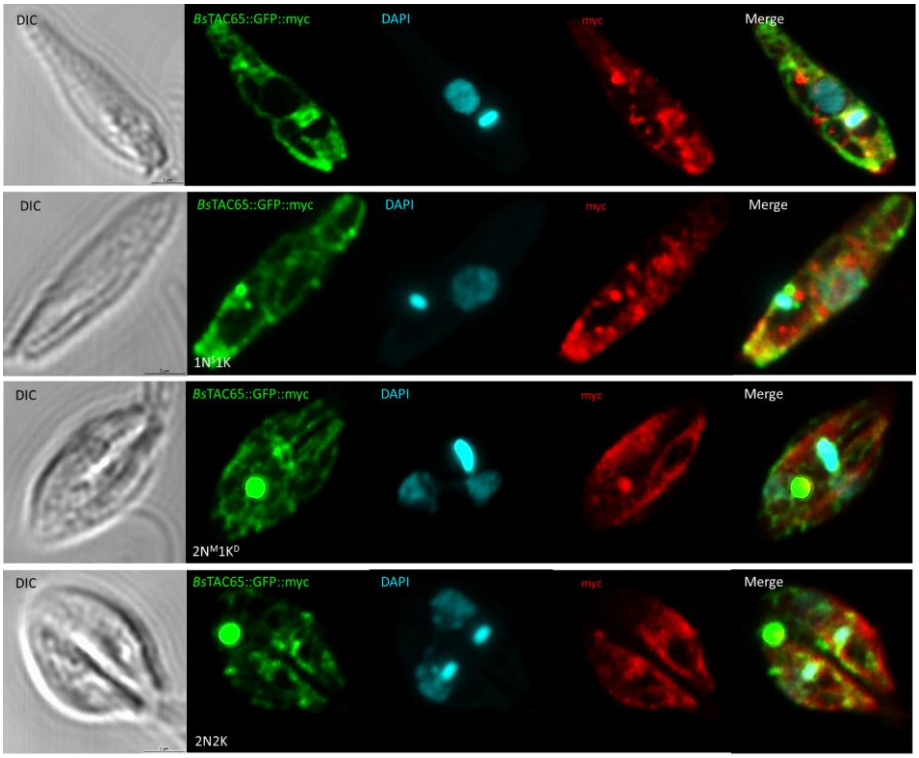

Figure 26 Myc Targeting of *Bs*TAC65 in *C. fasciculata*: Top panel – i) *Bs*TAC65 is distributed throughout the mitochondrion and flanks the kinetoplast. Monoclonal myc antibodies detect low level expression of *Bs*TAC65 with a large concentration around the kinetoplast and the basal body, as confirmed by co-localisation. ii) *Bs*TAC65 shows a bright localisation to the kinetoplast DNA during S phase and signal is concentrated at the flagellar base. iii) A bridge complex is formed between the newly synthesised cell, but *Bs*TAC65 remains distributed throughout both old and new mitochondria, a vibrant GFP puncta is present, and is also seen during cell division. Low level myc is detected within all chimeric GFP expressing cells.

3.8.5 *Bs*TAC60::GFP::myc Stably Associates to the Cell Membrane and Kinetoplast

Following optimisation of cytoskeletal extractions, whole cell mounts were blocked and targeted with primary mouse myc antibodies and secondary anti-mouse TRITC conjugates. *Bs*TAC60 appeared to remain anchored to the cell membrane. Distinct puncta are seen mainly at the mitochondrion periphery. Vibrant puncta also appear around the kinetoplast similar to whole cell mounts. Myc signals were diffuse throughout the cell with some co-localisation, suggesting poor penetrance of the antibody through the cell membrane. Despite the poor penetrance, myc signals are not present within wild type controls, the myc antibody may bind to low level of recombinant protein which produce a diffuse signal within the cell. However, puncta are seen around the kinetoplast and nuclear DNA with some co-localisation at these loci.

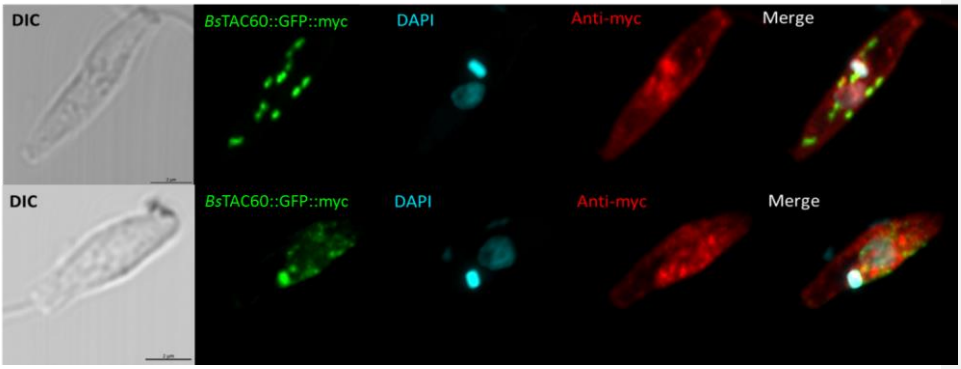

Figure 27 Myc Targeting of *Bs*TAC60 in *C. fasciculata*: Top panel – i) *Bs*TAC60 is distributed towards the mitochondrion periphery. ii) Monoclonal myc antibodies detect low level expression of *Bs*TAC60 with a large concentration around the kinetoplast and nuclear DNA. iii) Merge shows little colocalisation between myc and BsTAC60. Bottom panel: *Bs*TAC60 shows a bright localisation to the kinetoplast DNA and is primarily diffuse throughout the cell. Merge reveals little colocalisation between monoclonal myc antibodies and GFP signals.

3.9 Cytoskeletal Whole Cell Optimisation

3.9.1 Wild Type mounts required optimisation

To identify whether each protein stably associated with insoluble wild type cell components a series of detergent extractions were conducted. 0.2% and 1.0% Triton X-100 in PEME and 0.1% and 1.0% NP40 in PEME exposure for 30 and 60 seconds were tested. The majority of cells showed no or partial extraction with nuclear or kDNA being lysed indicating potential issues with the PEME buffer (Figure 28). Optimisation of cytoskeletal mounts showed that *C.fasciciulata* were relatively resistant to non-ionic surfactant extraction. 0.1% and 1.0% NP40 exposure for 1 minute produced cells which remained

relatively intact or partially extracted cells on wild type controls. Conversely, Triton X-100 mounts were more successful but resulted in complete destruction of the nuclear and kinetoplast DNA.

Fresh PEME buffer was made and a greater success was seen when 1% NP40 in PEME was applied for 30 to 60 seconds (Figure 28) Additionally, for IF of cytoskeletal whole cell mounts, 0.1% Triton X-100 in 1X PBS for five minutes was utilise proving better penetration of the antibodies used within this work.

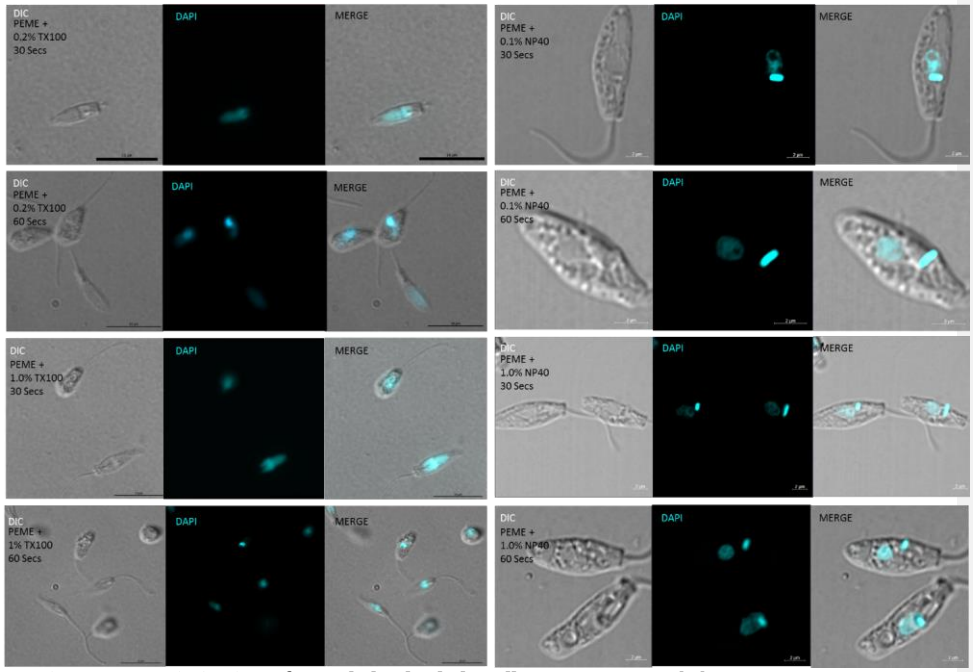

Figure 28 Optimisation of cytoskeletal whole cell extracts: Several detergent concentrations in PEME buffer were prepared and whole cell mounts exposed for 30 and 60 seconds. 1.0% NP40 in PEME proved most successful for whole cell extracts. Images were taken via wide field fluorescence. Scale bar 2 µm.

3.9.2 *Bs*Trett::GFP::myc Localises to the Cell Anterior

After extraction of soluble cell components with PEME and 1% NP40 localisations of the insoluble loci of *Bs*Trett were observed. The kinetoplast and nuclear DNA were full lysed providing little insight into the positioning of the kinetoplast. However, the flagellar pocket remains visible allowing probable deduction of kinetoplast compartment prior to detergent extraction (Figure 29; White arrows). Cytoskeletal mounts revealed a large insoluble granule at the anterior of the cell. Originally, primary observations showed a GFP signal at this position which was dismissed as being the product of a reflective bubble within the mount, closer observations of multiple cytoskeletal mounts revealed the

same morphology and signal within these positions. However, these granular insoluble areas are still unknown. Some extractions exhibited puncta adjacent to the flagellar pocket (possibly antipodal to the kinetoplast), yet this represented a minority of the population (Figure 29).

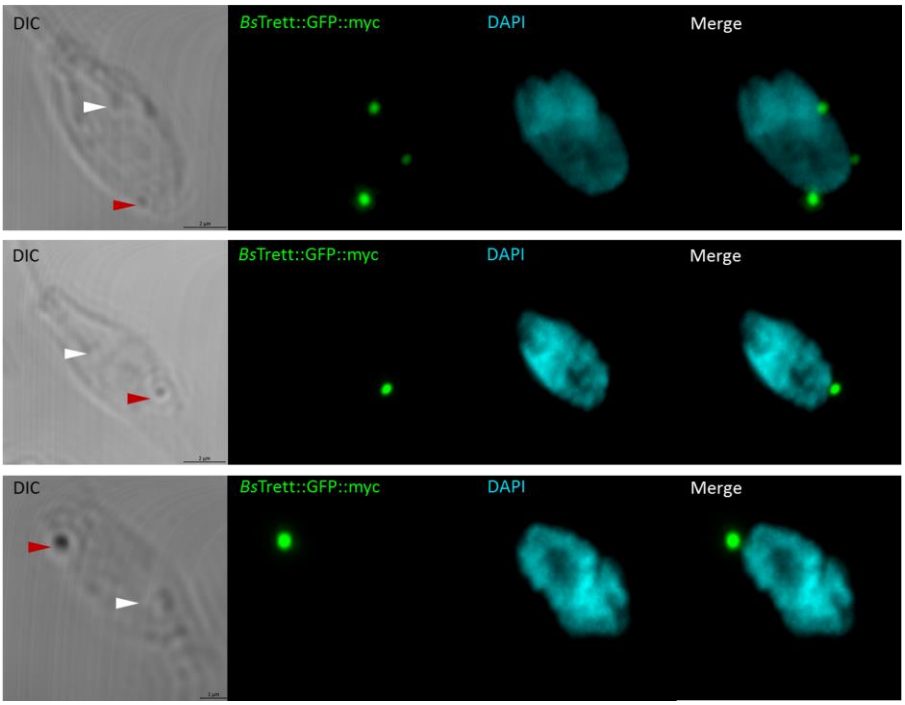

Figure 29 Whole cell mount cytoskeletal extractions of *Bs*Trett::GFP::myc: *Bs*Trett shows a punctate localisation at the anterior cell end. A single a localisations possibly antipodal to the kinetoplast can be seen within the top panel. Nuclear pocket and kinetoplast compartments were fully lysed during extraction. White arrows indicate the base of the flagellar pocket where the kinetoplast usually sits. Red arrows indicate the granular area revealed during extractions.

3.10 *Bs*TAC40::GFP::myc Showed No Expression

Transfections of *Bs*Trett::GFP::myc into *C. fasciculata* were conducted utilising 74 ng / µL DNA but showed little expression within all cell lines. Previous work by R.Reid within our group constructed the recombinant pNUS-GFPcH vector encoding *Bs*TAC40. PCR amplification of the *Bs*TAC40 gene appeared successful, insert DNA and recombinant plasmids appeared to run at the correct size with confirmation by Sanger sequencing (Reid, 2019 - Unpublished). Original cultures appeared to show full mitochondrial signal within her work with a main focus at the Tripartite Attachment Complex. However, subsequent generations of the culture failed to show any GFP signal when analysed by both wide field fluorescence microscopy and laser scanning confocal microscopy.

Following the loss of signal new transfections were performed from *Bs*TAC40 encoding plasmids. The growth of these transfections were slow with extensive death of the culture and poor recovery time possibly due to the poor DNA concentration revealed after NanoDrop™ analysis from *de novo* plasmids resulting in few cells expressing. Additionally, sequence information of *Bs*TAC40-pNUS showed multiple point mutations throughout the *Bs*TAC40 sequence. However, GFP and myc sequences appeared to suffer little mutations and were well annotated. Due to this, localisation of *Bs*TAC40 in transformant cell lines were unsuccessful despite original cultures showing expression.

3.11 Transfection Progeny Show Reduced GFP Expression after Several Generations

The loss of signal within progeny cell lines were apparent across all transfections. *Bs*TAC60 and *Bs*TAC40 expressing *C. fasciculata* cell lines appeared to have the least stable levels of expression. Transfection efficiency with the recombinant plasmids was poor, with dire levels of expressing cells present on mounts. The loss of signal also created difficulty for western blotting cell equivalents. To overcome the poor expression of progeny culture, glycerol stocks were taken in bulk from primary cultures that exhibited expression and new glycerol stock utilised for production of whole cell mounts, western blotting and cytoskeletal extracts. Although inefficient, this method appeared to overcome loss of signal and a greater expression was seen amongst *Bs*TAC65::GFP::myc *Bs*TAC60::GFP::myc and *Bs*Trett::GFP::myc.

3.12 *Bodo saltans* Show Puncta When Targeted with Trett Antibodies

Bodo saltans wild type cultures were cultured and grown for 5 days from passage prior to utilisation for whole cell mounts. Application of the *Bs*Trett C-terminal antibody produced within this thesis revealed several interesting localisations within *Bodo saltans*. First, large vibrant anterior puncta are seen within cells. These puncta appear to have a horse shoe morphology and localise with each other. Second, the puncta appear to localise away from the Pro-kDNA (which appears as a large mass) whereas within *Crithidia fasciculata Bs*Trett localises throughout the mitochondria and to the antipodal sites. Third, the DAPI stain of DNA also revealed bacterial DNA from the growth media, although not detrimental to ascertaining the localisation of Trett, nor identification of the nucleus. However, disruption to overall image quality, and fluorescence intensity is affected. To further confirm functionality of the antibody, further work is required to utilised the antibody on transformant *C, fasciculata* cell lines which carry *Bs*Trett expression. If a similar signal is present to that seen with GFP fluorescence the functionality will be confirmed. Additionally, this study purified second bleeds from Rabbit hosts. Terminal bleed purification will yield greater quantity of anti-sera and present a high IgG quantification for *Bs*Trett targeting.

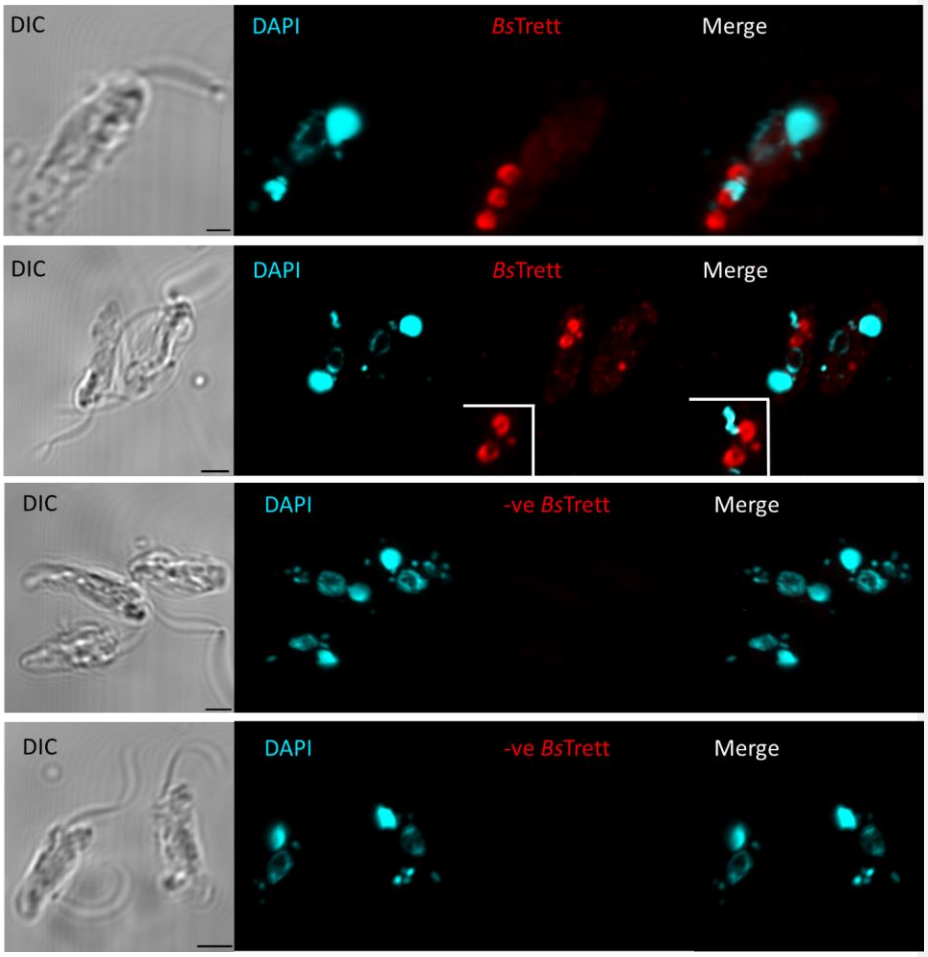

Figure 30 Whole Cell Mounts of *B. saltans* Targeting *Bs*Trett: A antibody specific to the C-terminus of *Bodo saltans* Trett was produced, purified and utilised within this work. Dot like structures were revealed within *B. saltans* at the cell anterior showing a horse shoe like structure. The Pro-kDNA is visable as a distinct round mass and nuclear DNA is more diffuse. DNA of bacteria from the *Bodo* growth media are also present. Negative controls show no non-specific targeting or auto-fluorescence on the same parameters.

4.0 Discussion

4.1 *Bs*Trett Associates With Kinetoplast Antipodal sites and Tripartite Attachment Complex

4.1.1 *Bs*Trett::GFP::myc Shows Antipodal localisations

Bs69260 has previously never been identified nor localised. Within *C.fasciuclata* the kinetoplast is secured to the basal body and flagella via the Tripartite Attachment Complex. This attachment ensures faithful replication of the kDNA throughout the cell cycle where crucial kDNA maturation complexes focussed at the antipodal sites (Povelones, 2014). Localisation of *Bs*Trett within *C. fasciculata* was possible due to the presence of a GFP tag and the DNA identified via staining with DAPI. *Bs*Trett::GFP::myc signals were punctate and present surrounding the kinetoplast DNA at the cell posterior. More interestingly a ring complex presents signals around the kinetoplast (Figures 16 and 20) and antipodal sights, especially within 1N1K and $1N^{S}1K^{D}$ cells. Previous research on minicircle replication by Lui *et al,* 2005 described a rotational movement between the kinetoplast and the antipodal sites in *Crithidia fasciculata, Trypanosoma cruzi* and *Leishmania* sp. which places newly replicated minicircles around the network periphery. The localisation of *Bs*Trett::GFP::myc at the antipodal site suggests a potential for canonical Trett to be involved within kinetoplast division or maturation. Alternatively, the proteomic mechanism leading to kinetoplast rotation is currently undescribed, further investigation into the functionality of *Cf*Trett via RNAi or CRISPR Cas9 could potentially allow divulsion of whether Trett is involved with kinetoplast rotation or translocation. The localisation of the *Bodo saltans* Trett provides important insights into the placement of *B. saltans* in Kinetoplastidea and the evolution of the TAC complex. Bodonids lack a Tripartite Attachment Complex but present a majority of the TAC forming complexes. Moreover, *Bodo saltans* has a Pro-kDNA disc so the presence of these proteins are unsurprising. However, *Tb*Trett localises to the antipodal sites and as *Bodo* lacks a TAC it serves to reason that *Bs*Trett may present a completely diffuse localisation. However, this study shows a focus of the *T. brucei* homologue around the kinetoplast, indicating there may be a possible functionality within mutant cell lines. Additionally, *Bs*Trett concentrates at the *C. fasciculata* kinetoplast, this further exemplifies the close evolutionary relationship between *Bodo saltans* and the parasitic trypanosomatids.

4.1.2 *Bs*Trett::GFP::myc Follows Kinetoplast Movement throughout Division

The positioning of *Bs*Trett throughout the cell cycle also exhibited interesting phenotypes. Log-phase *Crithidia* and newly divided cells present distinct signals correlating with the mitochondrial membrane pattern. However, $2N^{M}1K^{D}$ and 1N1K cells all showed more diffuse *Bs*Trett::GFP::myc signals. Additionally, *Crithidia fasciculata* cells undergoing division showed GFP fluorescence mirroring the kinetoplast position throughout cell division. *Crithidia* which were undergoing kinetoplast replication

produced a bridge complex (nabelschnur) of *Bs*Trett between the two cells, with the pattern mirrored by the kinetoplast. This signal appeared to follow the kinetoplast during cytokinesis and kinetoplast division of vibrant puncta over the kinetoplast DNA was seen within 2N2K cells. Myc targeting via IF showed co-localisation of antibody and Trett at the kinetoplast site confirming kinetoplast localisations which corroborate the hypothesis that *Bs*Trett is a kinetoplast associating protein. Within trypanosomes the basal body acts like centrioles and ensure the faithful replication of the kinetoplast by securing it to the TAC and mitochondrion throughout division. Although signal became diffuse within the mitochondrion for *Bs*Trett cell lines, there was still strong GFP signals at the kinetoplast. GFP signals within cytoskeletal mounts were present, however the complete lysis of nuclear membranes and kinetoplast compartment ultimately meant no signal could be recovered at the sites despite continuous

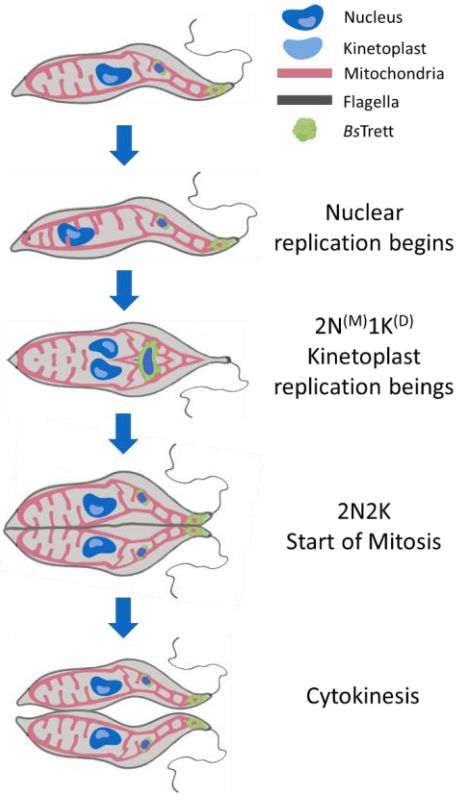

optimisation of the *C. fasciculata* detergent extracts.

Figure 31 Illustrations of BsTrett movement throughout the *C. fasciculata* cell cycle: *Bs*Trett favours antipodal sites of the kinetoplast. As the cell progresses throughout the cell cycle Trett appears focussed to the Tripartite Attachment Complex of the cell. Representative cell components are listed. Nucleus (N), Kinetoplast (K), Mitosis (M) and Division (D). Myc targeting confirmed localisation of *Bs*Trett within this study.

4.1.3 YL 1/2 May Recognise *Cf*RP2 within the Tripartite Attachment Complex

YL1/2 is an antibody classically used to detect α-tubulin epitopes. *Tb*RP2, a protein utilised within tubulin and flagellar assembly and possesses the epitope recognised by the antibody is also present within the golgi bi-lobe and flagellar associating *Tb*RP2 (Andre *et al.*, 2014). Within this piece of work I targeted tyrosinated α-tubulin with YL1/2 antibodies to co-localise *Bs*Trett and *Bs*TAC65 within *C. fasciculata*. Previous work on *Tb*RP2 revealed that a distinct signal present at the basal and pro-basal body were in fact *Tb*RP2 signals, and loss of YL1/2 signals were revealed with RNAi knock-down (Andre *et al.*, 2014). The loss of the YL1/2 signal suggests that the antibodies in fact target *Tb*RP2 instead of tyrosinated α-tubulin. During co-localisation experiments of *Bs*Trett and *Bs*TAC65 with monoclonal YL1/2 antibodies, basal body movement can be tracked with YL1/2 potentially localising *Cf*RP2 (Figure 21, Sup 1-3). A distinct basal body signal is visible within G0 cells, but a TAC associated localisation is seen during kinetoplast division and replication. Moreover, a signal flanking the kinetoplast is visible within $1N^{S}1K$ cells and during cytokinesis mirroring what is observed within *T. brucei* (Sup 3). Clustal alignment of this region between *C.fasciulata* RP2 and *T. brucei* RP2 revealed homologous areas between both proteins. As RP2 appears to be recognised by YL1/2, signals present may not be the basal body but in fact recognising the DDF epitope present in *Cf*RP2 (Sup 2). Regardless, even if YL1/2 recognises *Cf*RP2, the Tripartite Attachment Complex and flagellum are still revealed due to the presence of α-tubulin within these regions and RP2 role within flagellar maturation. However, as *Cf*RP2 is not the main focus of this work, more in-depth analysis of the protein is required, including direct analysis of the *Cf*RP2 protein, *Cf*RP2 localisation and knock-down studies. Whether or not the YL1/2 is detecting α-tubulin or *Cf*RP2 is not crucial for this study as both would result in basal body fluorescence which still allows determination of the Tripartite Attachment Complex and therefore *Bs*Trett::GFP::myc and *Bs*TAC65::GFP::myc. Although late cell cycle images of *Bs*Trett show a purely kinetoplast associated signal, a basal cell end association is seen within G0 cells and also at the start of kinetoplast division, indicating that Trett may be involved with kinetoplast segregation of maturation. However, this study employed a *Bodo saltans* orthologue, the functionality of this orthologue within *C. fasciculata*, or other trypanosomatids (*Trypanasoma sp.; Leishmania sp.*)

4.1.4 Detergent Extracts Show Cell Anterior Localisations

Following targeting of *Bs*Trett::GFP::myc with anti-myc polyclonal antibodies, whole cell extracts were performed to localise the protein within the cell. However, due to the nature of the non-ionic surfactants, lysis of the nuclear membrane and kinetoplast was seen within cell mounts, or a ballooning of cells. Although the kinetoplast and nucleus cannot be localised within the images presented here (Figure 29) the base of the flagellum where the kinetoplast and basal body sit are revealed (Figure 29: white arrows). Surprisingly, no signal at the flagellar base or the hypothetical kinetoplast position is present (possibly due to the lysis of these cellular compartments through over exposure) but an anterior signal is present.

Additionally, the Differential Interference Contrast (DIC) images provide little insight into the localisation of the *Bs*Trett::GFP::myc as subcellular structures were destroyed.

4.2 *Bs*TAC65::GFP::myc Surrounds the Kinetoplast

*Tb*TAC65 has previously been observed to colocalise with pATOM36 in *T. brucei* at the basal body and forms a dot like structure lateral of the kinetoplast (Käser *et al.*, 2016). Additionally, the same study described the pATOM26/TAC65 complex associating strongly with the Tripartite Attachment Complex and stably associates with isolated flagella. *Tb*TAC65 knockouts reduced the overall health of the cultures but also caused kDNA missegregation (Käser *et al.*, 2016). A complex is formed with pATOM36 which is diffuse throughout the mitochondrion. TAC65 localises at the kinetoplast where it stably associates with the basal body, pATOM36 and the flagellar base. Interestingly, *Bodo saltans* TAC65 utilised within this study appears to be diffuse throughout the mitochondrion and localises laterally to the kinetoplast of *C. fasciculata* similar to observations in *T. brucei.* The diffuse signal seen throughout the mitochondrion of *C. fasciculata* provides insights into the evolutionary development of the TAC. The *B. saltans* orthologue produces a signal indicating potential co-localisation and association with *Cf*pATOM36 indicating that the role of TAC65 has become more refined as the Tripartite Attachment Complex has developed in the trypanosomatids. Moreover, fluorescence of C-terminally tagged GFP showed potential localisation to the basal body of the cell.

Basal body targeting with YL1/2 showed *Bs*TAC65::GFP::myc not only associates laterally to the kinetoplast poles, but also localises to the basal body of the cell similar to canonical *Tb*TAC65. As mentioned before, TAC65 localises with isolated flagellar stably, localisations of *Bs*TAC65::GFP::myc showed localisation down the full length of the flagellar pocket during nuclear S-phase and cytokinesis. All stages of the cell cycle revealed signals were diffuse throughout the mitochondria but remained concentrated at the flagellar poles. Cytoskeletal extracts of *Bs*TAC65::GFP::myc were inconclusive possible due to the low expression rate of the protein and loss of signal after several generations.

4.3 *Bs*TAC60::GFP::myc is Diffuse within the Mitochondria

The mitochondria are fundamental to eukaryotic cells and are managed by a distinct array of voltage dependant anion channels (VDACs). The import of outer mitochondrial proteins are managed by VDACs and are frequently used to determine whether a protein anchors to the inner or outer mitochondrial membrane. *Tb*TAC60 relies on ATOM40 for import and anchoring into the outer mitochondrial membrane and is crucial for TAC function. *Tb*TAC60 appears to be distributed throughout the mitochondrion of the *T. brucei* and associates stably with isolated flagellum between the kDNA disc and the flagellum. Loss of TAC60 produces diskinetoplasty but no effect on cell growth (Käser *et al.*, 2017). *Bs*TAC60 is distributed evenly throughout the mitochondrion of *C. fasciculata*. However, some punctate localisations are present. *Bs*TAC60 appears to localise strongly to the

mitochondrion periphery and the kinetoplast of the cell reflecting that of the *Tb*TAC60. Furthermore, targeting of *Bs*TAC60::GFP::myc with anti-myc IgGs show colocalisation to the kinetoplast but also indicate low level expression throughout the mitochondria. Transfection efficiency of *Bs*TAC60 was low and most of the population exhibited no signal. The low expression levels within transfected cell lines was corroborated by Western blot analysis which showed low levels of expressions in comparison to *Bs*Trett and *Bs*TAC60. As with all the proteins investigated within this study, *Bs*TAC60 showed GFP fusion protein cleavage.

4.4 *Bs*TAC40 Requires Further Investigation

Like *Tb*TAC60, *Tb*TAC40 localises to the outer mitochondrial membrane acting as a VDAC-like porin. Previous work on the β-barrel protein TAC40, shows it complexes with TAC60 and TAC42. Five β-barrel mitochondrial outer membrane proteins have been previously identified within *T. brucei*, *Tb*Sam50, a *T. brucei* VDAC and ATOM40 and two additional porins (including TAC40). TAC40 cannot be grouped into any of the three subclasses of porin (TOM40, VDAC or MDM10), as functional analysis does not permit it (Kornmann and Walter, 2010; F. Schnarwiler *et al.*, 2014; Schneider and Ochsenreiter, 2018). Instead, TAC40 is currently classed as an integral member of the Tripartite Attachment Complex, linking the kDNA to the basal body. Within *Sacchromyces cerevisiae* mitochondria divide and fuse when propagating a new cell requiring a system to allow duplication and movement of the mitochondria and the mtDNA during budding (F. Schnarwiler *et al.*, 2014). The faithful replication of the mitochondrial genome bares striking similarities to the Tripartite Attachment Complex of the trypanosomatids. The three-membrane-spanning complex (TMS) of *S.cerevisiae* serves to faithfully replicate the yeast mtDNA connecting the endoplasmic reticulum to mitochondrial nucleoids (Kornmann and Walter, 2010). This endoplasmic reticulum-mitochondria encounter structure (ERMES) has several trypanosomatid orthologues, *Sc*MDM10 and *Sc*TOM40 are both crucial for DNA inheritance. In yeast MDM10 connects actin to mitochondrial DNA, whereas in Trypanosomes TAC40 mediates basal body and kDNA linkage (Figure 32). Despite their similarities TAC40 is not orthologous to MDM10, nor TOM40 and presents no co-localisation in *Trypanosoma brucei*.

Within this study I attempted to localise a *Bodo saltans* orthologue of TAC40 in *Crithidia fasciculata*, transfection efficiency was low with few cells showing expression. The recombinant pNUS-GFPcH vector encoding BSAL_82500 (*Bs*TAC40) was analysed via Sanger sequencing using two reverse primers to amplify the full length of TAC40. Initial sequences showed many point mutations and poor alignment to *Bs*TAC40, the GFP encoding region was well annotated with little discrepancy to the sequence. Sequences with both primers confirmed *Bs*TAC60, *Bs*TAC65 and *Bs*Trett all contained the appropriate sequence with GFP and myc tags. *Bs*TAC40, showed systemic point mutations throughout the sequence, though GFP and myc tags were all present with no alterations. The multiple mutations within TAC40 explain why no signal can be detected within the cells and the low level expression of

GFP seen within whole cell equivalents. The mutations within the plasmid can render the protein non-functional and prevent correct folding, expression and mitochondrial export.

Despite Western Blot analysis showing basal levels of TAC40 expression, few GFP expressing cells were visible on whole cell mounts and localisation of the protein was not possible. Optimisation of the transfection protocol for *C. fasciculata* is required to give greater transfection efficiency of the vector. Original work on TAC40 showed some localisation to the mitochondria and a concentration by the TAC (Reid, 2019 Unpublished), GFP signal is lost following multiple cell divisions so this work could not be corroborated. The point mutations visible within the sequence data will also be factor in the poor signal detected within transformant cell lines. Due to this, *Bs*TAC40 requires further work to confirm the localisation of the orthologue though preliminary data indicates it mirrors localisations seen by *Tb*TAC40.

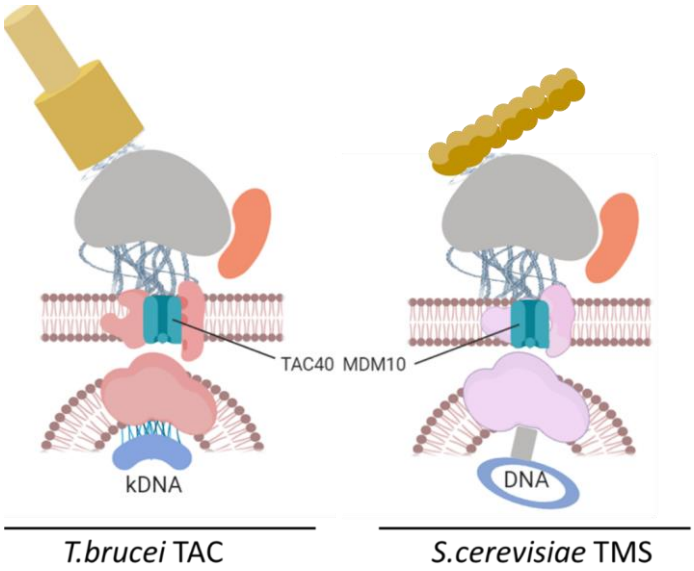

Figure 32 Comparison of the TAC and TMS within T. brucei and Saccharomyces cerevisiae: TAC40 and MDM10 are both outer membrane proteins which serve a vital role in DNA inheritance within the cells. Despite their identical function and similarity, TAC40 and MDM10 are not orthologues.

4.5 GFP::myc Is Truncated and Unstable

A modified pNUS-GFPcH vector was utilised for production of recombinant protein expression within this study. The vector features a C-terminal GFP fusion protein flanked by a N- and C-terminal myc tag for immunofluorescence localisation. Additionally, ampicillin and hygromycin B resistance were carried by the vector. Polyclonal mouse IgG targeting the myc tag were utilised for Western blots of

whole cell equivalents showed bands approximately 29 kDa myc::GFP::myc which is approximately 29 kDa (Figure 28). Cleavage of the fusion proteins is unsurprising giving the nature of the *Leishmania* and *Crithidia* proteasome. In 2006, a paper focussed on LmjKIN13-1 (a kinesin involved in nuclear mitosis), showed that post mitosis, proteolytic degradation of transfected proteins were abundant (Dubessay *et al.*, 2006). Furthermore, western blot analysis of *L.donovani* promastigotes showed recombinant proteins with a GFP fusion tag were actively cleaved in the stationary growth phase. Other studies have utilised protease inhibiters to prevent opportunistic degradation of the fusion proteins (Savoia, Allice and Tovo, 2005; Dubessay *et al.*, 2006; Kumar, Sundar and Singh, 2007).

As well as the truncation of the GFP fusion protein, photo bleaching of the GFP chromophore occurred frequently after low level laser exposure possibly due to the high energy carried by green light wavelengths. Recent developments with the mFruits series of fluorescent proteins have produced more resilient fluorophores which exhibit resistance to photo bleaching (Shaner *et al.*, 2004). Red fluorescent proteins (RFP) appeared to be more resistant to photobleaching than previous GFP and EGFP fluorophores (Day and Davidson, 2009) with several proponents arguing a shift away from GFP. However, more recent studies have shown EGFP has lower photobleaching rates than RFP in live cell imaging of HEK cells (Drobizhev *et al.*, 2009, 2014).

4.7 *Bodo saltans* Trett IgG is Possibly functional

Small scale protein expression and analysis via western blot confirmed overall functionality of the antibody produced and purified within this thesis. The same antibody which recognises canonical *B. saltans* Trett was utilised for localisation of Trett within *B. saltans* wild type cells. As *Bodo saltans* is the common ancestor of the trypanosomatids some similarities were expected between work previously done in *T. brucei* on the protein (Unpublished). Surprisingly, little similarities were detected, *Bs*Trett appears to form a scaffold within *Bodo saltans* indicating a structural role – as the protein localises to the TAC super-structure this was expected. Currently, this thesis is the first to describe Trett and insinuate its role as a structural protein within the Kinetoplastidae organisms. Trett appears conserved amongst the trypanosomes indicating an important structural role within the organism. However, due to time constraints the functionality of the protein was not investigated.

The distinct horse-shoe structure of *Bs*Trett, and repetition shows an organised structure which co-localises partially with nuclear DNA. The association with nuclear DNA may explain the close association with the kinetoplast within the trypanosomes, but also indicates that *Tb*Trett has evolved a primary function to serve kinetoplast DNA in a currently unknown manner – this obviously giving great scope for future work.

4.6 Bioinformatic Analysis of *B. saltans* Orthologues Provide Evolutionary Insights

The kinetoplastids are named after their disc-shaped mitochondrial DNA cassette – the kinetoplast. The best studied of these organisms are the obligate parasites, *Leishmania* and *Trypanosoma* which contribute to devastating mammalian diseases (Sibbald *et al.*, 2017; Tanifuji *et al.*, 2017). Recently the mitochondrial genome data for *Trypanosoma brucei* (TREU927) was analysed and hypothetical proteins revealed (Zhang *et al.*, 2010). BLASTP analysis of the *B. saltans* transcriptome against the *Tb*MitoCarta revealed 2,087 acquisitions of potential homology within *Bodo saltans.* As well as *B. saltans* (Lake Konstans), *Leishmania major (freidlin), Crithidia fasciculata (Cf-cl*), *Trypanoplasma borreli* and *Perkinsela sp. w*ere analysed giving insight into the evolutionary pathway of the parasitic kinetoplastids.

Recently, an effort has been made to sequence the mitochondrial genomes of these organisms. The enslaved amoeba endosymbiont *Perkinsela* is a relatively understudied kinetoplast with several distinct phenotypical features including a lack of flagella, singular outer membrane and glycosomes. *Perkinsela* is an endosymbiont of the *Paramoeba* genus amoeba with a significantly reduced genome size when compared to *Bodo saltans* and the parasitic trypanosomatids (Harmer *et al.*, 2018). Studies in Perkinsela show it coevolves with its host and has a reduce genome reflective of it symbiotic relationship (Nowak and Archibald, 2018). Despite the now well annotated genome, *Perkinsela* revealed no homology to other Kinetoplastids when analysed via tBLASTn within this work possibly due to having fewer protein-coding genes than *Trypanosoma brucei* (Table 16) or a result of the lack of in-depth sequencing and genome projects on the organism. Moreover, most of the analysis resulted in an empty database which was surprising giving it possesses some classical morphological traits of the kinetoplasts. Including, a kinetoplast, a singular large mitochondria and lead trans splicing (Sibbald *et al.*, 2017). *Trypanoplasma borreli* has one of the larger repertoire of protein-coding genes of the Kinetoplastids analysed within this study. *T. borreli* is a parasite of common carp (*Cyprinus carpio*). The full transcriptome was assembled in 2017 by Carrington *et al.*, and was utilised within this thesis as a representative of the lower branching *Kinetoplastida* organisms.

Despite having 13,640 putative proteins greater than 100 amino acids in length, *T. borreli* had 413 proteins revealing an empty database or with low homology to *T. brucei*. *Bodo saltans* is the common ancestor of the obligate parasitic trypanosomatids, and is more closely related than *T. borreli* (Simpson, Lukes and Roger, 2002; Cavalier-Smith *et al.*, 2014; Opperdoes *et al.*, 2016; Lukeš *et al.*, 2018). The close evolutionary relationship between the free-living ancestor and its parasitic cousins is echoed within this work. Lower branching Kinetoplastidae (*Perkinsela sp.* and *Trypanoplasma borreli)* show little homology to *T. brucei*, but homology increases within higher branching organisms, revealing several potential; future candidate proteins. Indeed, *T. borreli* and *Perkinsela* are relatively understudied

and further work is required to assemble their proteome, but tBLASTn did still result in potential candidates. *Bodo saltans* presents itself with minicircles that form small catenanes in dimers or trimers (Blom *et al.*, 2000). The orthology between *B. saltans* and *T. brucei* was substantial within this work with 621 of the 862 acquisitions analysed being potential *T. brucei* orthologues. Unsurprisingly *Leishmania major* and *Crithidia* both had vast orthology and homology to *T. brucei*, again reflecting their close relationship and position within the trypanosomes.

The positioning of each organism in the current phylogenetic model is reflected within this study. The more evolutionary divergent organisms (*Perkinsela* and *Trypanoplasma borreli*) show a reduced amount of orthology to *T. brucei* in comparison to those more closely related organisms. We also see a reduction in nuclear DNA quantity in higher branching organisms due to the removal of large expanses of non-coding DNA within *Bodo saltans* and *T. borreli* including a greater occurrence of moonlighting capabilities within the obligate parasites (Ginger, 2014; Jackson *et al.*, 2016). *Crithidia fasciculata* represents a morphologically distinct outgroup of the trypanosomatids possibly explaining is larger number of protein-coding genes being similar to that of *T. brucei* despite being more recently evolved than *Leishmania*. The analysis of the *B. saltans* transcriptome within this work has revealed several putative mitochondrial proteins which appear to be conserved within the representative genera which can be utilised and analysed further in future work. As the discovery and complete bioinformatic analysis was not the focus of this work this was not conducted.

Organism	DNA Amount (Mbp)	Protein-Coding Genes	Source
Trypanosoma brucei	77.9	9,598	Lukeš *et al.*, 2018
Leishmania major	32.3	8,272	Ivens, 2005; Harmer *et al.*, 2018
Crithidia fasciculata	32.6	9,489	Beverley *et al*, 2015
Bodo saltans	39.8	18,943	Harmer *et al.*, 2018
Trypanoplasma borreli	51.6	13,640	Carrington *et al.*, 2017; Lukeš *et al.*, 2018
Perkinsela sp.	9.5	5,252	Lukeš *et al.*, 2018

Table 16 Genome size and predicted number of protein-coding genes within each organism studied within this thesis: *C. fasciculata* data was obtained from data uploaded www.tritrypdb.org by Beverley *et al*, in 2015 - Unpublished.

Orthologue E-value totals	*T. brucei 927*	*L. major* Friedlin	*C. fasciculata*	*B. saltans*	*T. borreli*	*Perkinsela sp.*
<E-10	858	805	801	621	267	0
<E-4 to >E-10	3	15	21	76	31	0
>E-4	1	42	40	165	564	862
Total	862	862	862	862	862	862

Table 17 Amount of each acquisition separated by E-value of homology of each organisms studied within this work: *T. brucei* was compared to itself to give insight into the sequence quality being used.

5.0 Further Work

Indeed, the work presented within this thesis show the localisations of *Bodo saltans* orthologues of TAC65, TAC60 and Trett within *C. fasciculata*, with puncta present at the expected loci for each orthologue additional work is still required. All three Tripartite Attachment Complex proteins (65, 60 and 40) were constructed by R. Reid within our group for protein localisation studies; antibodies for each of these proteins are required for localisation within *Bodo saltans* to investigate its canonical localisation. Production of the antibodies can be prepared following the protocols presented throughout this body of work and that IF of fixed *Bodo saltans* cell lines. Production of C-terminal constructs encoding a 6XHis-tag™, induction of the recombinant proteins via an appropriate pET vector and purification with NiNTA would allow a thorough investigation to the localisation of these TAC and kinetoplast associated proteins within *Bodo saltans.* Removal of the soluble cell components with a PEME-NP40 solution would also allow more exquisite investigation to the true loci of these proteins in *Bodo saltans.*

The functionality of these proteins too is yet to be assessed, protein knockout via CRISPR/Cas9 of the proteins within *Bodo saltans* could yield promising insights into the role of these proteins within the cell. Trett has been shown to follow kinetoplastic movements throughout the cell cycle, ablation of Trett could result in distruption of kDNA segregation. Confirmation of true role of Trett could be conducted in *C. fasciculata*, knockdown of *Cf*Trett and recovery with *Bs*Trett could show whether Trett orthologues are functional within *Crithidia fasciculata* , functionality of this protein could give possible indicators into the importance of Trett within the trypanosomes and information of the evolutionary pathway taken by the obligatory parasites.

As previously stated, *Bodo saltans* lacks a Tripartite Attachment Complex. Within *T. brucei* TAC65 ablation effected the overall health of the cultures, knockout of the *Bodo saltans* orthologue could raise further insights into the evolutionary role of this protein. Additionally, TAC65 forms a complex with pATOM35 in *T. brucei*, co-localisations of the *Bs*pATOM35 within the TAC and throughout the outer mitochondrial membrane. *Bs*pATOM35::mOrange::myc (or any other mFruit monomeric fluorescent protein (Shaner, 2013)) recombinant protein could be expressed and purified for an antibody to be produced to infer colocalisation within *Bodo saltans.* CRISPR Cas9 of these proteins *Crithidia* or *Leishmania* and recovery with the *Bodo* orthologues could again provide information of the protein

functionality, but also indicate the TAC evolution beginning within *Bodo saltans* as indicated by its placement as the divergent ancestor of the parasitic trypanosomatids.

TAC40 and TAC60 are indicated within the literature to result in cell cycle arrest when knocked-down via RNAi. Construction of synthetic siRNA targeting *Bs*TAC40 AND *Bs*TAC60 should theoretically result in kDNA misregulation and cell cycle arrest as seen within *T. brucei* (Felix Schnarwiler *et al.*, 2014). Furthermore, knockdown and recovery studies similar to that proposed for TAC65 could also be conducted again to yield greater functional information about the relationship between *Bodo saltans* and the trypanosomatids.

Finally, the *Bs*Trett antibody produced within this thesis utilised the second bleed from two Rabbits. The terminal bleed was not purified due to time constraints but future work should seek to purify the anti-sera to gain a higher yield of anti-*Bs*Trett. The functionality of this further needs to be tested through application on *C. fasciculata* transformants expression *Bs*Trett. If merge reveals co-localisation of the antibody and *Bs*Trett the overall functionality of the antibody can be considered confirmed. Moreover, an additional western blot utilising *Bodo saltans* whole cell equivalents should also be performed and *Bs*Trett antibodies utilised as a primary. The steps outlined within this work can then be followed to confirm whether Trett is revealed through chemiluminescence.

6.0 Concluding Remarks

This thesis sought to probe the localisation and function of a novel Kinetoplast associated protein (here named *Bs*Trett) as discovered by bioinformatic analysis prior to the conceptualisation of this work. Furthermore, the localisation of *Bs*TAC40, *Bs*TAC60, and *Bs*TAC65 were probed to varying degrees of success within *C. fasciculata*. A *Bs*Trett antibody was produced and purified for *in vivo* targeting of the protein within *Bodo saltans* to allow future comparative analysis of the localisation of the protein to its *T. brucei* counterpart.

Furthermore, this body of work showed the localisation of *Bs*Trett is surprisingly different to that of its cousins yet still appears to form a structural role explaining its association to the Tripartite Attachment Complex. Antibodies produced showed functionality as demonstrated by western blot analysis and their application within co-localisation studies presented here, but further work is needed to concretely confirm this.

*Bs*TAC65 and *Bs*Trett were tagged with a chimeric GFP::myc tag and appeared to primarily localise to the kinetoplast within *C. fasciculata* mirroring the positioning of the protein within *T. brucei.* Due to time restraints the functionality of the proteins were not analysed, thus allowing room for future work with each protein. *Bs*TAC60 showed promising diffuse mitochondrial signalling similar to that of the *T. brucei* orthologue. All plasmids showed successful insertion of each gene, barring TAC40 which had multiple point mutations indicating the poor expression rates seen within samples. GFP expression was confirmed for each sample with greater expression within *Bs*TAC65 and *Bs*Trett. *Bodo saltans* lacks a Tripartite Attachment Complex but presents orthologues of each TAC associating protein. Differences between the peptide sequences of the parasitic TAC components and the free-living counterparts do exist however the localisations here indicate the starting formation of the TAC and therefore give potential future avenues for the rise of parasitism.

7.0 Works Cited

Abeliovich, H., Tzfati, Y. and Shlomai, J. (1993) 'A trypanosomal CCHC-type zinc finger protein which binds the conserved universal sequence of kinetoplast DNA minicircles: isolation and analysis of the complete cDNA from Crithidia fasciculata.', *Molecular and cellular biology*, 13(12), pp. 7766–73.

Alcolea, P. J. *et al.* (2014) 'An Insight into the Proteome of Crithidia fasciculata Choanomastigotes as a Comparative Approach to Axenic Growth, Peanut Lectin Agglutination and Differentiation of Leishmania spp. Promastigotes', *PLoS ONE*. Edited by Y. M. Traub-Csekö, 9(12), p. e113837. doi: 10.1371/journal.pone.0113837.

Andre, J. *et al.* (2013) 'The tubulin cofactor C family member TBCCD1 orchestrates cytoskeletal filament formation', *Journal of Cell Science*, 126(23), pp. 5350–5356. doi: 10.1242/jcs.136515.

Andre, J. *et al.* (2014) 'An Alternative Model for the Role of RP2 Protein in Flagellum Assembly in the African Trypanosome', *Journal of Biological Chemistry*, 289(1), pp. 464–475. doi: 10.1074/jbc.M113.509521.

Aphasizhev, R. and Aphasizheva, I. (2014) 'Mitochondrial RNA editing in trypanosomes: Small RNAs in control', *Biochimie*, 100, pp. 125–131. doi: 10.1016/j.biochi.2014.01.003.

Blom, D. *et al.* (1998) 'RNA editing in the free-living bodonid Bodo saltans.', *Nucleic acids research*, 26(5), pp. 1205–13.

Blom, D. *et al.* (2000) 'Mitochondrial minicircles in the free-living bodonid Bodo saltans contain two gRNA gene cassettes and are not found in large networks.', *RNA (New York, N.Y.)*, 6(1), pp. 121–35. Available at: http://www.ncbi.nlm.nih.gov/pubmed/10668805.

Bonhivers, M. *et al.* (2008) 'A monoclonal antibody marker for the exclusion-zone filaments of Trypanosoma brucei.', *Parasites & vectors*, 1(1), p. 21. doi: 10.1186/1756-3305-1-21.

Borghi, S. M. *et al.* (2017) 'Leishmania infection: painful or painless?', *Parasitology Research*, 116(2), pp. 465–475. doi: 10.1007/s00436-016-5340-7.

Botero, A. *et al.* (2018) 'The kinetoplast DNA of the Australian trypanosome, Trypanosoma copemani , shares features with Trypanosoma cruzi and Trypanosoma lewisi', *International Journal for Parasitology*, 48(9–10), pp. 691–700. doi: 10.1016/j.ijpara.2018.02.006.

Brugerolle, G., Lom, J., Nohỳnkovà, E., & Joyon, L. (1979) 'Comparison et evolution des structures cellulaires chez plusiers éspeces de Bodonides et Cryptobiides appartenant genres Bodo, Cryptobia et Trypanoplasma', *Protistologica*, 15, pp. 197–221.

Carrington, M. *et al.* (2017) 'Transcriptome Sequence of the Bloodstream Form of Trypanoplasma borreli, a Hematozoic Parasite of Fish Transmitted by Leeches.', *Genome announcements*, 5(9). doi: 10.1128/genomeA.01712-16.

Cavalier-Smith, T. *et al.* (2014) 'Multigene eukaryote phylogeny reveals the likely protozoan

ancestors of opisthokonts (animals, fungi, choanozoans) and Amoebozoa', *Molecular Phylogenetics and Evolution*, 81, pp. 71–85. doi: 10.1016/j.ympev.2014.08.012.
Cavalier-Smith, T. (2016) 'Higher classification and phylogeny of Euglenozoa', *European Journal of Protistology*, 56, pp. 250–276. doi: 10.1016/j.ejop.2016.09.003.
Dacks, J. B. *et al.* (2016) 'The changing view of eukaryogenesis - fossils, cells, lineages and how they all come together.', *Journal of cell science*, 129(20), pp. 3695–3703. doi: 10.1242/jcs.178566.
Day, R. N. and Davidson, M. W. (2009) 'The fluorescent protein palette: tools for cellular imaging', *Chemical Society Reviews*, 38(10), p. 2887. doi: 10.1039/b901966a.
Drobizhev, M. *et al.* (2009) 'Absolute Two-Photon Absorption Spectra and Two-Photon Brightness of Orange and Red Fluorescent Proteins', *The Journal of Physical Chemistry B*, 113(4), pp. 855–859. doi: 10.1021/jp8087379.
Drobizhev, M. *et al.* (2014) 'Multiphoton Photochemistry of Red Fluorescent Proteins in Solution and Live Cells', *The Journal of Physical Chemistry B*, 118(31), pp. 9167–9179. doi: 10.1021/jp502477c.
Dubessay, P. *et al.* (2006) 'Cell cycle-dependent expression regulation by the proteasome pathway and characterization of the nuclear targeting signal of a Leishmania major Kin-13 kinesin', *Molecular Microbiology*, 59(4), pp. 1162–1174. doi: 10.1111/j.1365-2958.2005.05013.x.
Fenn, K. and Matthews, K. R. (2007) 'The cell biology of Trypanosoma brucei differentiation', *Current Opinion in Microbiology*, 10(6), pp. 539–546. doi: 10.1016/j.mib.2007.09.014.
Fidalgo, L. M. and Gille, L. (2011) 'Mitochondria and Trypanosomatids: Targets and Drugs', *Pharmaceutical Research*, 28(11), pp. 2758–2770. doi: 10.1007/s11095-011-0586-3.
Flegontov, P. *et al.* (2013) 'Paratrypanosoma Is a Novel Early-Branching Trypanosomatid', *Current Biology*, 23(18), pp. 1787–1793. doi: 10.1016/j.cub.2013.07.045.
Galvez Rojas, R. L. *et al.* (2008) 'l-Proline uptake in Crithidia deanei is influenced by its endosymbiont bacterium', *FEMS Microbiology Letters*, 283(1), pp. 15–22. doi: 10.1111/j.1574-6968.2008.01125.x.
Gažiová, I. and Lukeš, J. (2003) 'Mitochondrial and Nuclear Localization of Topoisomerase II in the Flagellate Bodo saltans (Kinetoplastida), a Species with Non-catenated Kinetoplast DNA', *Journal of Biological Chemistry*, 278(13), pp. 10900–10907. doi: 10.1074/jbc.M202347200.
Ginger, M. L. (2014) 'Protein moonlighting in parasitic protists.', *Biochemical Society transactions*, 42(6), pp. 1734–9. doi: 10.1042/BST20140215.
Gould, M. K. (2009) *Putative phosphodiesterase inhibitors as potential new chemotherapies against African Trypanosomiasis*. Univeristy of Glasgow.
Guilbride, D. L. and Englund, P. T. (1998) 'The replication mechanism of kinetoplast DNA networks in several trypanosomatid species', *Journal of Cell Science*, 111(6), p. 675 LP-679. Available at: http://jcs.biologists.org/content/111/6/675.abstract.
Hajduk, S. L., Siqueira, A. M. and Vickerman, K. (1986) 'Kinetoplast DNA of Bodo caudatus: a noncatenated structure.', *Molecular and cellular biology*, 6(12), pp. 4372–8. Available at:

http://www.ncbi.nlm.nih.gov/pubmed/2432399.
Harmer, J. *et al.* (2018) 'Farming, slaving and enslavement: histories of endosymbioses during kinetoplastid evolution', *Parasitology*, 145(10), pp. 1311–1323. doi: 10.1017/S0031182018000781.
Harteis, S. and Schneider, S. (2014) 'Making the Bend: DNA Tertiary Structure and Protein-DNA Interactions', *International Journal of Molecular Sciences*, 15(7), pp. 12335–12363. doi: 10.3390/ijms150712335.
Hoffmann, A. *et al.* (2018) 'Molecular model of the mitochondrial genome segregation machinery in Trypanosoma brucei', *Proceedings of the National Academy of Sciences*, 115(8), pp. E1809–E1818. doi: 10.1073/pnas.1716582115.
Ivens, A. C. (2005) 'The Genome of the Kinetoplastid Parasite, Leishmania major', *Science*, 309(5733), pp. 436–442. doi: 10.1126/science.1112680.
Jackson, A. P. *et al.* (2016) 'Kinetoplastid Phylogenomics Reveals the Evolutionary Innovations Associated with the Origins of Parasitism', *Current Biology*, 26(2), pp. 161–172. doi: 10.1016/j.cub.2015.11.055.
Jackson, A. P., Quail, M. A. and Berriman, M. (2008) 'Insights into the genome sequence of a free-living Kinetoplastid: Bodo saltans (Kinetoplastida: Euglenozoa)', *BMC Genomics*, 9(1), p. 594. doi: 10.1186/1471-2164-9-594.
Kamashev, D. *et al.* (2017) 'Comparison of histone-like HU protein DNA-binding properties and HU/IHF protein sequence alignment', *PLOS ONE*. Edited by D. Chatterji, 12(11), p. e0188037. doi: 10.1371/journal.pone.0188037.
Käser, S. *et al.* (2016) 'Outer membrane protein functions as integrator of protein import and DNA inheritance in mitochondria', *Proceedings of the National Academy of Sciences*, 113(31), pp. E4467–E4475. doi: 10.1073/pnas.1605497113.
Käser, S. *et al.* (2017) 'Biogenesis of the mitochondrial DNA inheritance machinery in the mitochondrial outer membrane of Trypanosoma brucei', *PLOS Pathogens*. Edited by K. L. Hill, 13(12), p. e1006808. doi: 10.1371/journal.ppat.1006808.
Kaufer, A. *et al.* (2017) 'The evolution of trypanosomatid taxonomy', *Parasites & Vectors*, 10(1), p. 287. doi: 10.1186/s13071-017-2204-7.
Koch, H. and Schmid-Hempel, P. (2011) 'Socially transmitted gut microbiota protect bumble bees against an intestinal parasite', *Proceedings of the National Academy of Sciences*, 108(48), pp. 19288–19292. doi: 10.1073/pnas.1110474108.
Koga, H. *et al.* (1988) 'Hypersensitive cell death, autofluorescence, and insoluble silicon accumulation in barley leaf epidermal cells under attack by Erysiphe graminis f. sp. hordei', *Physiological and Molecular Plant Pathology*, 32(3), pp. 395–409. doi: 10.1016/S0885-5765(88)80033-X.
Kornmann, B. and Walter, P. (2010) 'ERMES-mediated ER-mitochondria contacts: molecular hubs for the regulation of mitochondrial biology.', *Journal of cell science*, 123(Pt 9), pp. 1389–93. doi:

10.1242/jcs.058636.
Kumar, P., Sundar, S. and Singh, N. (2007) 'Degradation of pteridine reductase 1 (PTR1) enzyme during growth phase in the protozoan parasite Leishmania donovani', *Experimental Parasitology*, 116(2), pp. 182–189. doi: 10.1016/j.exppara.2006.12.008.
Liu, B. *et al.* (2005) 'Fellowship of the rings: the replication of kinetoplast DNA', *Trends in Parasitology*, 21(8), pp. 363–369. doi: 10.1016/j.pt.2005.06.008.
Liu, Y. and Englund, P. T. (2007) 'The rotational dynamics of kinetoplast DNA replication', *Molecular Microbiology*, 64(3), pp. 676–690. doi: 10.1111/j.1365-2958.2007.05686.x.
Liu, Y., Motyka, S. A. and Englund, P. T. (2005) 'Effects of RNA Interference of Trypanosoma brucei Structure-specific Endonuclease-I on Kinetoplast DNA Replication', *Journal of Biological Chemistry*, 280(42), pp. 35513–35520. doi: 10.1074/jbc.M507296200.
Lukeš, J. *et al.* (1998) 'Pankinetoplast DNA structure in a primitive bodonid flagellate, Cryptobia helicis.', *The EMBO journal*, 17(3), pp. 838–46. doi: 10.1093/emboj/17.3.838.
Lukeš, J. *et al.* (2002) 'Kinetoplast DNA network: Evolution of an improbable structure', *Eukaryotic Cell*. doi: 10.1128/EC.1.4.495-502.2002.
Lukeš, J. *et al.* (2014) 'Evolution of parasitism in kinetoplastid flagellates', *Molecular and Biochemical Parasitology*, 195(2), pp. 115–122. doi: 10.1016/j.molbiopara.2014.05.007.
Lukeš, J. *et al.* (2018) 'Massive mitochondrial DNA content in diplonemid and kinetoplastid protists', *IUBMB Life*, 70(12), pp. 1267–1274. doi: 10.1002/iub.1894.
Marande, W., Lukes, J. and Burger, G. (2005) 'Unique Mitochondrial Genome Structure in Diplonemids, the Sister Group of Kinetoplastids', *Eukaryotic Cell*, 4(6), pp. 1137–1146. doi: 10.1128/EC.4.6.1137-1146.2005.
Maslov, D. A. *et al.* (2013) 'Diversity and phylogeny of insect trypanosomatids: all that is hidden shall be revealed', *Trends in Parasitology*, 29(1), pp. 43–52. doi: 10.1016/j.pt.2012.11.001.
Milman, N. *et al.* (2007) 'Mitochondrial origin-binding protein UMSBP mediates DNA replication and segregation in trypanosomes', *Proceedings of the National Academy of Sciences*, 104(49), pp. 19250–19255. doi: 10.1073/pnas.0706858104.
Nowak, B. F. and Archibald, J. M. (2018) 'Opportunistic but Lethal: The Mystery of Paramoebae', *Trends in Parasitology*, 34(5), pp. 404–419. doi: 10.1016/j.pt.2018.01.004.
Ochsenreiter, T. *et al.* (2008) 'Alternative RNA Editing Produces a Novel Protein Involved in Mitochondrial DNA Maintenance in Trypanosomes', *Molecular and Cellular Biology*. doi: 10.1128/MCB.00637-08.
Ogbadoyi, E. O., Robinson, D. R. and Gull, K. (2003) 'A high-order trans-membrane structural linkage is responsible for mitochondrial genome positioning and segregation by flagellar basal bodies in trypanosomes.', *Molecular biology of the cell*, 14(5), pp. 1769–79. doi: 10.1091/mbc.e02-08-0525.
Opperdoes, F. R. *et al.* (2016) 'Comparative Metabolism of Free-living Bodo saltans and Parasitic Trypanosomatids', *Journal of Eukaryotic Microbiology*, 63(5), pp. 657–678. doi: 10.1111/jeu.12315.

Poinar, G. (2011) ‘The Origin of Insect-Borne Human Diseases as Revealed in Amber’, *American Entomologist*, 57(3), pp. 170–178. doi: 10.1093/ae/57.3.170.
Povelones, M. L. (2014) ‘Beyond replication: division and segregation of mitochondrial DNA in kinetoplastids.’, *Molecular and biochemical parasitology*, 196(1), pp. 53–60. doi: 10.1016/j.molbiopara.2014.03.008.
Reid, R. (2019) *Evolution of a Mitochondrial-genome Attachment Structure in Trypanosomatid Protists*. The Univeristy of Huddersfeild.
Ro, Y. T., Scheffter, S. M. and Patterson, J. L. (1997) ‘Hygromycin B resistance mediates elimination of Leishmania virus from persistently infected parasites.’, *Journal of virology*, 71(12), pp. 8991–8. Available at: http://www.ncbi.nlm.nih.gov/pubmed/9371555.
Robinson, D. R. and Gull, K. (1994) ‘The configuration of DNA replication sites within the Trypanosoma brucei kinetoplast.’, *The Journal of cell biology*, 126(3), pp. 641–8. doi: 10.1083/jcb.126.3.641.
Rodrigues, J. C. F., Godinho, J. L. P. and de Souza, W. (2014) ‘Biology of Human Pathogenic Trypanosomatids: Epidemiology, Lifecycle and Ultrastructure’, in, pp. 1–42. doi: 10.1007/978-94-007-7305-9_1.
Santos, H. J., Makiuchi, T. and Nozaki, T. (2018) ‘Reinventing an Organelle : The Reduced Mitochondrion in Parasitic Protists’, *Trends in Parasitology*. Elsevier Ltd, 34(12), pp. 1038–1055. doi: 10.1016/j.pt.2018.08.008.
Savoia, D., Allice, T. and Tovo, P.-A. (2005) ‘Antileishmanial activity of HIV protease inhibitors’, *International Journal of Antimicrobial Agents*, 26(1), pp. 92–94. doi: 10.1016/j.ijantimicag.2005.04.003.
Schnarwiler, F. *et al.* (2014) ‘Trypanosomal TAC40 constitutes a novel subclass of mitochondrial -barrel proteins specialized in mitochondrial genome inheritance’, *Proceedings of the National Academy of Sciences*, 111(21), pp. 7624–7629. doi: 10.1073/pnas.1404854111.
Schnarwiler, F. *et al.* (2014) ‘Trypanosomal TAC40 constitutes a novel subclass of mitochondrial β-barrel proteins specialized in mitochondrial genome inheritance.’, *Proceedings of the National Academy of Sciences of the United States of America*, 111(21), pp. 7624–9. doi: 10.1073/pnas.1404854111.
Schneider, A. and Ochsenreiter, T. (2018) ‘Failure is not an option – mitochondrial genome segregation in trypanosomes’, *Journal of Cell Science*, 131(18), p. jcs221820. doi: 10.1242/jcs.221820.
Séguin, O. and Descoteaux, A. (2016) ‘Leishmania , the phagosome, and host responses: The journey of a parasite’, *Cellular Immunology*, 309, pp. 1–6. doi: 10.1016/j.cellimm.2016.08.004.
Shaner, N. C. *et al.* (2004) ‘Improved monomeric red, orange and yellow fluorescent proteins derived from Discosoma sp. red fluorescent protein’, *Nature Biotechnology*, 22(12), pp. 1567–1572. doi: 10.1038/nbt1037.

Shaner, N. C. (2013) ‘The mFruit Collection of Monomeric Fluorescent Proteins’, *Clinical Chemistry*, 59(2), pp. 440–441. doi: 10.1373/clinchem.2012.194837.
Shapiro, T. A. (1993) ‘Kinetoplast DNA maxicircles: networks within networks.’, *Proceedings of the National Academy of Sciences of the United States of America*, 90(16), pp. 7809–13. Available at: http://www.ncbi.nlm.nih.gov/pubmed/8395055.
Sibbald, S. J. *et al.* (2017) ‘Diversity and Evolution of Paramoeba spp. and their Kinetoplastid Endosymbionts’, *Journal of Eukaryotic Microbiology*, 64(5), pp. 598–607. doi: 10.1111/jeu.12394.
Silvester, E., McWilliam, K. and Matthews, K. (2017) ‘The Cytological Events and Molecular Control of Life Cycle Development of Trypanosoma brucei in the Mammalian Bloodstream’, *Pathogens*, 6(4), p. 29. doi: 10.3390/pathogens6030029.
Simpson, A. G. B., Lukes, J. and Roger, A. J. (2002) ‘The evolutionary history of kinetoplastids and their kinetoplasts.’, *Molecular biology and evolution*, 19(12), pp. 2071–83. doi: 10.1093/oxfordjournals.molbev.a004032.
Souza, F. S. P. de *et al.* (2010) ‘Knockout of the gene encoding the kinetoplast-associated protein 3 (KAP3) in Trypanosoma cruzi: Effect on kinetoplast organization, cell proliferation and differentiation’, *Molecular and Biochemical Parasitology*, 172(2), pp. 90–98. doi: 10.1016/j.molbiopara.2010.03.014.
de Souza, S. S. *et al.* (2017) ‘Expanded repertoire of kinetoplast associated proteins and unique mitochondrial DNA arrangement of symbiont-bearing trypanosomatids’, *PLOS ONE*. Edited by V. Yurchenko, 12(11), p. e0187516. doi: 10.1371/journal.pone.0187516.
Sunter, J. and Gull, K. (2017) ‘Shape, form, function and Leishmania pathogenicity: from textbook descriptions to biological understanding’, *Open Biology*, 7(9), p. 170165. doi: 10.1098/rsob.170165.
Sykes, S. E. and Hajduk, S. L. (2013) ‘Dual functions of α-ketoglutarate dehydrogenase E2 in the Krebs cycle and mitochondrial DNA inheritance in Trypanosoma brucei’, *Eukaryotic Cell*. doi: 10.1128/EC.00269-12.
Talamond, P., Verdeil, J.-L. and Conéjéro, G. (2015) ‘Secondary Metabolite Localization by Autofluorescence in Living Plant Cells’, *Molecules*, 20(3), pp. 5024–5037. doi: 10.3390/molecules20035024.
Tanifuji, G. *et al.* (2017) ‘Genome sequencing reveals metabolic and cellular interdependence in an amoeba-kinetoplastid symbiosis’, *Scientific Reports*, 7(1), p. 11688. doi: 10.1038/s41598-017-11866-x.
Tetaud, E. *et al.* (2002) ‘A new expression vector for Crithidia fasciculata and Leishmania’, *Molecular and Biochemical Parasitology*, 120(2), pp. 195–204. doi: 10.1016/S0166-6851(02)00002-6.
Towbin, H., Staehelin, T. and Gordon, J. (1979) ‘Electrophoretic transfer of proteins from polyacrylamide gels to nitrocellulose sheets: procedure and some applications.’, *Proceedings of the National Academy of Sciences of the United States of America*, 76(9), pp. 4350–4. doi:

10.1073/pnas.76.9.4350.
Trikin, R. *et al.* (2016) 'TAC102 Is a Novel Component of the Mitochondrial Genome Segregation Machinery in Trypanosomes', *PLOS Pathogens*. Edited by K. L. Hill, 12(5), p. e1005586. doi: 10.1371/journal.ppat.1005586.
Wong, R. G. *et al.* (2015) 'U-insertion/deletion RNA editing multiprotein complexes and mitochondrial ribosomes in Leishmania tarentolae are located in antipodal nodes adjacent to the kinetoplast DNA', *Mitochondrion*, 25, pp. 76–86. doi: 10.1016/j.mito.2015.10.006.
Woods, A. *et al.* (1989) 'Definition of individual components within the cytoskeleton of Trypanosoma brucei by a library of monoclonal antibodies.', *Journal of cell science*, 93 (Pt 3), pp. 491–500. Available at: http://www.ncbi.nlm.nih.gov/pubmed/2606940.
Xu, C. W. *et al.* (1996) 'Nucleus-encoded histone H1-like proteins are associated with kinetoplast DNA in the trypanosomatid Crithidia fasciculata.', *Molecular and Cellular Biology*, 16(2), pp. 564–576. doi: 10.1128/MCB.16.2.564.
Zhang, W.-W. and Matlashewski, G. (2015) 'CRISPR-Cas9-Mediated Genome Editing in Leishmania donovani', *mBio*. Edited by L. D. Sibley, 6(4). doi: 10.1128/mBio.00861-15.
Zhang, X. *et al.* (2010) 'The Trypanosoma brucei MitoCarta and its regulation and splicing pattern during development', *Nucleic Acids Research*, 38(21), pp. 7378–7387. doi: 10.1093/nar/gkq618.
Zhao, Z. *et al.* (2008) 'p166, a link between the trypanosome mitochondrial DNA and flagellum, mediates genome segregation.', *The EMBO journal*, 27(1), pp. 143–54. doi: 10.1038/sj.emboj.7601956.
Zhou, Q. *et al.* (2010) 'A Comparative Proteomic Analysis Reveals a New Bi-Lobe Protein Required for Bi-Lobe Duplication and Cell Division in Trypanosoma brucei', *PLoS ONE*. Edited by M. Polymenis, 5(3), p. e9660. doi: 10.1371/journal.pone.0009660.

Appendices

8.0 Supplementary Materials

8.1 YL1/2 may recognise *Cf*RP2

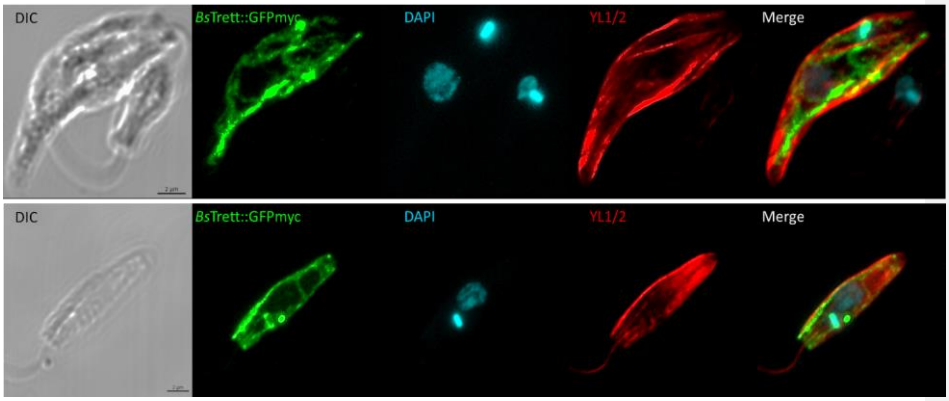

Sup 1 YL1/2 Targeting in *Crithidia fasciculata*: YL1/2 appears to associate down the flagellar and outer cell membrane possibly due to recognition of *Cf*RP2

Sup2 Clustal omega analysis of *Tb*RP2 and *Cf*RP2: Clustal alignment of *Tb*RP2 and *Cf*RP2 shows homologous regions between both proteins possibly leading to the identification of RP2 with YL1/2

```
TbRP2
MTYQAKEVVTEEFLRKKLEVSGELARMRAMIVDTALKTLSEDPNIKSRLFSPTPRLKAEKESAKGRQS
LSVVMEYLEHMGLNYTLSVLKQEAALTECALQSRQDIVRELGLPEGSGPILTTIMGAPGAAGANSGVS
KDNIGLPTTTPESAPVPRAPVAQTKTEDGEDTTYFISKWSGRTFYRSGGQVSGQQVQLEYLTNCTVYV
LDPLDSITVDDCEGGELIIAACEGSVFLRNCKNMTVHVACKQLRTRDCEYITLHIFATTDPVVESSHH
INFKPFYIRLPGLQASFKSARLDPKTNRFVHVYDFTEDDPKLPKPHFTVTYKGHGLCMKDLCGEKGKP
DCPQEIEDFLAGRLGPAASSESGHNKSYNIKTGAEEWTGNKESSSPERGKEATPPESASRSDSSAPTT
PHSRKDDAVPAPAAATGDALDGSYSSFDDDEDEDENDSQSDKKSEDDDDDDSDDF

CfRP2
MATSDPAETERVIRQKLESSGQYGKMRAMIMEAALQTVQSSSNSSNGAAKPSFAPSAALIEAKANGVV
ELSIVLEYIRALGLQYTESVLCLEAGLSAASLHTSADLRQRFGVTAPCTCLTALVKGGGDSSAPPAAT
QQAPPPTSAAAVVAVEEPADEKGDKSDHDQPGAEDSTYFISGWKRRHFVRHQQVTGQQVQLDRLTDCQ
TIVLDELDSMTADDCEGGELVVAACEGSVFLRNCKNMTVHVACKQLRTRDCANINLHIFTTTDPVVEM
SHNVHFYPFHLRLPSLRKLFADARLDAKLNRFVHVYDFTPSEPGLPQPHFQVHFPDHGQQMENRCGSY
GTPECPPEVEQLLALQLMPAASSESGKNKSYDIKTGAHVWAAGGVSAVPVVAAAAAAAAAVSVAPQGQ
AASSSADHSSVHSSSVSDVESDSESSGSDDDSDKAAAAAQAKRAAALGAVPAPLAAAAPAATHAAIPG
GFDNEEYSSFDDESDAHDADDKYEVDEDEDDF

CLUSTAL format alignment by MAFFT FFT-NS-i (v7.397)


TbRP2           MTYQAKEVVTEEFLRKKLEVSGELARMRAMIVDTALKTLSEDPNIKSRLFSPT--PRLKA
CfRP2           MA-TSDPAETERVIRQKLESSGQYGKMRAMIMEAALQTVQSSSNSSNGAAKPSFAPSAAL
                *:  :. . **..:*:*** **: .:*****:::**:*:....* ..   .*:  *
```

```
TbRP2           EKESAKGRQSLSVVMEYLEHMGLNYTLSVLKQEAALTECALQSRQDIVRELGLPEGSGPI
CfRP2           IEAKANGVVELSIVLEYIRALGLQYTESVLCLEAGLSAASLHTSADLRQRFGV---TAP-
                 : .*:*  .**:*:**:. :**:** ***  **.*: .:*::  *: :.:*:   :.*

TbRP2           LTTIMGAPGAAGANSGVSKDNIGLPTTTPESAPVPRAPVAQTKTED--------------
CfRP2           -CTCLTALVKGGGDSSA-------PPAATQQAPPPTSAAAVVAVEEPADEKGDKSDHDQP
                  * : *   .*.:*..       *.::.:.** * :..* . .*:

TbRP2           -GEDTTYFISKWSGRTFYRSGGQVSGQQVQLEYLTNCTVYVLDPLDSITVDDCEGGELII
CfRP2           GAEDSTYFISGWKRRHFVRH-QQVTGQQVQLDRLTDCQTIVLDELDSMTADDCEGGELVV
                 .**:***** *. * * *   **:******: **:* . *** ***:*.********::

TbRP2           AACEGSVFLRNCKNMTVHVACKQLRTRDCEYITLHIFATTDPVVESSHHINFKPFYIRLP
CfRP2           AACEGSVFLRNCKNMTVHVACKQLRTRDCANINLHIFTTTDPVVEMSHNVHFYPFHLRLP
                ****************************  *.****:******* **:::* **::***

TbRP2           GLQASFKSARLDPKTNRFVHVYDFTEDDPKLPKPHFTVTYKGHGLCMKDLCGEKGKPDCP
CfRP2           SLRKLFADARLDAKLNRFVHVYDFTPSEPGLPQPHFQVHFPDHGQQMENRCGSYGTPECP
                .*:  * .****.* ********** .:* **:*** * : .**  *:: **. *.*:**

TbRP2           QEIEDFLAGRLGPAASSESGHNKSYNIKTGAEEWTGNKESSSP---------------ER
CfRP2           PEVEQLLALQLMPAASSESGKNKSYDIKTGAHVWAAGGVSAVPVVAAAAAAAAAVSVAPQ
                 *:*::** :* ********:****:*****. *:..  *: *               :

TbRP2           GKEATPP------ESASRSDSSAPTTPHSRKDD-----------------AVPAP-----
CfRP2           GQAASSSADHSSVHSSSVSDVESDSESSGSDDDSDKAAAAAQAKRAAALGAVPAPLAAAA
                *: *:..      .*:* ** .: : . . .**                 *****

TbRP2           AAATGDALDG-----SYSSFDDDEDEDENDSQSDKKSEDDDDDDSDDF
CfRP2           PAATHAAIPGGFDNEEYSSFDDESDAHDADDKYEV------DEDEDDF
                .***  *: *     .******:.* .: *.: :       *:*.***
```

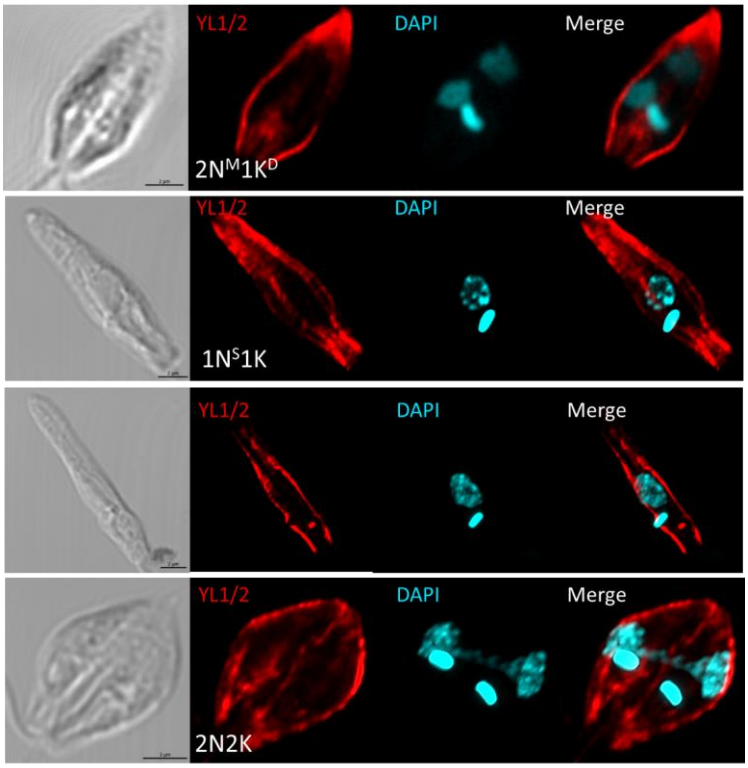

Sup 3 YL1/2 Movement through the *C.fasciulata* cell cycle: YL 1/2 movement throughout the cell cycle reveals the basal body and highlights the cell periphery

Sup 4 Central region of TAC40 showing mutations throughout

```
TAC40_Seq      ATCCACNNNNGATCCGGATCNNNNGTGCACNNNNNNTCCGGANNNNNNGTGTTAACNNNN 1800
TAC40          ATGAACATTCCAGAAGTATGCGATG---------TCT-----------CTCAAAAGATTC 331
               **  **     *   * **     *          *           *   **

TAC40_Seq      NNGTGCGCACNNNNNNGTTAAGCACCCANNNGTTAACNNNTGGGTGCAACNNNAACGTGC 1860
TAC40          TTGTGGACACGGATGG-CAAAGCTACCGGCACTC----------TACAGCTCAAAGAACT 380
                 ***  ***         ****  **     *          * ** *   **

TAC40_Seq      NNGTGCGCACNNGCACGTTNNNGTTAACGCACTAGTGCGTTGCACNAACTAGTTNGTGCA 1920
TAC40          CATCGAGGGATTGAAAATTCGAGGGACAGTCGTTGTG-----AATACCATTGCGCCAGCA 435
                   * *     * *  **   *  *  *   * ***      *     * *     ***

TAC40_Seq      ACNAACTAGTG------CGTGCGCACGCACTAGTTNGTTAACTAGTNNGTGCGCACNNAC 1974
TAC40          ACGAACGACGACTCCGCCATTCACGCGAAGTTCTTCAAGAATGACTTTTATTGCTCC--- 492
               ** *** *         * * * * ** * *  **    **  * *      ** *

TAC40_Seq      TAGTTAACNNACTAGTGCGCACTAGTNNGTTGGCCNNNNNGGC---CGAACNNNNNNTAC 2031
TAC40          --------ACAGCTGCAAGCAAGAATGGATTTGGCTCCACTGCAACCGGCGTTGACTTCG 544
                       *   *  ***  * *   ** * *      **   **         *

TAC40_Seq      GTANNNNNNGTTCGCACNN---------NNNNGTTATAACNNNNNNGTGCTTATAACNNN 2082
TAC40          GTGGGCGTTTTCAGGATTTAATTCTTGGCGCTGGCATCACACGAAAGTACTTCTCCGCAG 604
               **        *  * *               *  ** **      ** *** *
```

```
TAC40_Seq      NNNGTGCGCACNNNNNNGTTATAACCAGGWCCTGGCCWGGGWCCTGGCCAGGWCCCWGGC 2142
TAC40          AAGAGGCCGACCA-----------GCGGATGCTTGCCATGCAG----------------- 636
                     **  **             * *   ** ***  *

TAC40_Seq      CAGGWCCYRGGWCCTGGGAACNNNNNCTCGAGNNNNNGTTCAACNNGCACGTGCNNGTTA 2202
TAC40          -------------------------------ATCCAACAGGACGAGGATACACAGGTCT 664
                                                    **  * *    *  **

TAC40_Seq      TCTATGTCGGGTGCGGAGAAAGAGGTAATGAAATGGCCATTTCATTACCTCTTTCTCCGC 2262
TAC40          ACATTG----GTGGGGGCATGCATGGAAGGAATTGGGCCTTTGGTGGACGACTTGTGCGT 720
                *  **    *** **  *   * * ** *** *** * ***  *   *   ** * **

TAC40 Seq      ACCCGACATAGATTGGCAAACAGCTATTATGGGTATTATGGGTACCCATAATACCCATAA 2322
TAC40          GTCAACGA-CTTGTGGAACACTGCTGAGCTTGTCATGTTTGGTGGACGACTTGTGCGTGT 779
                 *    *     *** * ** ***    * *  **  * ***   *    *   * *

TAC40 Seq      TAGCTGTTTGCCAAACGCA----CATGTGCGTTGCACNAACATGTTNGTGCAACNAACAT 2378
TAC40          CAACGACTTGTGGAACAATGCCGAGCTTGCCATGTTCCGTAAGATTGAAG---------- 829
                * *   ***   ***           ***  **  *    *  **   *

TAC40 Seq      GTGCGTGCGCACGCACATGTTNGTTGATCGCGATCCCWGGNNCCGGNNCCWGGCCWGGCG 2438
TAC40          ----CTTCCACCGCAGTTGCTTGTGCCTACGG---------------------------- 857
                    * *   ****  ** * **   *   *
```

9.0 Plasmid Maps

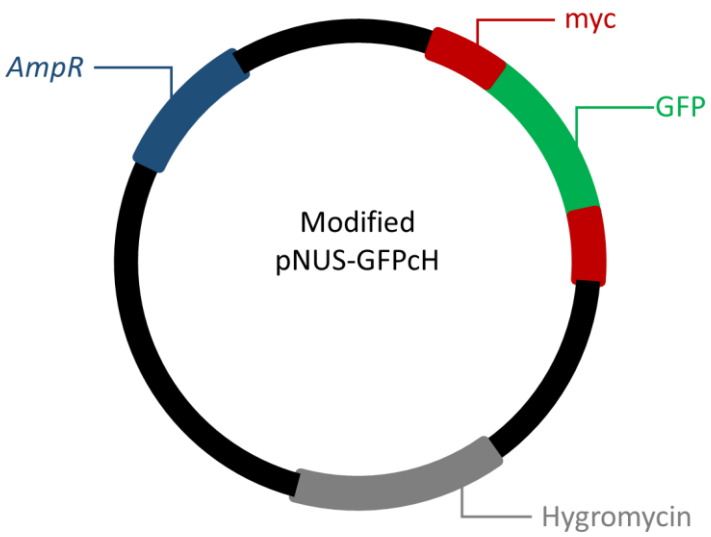

Sup 5 Plasmid map of modified pNUS-GFPcH used in this study: The plasmid features an N and C terminal myc tag flanking the GFP tag, usually there is only a C-terminal myc tag within this vector

Sup 6 Plasmid map of pET-28a (+) used in this study: pET-28a (+) encodes Kanamycin resistance and expression is initiated via a lac operon.